Hill-Robertson interference may bias the inference of fitness effects of new mutations in highly selfing species

Austin Daigle[1,2,3] and Parul Johri[1,2,4,*]

[1]Department of Biology, University of North Carolina, Chapel Hill, NC 27599
[2]Department of Genetics, University of North Carolina, Chapel Hill, NC 27599
[3]Curriculum in Bioinformatics and Computational Biology, University of North Carolina, Chapel Hill, NC 27599
[4]Integrative Program for Biological & Genome Sciences, University of North Carolina, Chapel Hill, NC 27599

*Correspondence can be addressed to these authors

Parul Johri
pjohri@unc.edu

Running title: Inferring fitness effects in selfing populations

Keywords: distribution of fitness effects, self-fertilization, Hill-Robertson interference, background selection, population structure

ABSTRACT

The accurate estimation of the distribution of fitness effects (DFE) of new mutations is critical for population genetic inference but remains a challenging task. While various methods have been developed for DFE inference using the site frequency spectrum of putatively neutral and selected sites, their applicability in species with diverse life history traits and complex demographic scenarios is not well understood. Selfing is common among eukaryotic species and can lead to decreased effective recombination rates, increasing the effects of selection at linked sites, including interference between selected alleles. We employ forward simulations to investigate the limitations of current DFE estimation approaches in the presence of selfing and other model violations, such as linkage, departures from semidominance, population structure, and uneven sampling. We find that distortions of the site frequency spectrum due to Hill-Robertson interference in highly selfing populations lead to mis-inference of the deleterious DFE of new mutations. Specifically, when inferring the distribution of selection coefficients, there is an overestimation of nearly neutral and strongly deleterious mutations and an underestimation of mildly deleterious mutations when interference between selected alleles is pervasive. In addition, the presence of cryptic population structure with low rates of migration and uneven sampling across subpopulations leads to the false inference of a deleterious DFE skewed towards effectively neutral/mildly deleterious mutations. Finally, the proportion of adaptive substitutions estimated at high rates of selfing is substantially overestimated. Our observations apply broadly to species and genomic regions with little/no recombination and where interference might be pervasive.

INTRODUCTION

The distribution of fitness effects (DFE) of new mutations describes the continuum of selective effects of spontaneous mutations in a population and is critical for understanding the effects of natural selection on genetic variation (Eyre-Walker and Keightley 2007). Because of the considerable impact deleterious mutations can have on allele frequency patterns in a population, knowledge of the DFE is often necessary to produce accurate evolutionary models, which are required for unbiased estimates of both the demographic history of a population and the proportion of adaptive nucleotide substitutions in a lineage (Charlesworth 1994; Eyre-Walker

53 and Keightley 2007; Bank et al. 2014; Johri, Aquadro, et al. 2022). While the DFE can be
54 estimated with experimental approaches using random mutagenesis or mutation-accumulation
55 lines (*e.g.*, Wloch *et al.* 2001; Estes *et al.* 2004; Sanjuán *et al.* 2004), it can also be inferred from
56 the distribution of allele frequencies from population genetic data (Williamson et al. 2005; Eyre-
57 Walker et al. 2006; Keightley and Eyre-Walker 2007; Galtier 2016). As many organisms cannot
58 easily be cultured in laboratories, are not genetically manipulatable, and/or have large generation
59 times, a population genetic approach remains an important and the only possible approach to
60 estimating the DFE in some species.

61 Population genetic methods use putatively neutral sites to fit the demographic history or
62 to account for other potential nuisance parameters, while selected sites are used to infer the DFE
63 (by inferring the parameters of a prespecified probability distribution), conditional on the
64 demographic history obtained from neutral sites (reviewed in Johri *et al.* 2022b). While most
65 two-step population genetic approaches that infer the DFE make a series of assumptions, like
66 random mating and the absence of effects of selection at linked sites, they appear to be robust to
67 certain model violations like mutation rate variability (Tataru et al. 2017), background selection
68 (Huber et al. 2017; Kim et al. 2017; Huang et al. 2021), population substructure (Kim et al.
69 2017), and some complex demographic changes (Kousathanas and Keightley 2013). This is
70 because two-step inference methods are usually employed using interdigitated neutral and
71 selected sites and might therefore correct for model violations that skew the neutral and selected
72 SFS similarly. As an aside, because demographic history is unlikely to affect the SFS of neutral
73 and very strongly deleterious mutations equally (Eyre-Walker et al. 2006), this might lead to
74 slight inaccuracies in inference using methods that do not explicitly model population size
75 changes.

76 Despite significant progress, not much work has been done on understanding the effects
77 of non-random mating, in particular self-fertilization, on the inference of the DFE using
78 population genetic approaches. Self-fertilization or selfing (*i.e.*, an individual mating with itself)
79 is common across all eukaryotic species - about 35% of all seed plants and ~50% of all animals
80 exhibit moderate to high rates (50-100%) of selfing (Goodwillie et al. 2005; Jarne and Auld
81 2006). A transition from random mating to partial selfing has several effects on the population.
82 Firstly, the increase of nonrandom mating in a partially selfing population decreases the effective
83 population size (N_e), due to a reduction in the amount of independently sampled gametes (Pollak

84 1987) . There is no change in the probability of fixation of semidominant mutations, but the
85 probability of fixation of recessive or partially recessive beneficial mutations is increased by
86 selfing, and the probability of fixation of recessive or partially recessive deleterious mutations is
87 slightly reduced (Caballero and Hill 1992; Charlesworth 1992). Thirdly, increased homozygosity
88 in the genomes of partially selfing organisms results in a higher proportion of recombination
89 events occurring on nearly identical chromosomes, which decreases the effective rate of
90 recombination (Nordborg 2000). This effect increases the extent of background selection (BGS;
91 Charlesworth *et al.* 1993; Charlesworth and Charlesworth 1998; Charlesworth 2003) and
92 selective sweeps (Hedrick 1980; Hartfield and Bataillon 2020) experienced by the population.
93 Finally, as the effective rate of recombination is lowered drastically in highly selfing
94 populations, there can be a further decrease in the efficacy of selection due to Hill-Robertson
95 interference (HRI) between selected loci (Hill and Robertson 1966; McVean and Charlesworth
96 2000; Comeron and Kreitman 2002; Hartfield and Glémin 2014; Hartfield and Glémin 2016).
97 Hill-Robertson interference (HRI) describes how the efficacy of selection at an allele at
98 one locus can be reduced due to the segregation of selected alleles at a second linked locus (Hill
99 and Robertson 1966; Felsenstein 1974). While BGS and selective sweeps are also a type of HRI,
100 those models assume that selection is strong and that there is no interference between selected
101 sites (reviewed in Charlesworth and Jensen 2021). However, because weakly selected mutations
102 can segregate in the population at higher frequencies, interference between them can result in
103 reduced efficacy of selection and has been termed interference selection (Comeron et al. 1999;
104 Comeron and Kreitman 2002) or weak selection HRI (McVean and Charlesworth 2000; Kaiser
105 and Charlesworth 2009). Moreover, the effects of such interference have been shown to extend
106 to more strongly selected mutations in cases where recombination is greatly reduced (Kaiser and
107 Charlesworth 2009). We therefore refer to the effects of interference selection/weak selection
108 HRI as simply HRI in this study. Since the entire genomes of populations with high selfing rates
109 have greatly reduced effective recombination rates (Nordborg 2000) and deleterious mutations
110 are prevalent across the genome (Bank et al. 2014), HRI is likely to play an important role in
111 determining the dynamics of deleterious mutations in such populations.
112 Unlike the model of classical BGS, where deleterious alleles are at deterministic
113 mutation-selection equilibrium, selected sites in populations or genomic regions with pervasive
114 HRI depart from the standard equilibrium (Comeron and Kreitman 2002; Kaiser and

Charlesworth 2009; O'Fallon et al. 2010; Seger et al. 2010; Nicolaisen and Desai 2013). The site frequency spectra (SFS) of neutral and selected sites affected by HRI are skewed towards rare variants and become more similar to each other as the strength of HRI increases, and these changes cannot be summarized as a simple change in effective population size (Comeron and Kreitman 2002; Kaiser and Charlesworth 2009; O'Fallon et al. 2010; Seger et al. 2010; Nicolaisen and Desai 2013; Good et al. 2014). More recent work assuming equal selection coefficients across deleterious alleles has shown that when HRI is sufficiently common, the nucleotide site diversity can be entirely described by the variation of fitness between individuals in the population. However, populations with different combinations of average selection coefficients, recombination, and mutation rates can have the same nucleotide diversity in this regime (Good et al. 2014), suggesting difficulties in estimating a distribution of selection coefficients along with other population genetic parameters in populations with little/no recombination. While, a recent study suggested that the population-scaled fitness effects of mutations are mis-inferred due to linked effects of selection when the probability of selfing is sufficiently high (Gilbert et al. 2022), the role of HRI (specifically interference) remains unclear. Here, we thoroughly characterize how HRI and other linked effects of selection might bias the inference of both population-scaled as well as direct estimates of selection coefficients in highly selfing species and in regions of low recombination for a variety of DFE shapes. To investigate other potential causes of DFE mis-inference in partially selfing natural populations, we explore the effects of changing the dominance coefficients, coding density, and number of selected sites, as well as the effects of cryptic population structure and sampling on DFE inference. Moreover, we characterize the accuracy of inference of both the DFE of new deleterious mutations as well as the proportion of adaptive substitutions.

METHODS

Simulations

All simulations were performed using the forward simulator SLiM (version 4.0.1; Haller and Messer 2023). The genome architecture and population parameters were modeled to mimic the genomes of *C. elegans* populations because they have a high rate of selfing, which has been estimated to be 98%-99.9% using laboratory observations (Hodgkin 1983; Anderson et al. 2010),

146 field work, and population genetic analyses (Barrière and Félix 2005; Barrière and Félix 2007).
147 A chromosome with an intron-exon structure was simulated such that each gene consisted of 6
148 exons (250 bp in length) and 5 introns (100 bp in length). Genes were interspersed with
149 intergenic regions of length 3000 bp each. These numbers were close to the median of the length
150 of exons, introns, and intergenic regions observed in the *C. elegans* genome with a gene density
151 of ~1 gene every 5kb (*C. elegans* Sequencing Consortium 1998). The *C. elegans* genome
152 comprises 30% coding, 25% intronic, and 45% intergenic regions (*C. elegans* Sequencing
153 Consortium 1998). In line with these genome-wide characteristics, our simulated genome
154 comprised 30% coding, 10% intronic, and 60% intergenic regions, and a total of 500 genes,
155 resulting in a full chromosomal length of 2,503,000 bp. All introns and intergenic regions were
156 assumed to be neutral, while exons experienced selection.

157 To take synonymous sites into account, 25% ($= f_{neu}$) of all mutations in exons were
158 assumed to be fully neutral (with s=0) while the rest were under selection. Fitness was calculated
159 multiplicatively across loci. Epistasis, which could increase or decrease HRI due to changes in
160 the mean equilibrium frequency of deleterious mutations, was not modeled in this study. Of the
161 selected mutations, a fraction f_{pos} were assumed to be beneficial, where f_{pos} was assumed to be
162 either 0.0, 0.01, or 0.001, and the rest ($1 - f_{pos} - f_{neu}$) were deleterious. The DFE of deleterious
163 mutations was assumed to be a gamma distribution, parametrized by the shape parameter (β) and
164 the mean population-scaled selection coefficient ($\gamma = 2N_e\overline{s_d}$), where $\overline{s_d}$ is the mean selective
165 disadvantage of the mutant homozygote relative to wildtype. Three different deleterious DFEs
166 were modeled, representing fitness effects skewed towards mildly, moderately, and strongly
167 deleterious classes respectively (Table 1). The DFE of beneficial mutations was assumed to be
168 exponential with mean $2N_e\overline{s_a} = 200$, where $\overline{s_a}$ is the mean selective advantage of the mutant
169 homozygote relative to wildtype. All mutations were assumed to be semidominant (where $h =$
170 0.5) unless otherwise specified.

171 A Wright-Fisher population under equilibrium was simulated with a population size (N)
172 of 500,000 diploid individuals (following Gilbert et al. 2022) and with varying probabilities of
173 selfing – 0%, 50%, 80%, 90%, 95%, and 99%. Mutation (μ) and recombination (r) rates were
174 assumed to be constant at 3.3×10^{-9} per site/generation (Denver et al. 2004; Konrad et al. 2019;
175 Saxena et al. 2019) and 3.12×10^{-8} per site/generation (Rockman and Kruglyak 2009),
176 respectively. Simulations were conducted with a population size of 5000 diploid individuals,

with a rescaling factor (Q) of 100, and rates of mutation and recombination as well as selection coefficients were correspondingly adjusted so that the population-scaled parameters $N\mu$, Nr, and Ns were equivalent to a population of 500,000. Simulations were run for a total of $14N$ generations, where $10N$ generations corresponded to the burn-in period and $4N$ generations were used to calculate the number of substitutions and where N represents the scaled population size. Five replicates of each evolutionary scenario were simulated and the DFE was estimated for each replicate separately.

Single-locus simulations with selfing: To investigate the effects of selfing on DFE inference without linkage, selected, semidominant mutations were simulated at single sites with probabilities of selfing of 0%, 50%, and 99%. As allele frequencies of neutral mutations are unaffected by linkage in the absence of selected mutations, 187,500 linked neutral sites were simulated, equivalent to the number of neutral sites present in 500 *C. elegans* genes. 50,000 selected sites were simulated for each scenario (compared to 562,500 selected sites in previous simulations), then paired with neutral mutations simulated with the appropriate selfing rate. The simulations were rescaled by a factor of 100 and run for $14N$ generations with $10N$ burn-in generations.

Simulations under low recombination rates with no selfing: To clarify if the lower effective recombination rates in a partially selfing population were responsible for DFE mis-inference, we conducted simulations with low recombination rates and 0% selfing. As before, these simulations were rescaled by a factor of 100. The *C. elegans* rescaled recombination rate of 3.12×10^{-6} was multiplied by 0.5, 0.1, 0.05, 0.01, 0.005, or 0.001. Beneficial mutations were not included in these simulations.

Simulations with varying dominance coefficients: All selected mutations shared a single dominance coefficient of 0.1, 0.25, or 0.75. Populations with selfing probabilities of 0%, 50%, and 99% were simulated and compared to the original simulations (where $h = 0.5$).

Simulations under varying coding density and chromosome size: Simulations were performed with varying coding densities by varying the intergenic lengths - 1500 bp and 500 bp. The total

208 number of genes was not increased in these simulations. Thus, in the simulations with 1500 bp
209 intergenic regions, the simulated genome was comprised of ~43% coding, ~14% intronic, and
210 ~43% intergenic regions, with a total length of 1,752,100 bp. In the simulations with 500 bp
211 intergenic regions, the genome was comprised of ~55% coding, ~18% intronic, and ~27%
212 intergenic regions, with a total length of 1,376,650 bp. These simulations were run with
213 probabilities of selfing equal to 0%, 50%, and 99%.
214 To study the effects of a more realistically sized chromosome on DFE inference in
215 selfers, the total number of genes was increased from 500 to 3000, corresponding to
216 approximately the number of genes observed on the first chromosome of the *C. elegans* genome,
217 with a total simulated length of 15,018,000 bp, close to the true size of *C. elegans* chromosome I
218 (15,072,434 bp) (https://www.ncbi.nlm.nih.gov/datasets/genome/GCF_000002985.6/; last
219 accessed in Dec. 2023).
220
221 *Simulations with varying rescaling factors:* To investigate the impact of rescaling of population
222 sizes, simulations were conducted with the rescaling factor $Q = 50$, 20, and 10, where the
223 population-scaled parameters $N\mu$, Nr, and Ns were equivalent to a population of 500,000.
224 Simulations were run for a total of $14N$ generations, where $10N$ generations corresponded to the
225 burn-in period and $4N$ generations were used to calculate the number of substitutions and where
226 N represents the scaled population size. Due to the excessive run time of unscaled simulations,
227 simulations were only run with selfing rates of 95% and 99%. For $Q = 10$, only one replicate of
228 DFE3 at 95% selfing and three replicates each for DFE2 and DFE3 at 99% selfing reached
229 completion.
230
231 **Quantifying the effect of BGS in simulated data**
232 To determine the theoretically expected neutral nucleotide diversity (π) in simulations with
233 partial selfing, we calculated the expected effective population size after correcting for selfing
234 (N_{self}) as $N_{self} = N/(1 + F)$, where $F = P_{self}/(2 - P_{self})$, and P_{self} represents the proportion
235 of selfing individuals in a population per generation (Pollak 1987). Without the linked effects of
236 selection, the neutral π is expected to be approximated by $\pi \sim \theta = 4N_{self}\mu$. In simulations with
237 deleterious mutations, the extent of BGS was quantified as the observed nucleotide diversity
238 (π_{obs}) at neutral sites relative to that expected under strict neutrality, *i.e.*,

$$B = \frac{\pi_{obs}}{4N_{self}\mu} \quad (1)$$

Simulations with population structure

To study the effects of population structure on DFE inference in selfers, a finite island model (Maruyama 1970) with five demes and an equal probability of exchange of migrants between all demes was considered. Note that in this model the migration rate is independent of the selfing rate, which applies well to animals but is not necessarily the case in plant species because selfing can prevent pollen dispersal (reviewed in Sicard and Lenhard 2011). Scenarios with different migration rates were simulated such that the effective metapopulation size remained constant and equivalent to the size of the panmictic population simulated above. Genome structure was identical to that in the previous simulations mimicking *C. elegans* genome architecture. In a metapopulation with d demes and a deme effective population size N_{deme}, the mean coalescence time for a pair of alleles sampled from the same deme (T_S) is given by the following equation (Nei 1973; Slatkin and Voelm 1991; Charlesworth and Charlesworth 2010):

$$T_S \sim 2dN_{deme} \quad (2)$$

The mean coalescence time for a pair of alleles sampled from different demes (T_B) is given by (Nei 1973; Slatkin and Voelm 1991; Charlesworth and Charlesworth 2010):

$$T_B \sim 2dN_{deme} + \frac{(d-1)}{2m} \quad (3)$$

where the migration rate m is the probability that an allele in one deme is derived by migration from any other deme in a generation (which means that the migration rate between any two demes is equal to $\frac{m}{d}$). Combining these two equations gives the mean coalescence time (T_T) for a

267 pair of alleles drawn from the entire metapopulation (Nei 1973; Slatkin and Voelm 1991;
268 Charlesworth and Charlesworth 2010):
269

270 $$T_T \sim 2dN_{deme} + \frac{(d-1)^2}{2dm} \quad (4)$$

271
272
273 To keep the effective size of the metapopulation ($0.5T_T$) equivalent to the rescaled size of
274 5,000 individuals used in previous simulations, N_{deme} and m were varied such that T_T remained
275 equal to 10,000. To allow a wide range of migration rates, $N_{deme}m$ was varied from 10, 2, 1, 0.5,
276 and 0.1 in populations with 0%, 50%, and 99% selfing, with separate simulations for DFE1,
277 DFE2, and DFE3. The exact parameters used in each simulation can be found in Supplementary
278 Table 7. Parameters were chosen so that the predicted F_{ST} of the entire metapopulation ($F_{ST} =$
279 $\frac{T_T - T_S}{T_T}$) would cover a range of values (from 0.02 to 0.76) matching previously estimated values
280 for *C. elegans* populations in the literature (from 0.15 to 0.43; Cutter 2006). Neutral simulations
281 with identical genome structure and migration parameters were used to verify the joint effects of
282 population structure and selfing on neutral nucleotide diversity and F_{ST}, and were found to yield
283 expected results (Supplementary Table 8). The expected neutral nucleotide diversity for partially
284 selfing populations was calculated assuming that the effective size of each deme will be
285 equivalent to $N_{deme,self} = \frac{N_{deme}}{1+F}$, which was used to calculate the appropriate T_T and T_S values
286 for each evolutionary scenario. In SLiM, m represents the proportion of individuals in a deme
287 that are migrants each generation. Therefore, m still represents the probability that an allele is
288 derived from migration each generation, and $N_{deme}m$ represents the number of diploid migrants
289 per deme per generation.
290 Twenty genomes were sampled from each deme (totaling 100 genomes from the
291 metapopulation) for DFE inference. To understand the effects of uneven sampling on DFE
292 inference, two alternative sampling schemes were employed. In the first, 60 genomes were
293 sampled from one deme, while 10 genomes were drawn from the remaining four demes. In the
294 second, 35 genomes were drawn from two demes, while 10 genomes were drawn from the
295 remaining three demes.
296

297 **Calculating the SFS and the number of adaptive substitutions from simulations**

298 The full output provided by SLiM was used to generate the site frequency spectra of neutral and
299 selected mutations in exonic regions individually. The fixed class was obtained as the number of
300 substitutions that occurred after the burn-in period ($= 10N$ generations). The zero class was
301 calculated by subtracting the number of polymorphic and fixed sites from the total number of
302 sites for both neutral ($= 0.25 \times$ number of exonic sites) and selected ($= 0.75 \times$ number of
303 exonic sites) mutations respectively. Scripts to calculate the SFS are available at
304 https://github.com/JohriLab/DFESelfing/tree/main/calculateSFS.

305

306 The true fraction of beneficial substitutions (α) in simulations was obtained as follows:

307

308 $$\alpha = \frac{number\ of\ substitutions\ with\ 2N_e s_a > 5}{number\ of\ substitutions\ at\ selected\ sites} \quad (5)$$

309

310

311 Only substitutions that occurred after the burn-in with $2N_e s_a > 5$ were included when
312 calculating the true value of α in order to match the assumptions of GRAPES.

313

314 **DFE-alpha**

315 *Est_dfe* (Keightley and Eyre-Walker 2007) was employed to infer the DFE of deleterious
316 mutations. We fitted a two-epoch model, with starting values of $t2$ (time of change), β, and $\overline{s_d}$
317 equal to 50, 0.5, and -0.01 respectively. $N2$ (current size) and $t2$ were set to be variable. In the
318 absence of positive selection, the unfolded SFS was used as input, and the fold setting was set to
319 0. In the presence of beneficial mutations, the folded SFS was used in addition to the unfolded
320 SFS because DFE-alpha has been shown to be sensitive to high frequency beneficial alleles in
321 the SFS (Tataru et al. 2017). DFE-alpha provides the most likely estimate of the expected value
322 of $\overline{s_d}$, the shape parameter (β) of the gamma distribution, and a weighted effective population
323 size (N_w). These parameters were used to obtain the proportion of mutations (f_0, f_1, f_2, f_3) in the
324 four classes- effectively neutral ($0 \leq 2N_w s_d < 1$), weakly deleterious ($1 \leq 2N_w s_d < 10$),
325 moderately deleterious ($10 \leq 2N_w s_d < 100$), and strongly deleterious ($100 \leq 2N_w s_d$),
326 respectively.

327

328 **GRAPES**

329 The program GRAPES (Eyre-Walker and Keightley 2009; Galtier 2016), Version 1.1.1
330 (https://github.com/BioPP/grapes/releases/tag/v1.1.1) was used to infer the full DFE using
331 simulations with and without positive selection. GRAPES provides the maximum likelihood
332 estimate of the shape parameter (β) and the expected population-scaled mean strength of
333 selection in terms of $2N_e\overline{s_d}$, in order to characterize the gamma distribution representing the
334 deleterious DFE. GRAPES also infers the parameters of the beneficial DFE, including the
335 proportion of substitutions that are beneficial mutations (α) and the mean population-scaled
336 strength of selection favoring new advantageous mutations $2N_e\overline{s_a}$, assuming that advantageous
337 selection coefficients are exponentially distributed. The unfolded SFS was provided as input for
338 both scenarios (with and without positive selection). In simulations without positive selection,
339 the default parameters for the GammaZero model were used (*i.e.*, parameters of the beneficial
340 DFE were not inferred). In the presence of positive selection, the estimated beneficial DFE was
341 assumed to follow an exponential distribution (*i.e.*, the GammaExpo model was used). As
342 GRAPES can use either the folded or the unfolded SFS to provide estimates of the beneficial
343 DFE, we performed inference using the unfolded and folded SFS separately to compare the
344 results of both estimation methods. These parameters were accordingly used to obtain the values
345 f_0, f_1, f_2, f_3, representing the classes of the deleterious DFE as described above.

346

347 **Comparison of the expected and estimated DFE when mutations are semidominant**

348 In a partially selfing population, diffusion theory provides the following mean ($M_{\Delta q}$) and
349 variance ($V_{\Delta q}$) of the change in allele frequency (q) assuming that the change (Δq) in allele
350 frequency is small (Caballero et al. 1991):

351

352 $$M_{\Delta q} = q(1-q)s[h + q(1-2h) + F(1-q-h+2qh)] \quad (6)$$

353

354

355 $$V_{\Delta q} = \frac{q(1-q)}{2N_{self}} = \frac{q(1-q)(1+F)}{2N} \quad (7)$$

356

For completely additive mutations ($h = 0.5$), the mean reduces to:

$$M_{\Delta q} = \frac{q(1-q)s(1+F)}{2} \tag{8}$$

In a panmictic population (of size N) with random mating, the mean and variance of change in allele frequency (assuming semidominance) is given by:

$$M_{\Delta q} = \frac{q(1-q)s}{2} \tag{9}$$

$$V_{\Delta q} = \frac{q(1-q)}{2N} \tag{10}$$

Thus, by comparing the above set of equations, a selfing population of size N experiences more genetic drift than a randomly mating population of the same size (Caballero and Hill 1992). However, the mean change in allele frequency in selfing populations is also larger, by the same factor, $(1 + F)$, and thus the fixation probability of mutations remains the same in a selfing *vs*. a randomly mating population (Charlesworth and Charlesworth 1987; Caballero and Hill 1992; Charlesworth 1992). Thus, for the case of additive mutations and not taking selection at linked sites into account, the expected DFE would be determined by $2N_{self}s_d(1+F) = 2\frac{N}{(1+F)}s_d(1+F) = 2Ns_d$. To account for the relative decrease in population size due to BGS or selective sweeps, the simulated DFE was adjusted and presented as $2NBs_d$, where B was calculated using equation 1.

In the case of the estimated DFE, because DFE-alpha only infers a relative increase or decrease in population size ($\frac{N_2}{N_1}$), these estimates of demographic parameters should not be

384 affected by selfing rates (where the factor $1 + F$ will cancel out). We thus present our inferred
385 DFE as $2N_w s_d$.
386
387 **Comparison of the expected and estimated DFE when mutations are not semidominant**
388 When mutations were not additive, our expected DFE was parameterized by $2N_{self} s_d h_{self}$,
389 where
390
391 $$N_{self} = \frac{N}{1 + F} \quad (11)$$
392
393
394 and
395 $$h_{self} = h + q(1 - 2h) + F(1 - q - h + 2qh) \quad (12)$$
396
397
398 Assuming that $q << 1$, this equation simplifies to:
399
400 $$h_{self} \sim h + F(1 - h) \quad (13)$$
401
402 Note that this approximation is less accurate when selection is weak ($2Ns_d \sim 1$) and thus might
403 not be as accurate for the DFE comprising predominantly weakly deleterious mutations. The
404 estimated DFE (using DFE-alpha and GRAPES) was parameterized by $2N_w s_d h$ where $h = 0.5$
405 is assumed by both the programs.
406
407 **Calculation of summary statistics from simulated data**
408 In order to quantify the effects of HRI, the skew in the SFS towards rare alleles was measured
409 using the summary statistic $\Delta\theta_w = 1 - (\frac{\pi}{\theta_w})$, which has been demonstrated to be less sensitive
410 than Tajima's *D* to the number of SNPs used in the calculation (Becher et al. 2020). Here, π is
411 the nucleotide diversity (Nei and Tajima 1981) and θ_w denotes Watterson's θ (Watterson 1975).
412 In addition, the number of singletons ($sing$) and haplotype diversity (hapdiv; Ferrer-Admetlla et
413 al. 2014) were calculated. To summarize linkage disequilibrium, r^2 (Hill and Robertson 1968),

414 D, and D' (Lewontin 1964) were calculated using minor alleles for pairs of polymorphisms at
415 frequencies between 1% and 5%. Only low-frequency SNPs were used for D' calculations to
416 correct for the allele frequency dependence of linkage disequilibrium statistics (Lewontin 1988).
417 All summary statistics were calculated separately for neutral and selected polymorphisms in
418 exonic regions in nonoverlapping 5000 bp windows using *pylibseq* v. 0.2.3 (Thornton 2003).
419

420 **Estimation of the extent of background selection in highly selfing species**

421 To estimate the levels of background selection (B) in highly selfing species, we collated previous
422 estimates for the mutation (μ) and recombination rate (r) per site/generation, the fraction of the
423 genome that is coding (f_{coding}), and selfing rates for highly selfing species that have publicly
424 available genome assemblies. In species where the mutation rate had not been measured, we used
425 closely-related species to approximate the rate (see Supplementary Table 9 for details). Estimates
426 of B were obtained for each species using $B = \exp\left(-\frac{U_d}{R_{self}}\right)$ (Nordborg *et. al* 1996), where U_d
427 (the genome-wide mutation rate for a diploid individual) was estimated as $U_d =$
428 $2 \times L \times f_{coding} * \mu \times 0.7$, where L is the total length of the genome, 0.7 represents the fraction
429 of nonsynonymous sites, and $R_{self} = R \times F$, where R was estimated as $R = r \times L$.
430
431

432 **RESULTS**

433 **Inference of the DFE of new deleterious mutations in self-fertilizing populations**

434 We simulated a single *C. elegans*-like population with varying rates of selfing – 0, 50, 80, 90, 95,
435 and 99% and three different DFEs (following a gamma distribution; parameters specified in
436 Table 1) skewed towards mildly (DFE1), moderately (DFE2), and strongly deleterious (DFE3)
437 classes respectively. Here we assumed that all new mutations were semidominant. We used
438 DFE-alpha and GRAPES to infer the parameters of the deleterious DFE, specified to be gamma-
439 distributed. As expected, when there is no selfing, inference was accurate (Figure1,
440 Supplementary Figure 1, Supplementary Table 1, Supplementary Table 2). As the selfing rate
441 increased ($\geq 90\%$), the estimated DFE (*i.e.*, distribution of population-scaled selection
442 coefficients) was skewed strongly towards the class of mildly deleterious mutations (Figure 1),
443 when compared to the simulated DFE, with a particularly substantial skew in the most highly

selfing population, consistent with Gilbert *et al.* (2022). While the inferred $2N\bar{s}_d$ was highly underestimated (Supplementary Figure 1)., the β parameter of the gamma distribution was also mis-inferred as the selfing rate increased, with the inferred β becoming 2-3× smaller than the simulated value at 99% selfing (Supplementary Table 2). The mean population-scaled selection coefficients remained slightly biased even when selfing rates were as low as 80% (*e.g.* for DFE2; Figure 1, Supplementary Table 2).

Because BGS will lead to a decrease in the effective population size, we hypothesized that the true population-scaled selection coefficients in our simulated populations are likely to be smaller than those simulated (*i.e.*, $2Ns_d$). To account for the reduction in the efficacy of purifying selection due to BGS, we corrected the simulated DFE with the relative rate of coalescence (B) with and without BGS observed in the simulated population. Note that this adjusted DFE accounts for the relative decrease in population size due to linked effects of selection only, not due to selfing (see details in Methods). While the inferred DFE matches the corrected expected DFE substantially well for moderate levels of selfing (Figure 1; Supplementary Figure 1), the DFE accounting for BGS is somewhat inaccurate at high selfing levels (Figure 1C; Supplementary Figure 1).

We next estimated the distribution of selection coefficients by accounting for the decrease in the effective population size due to BGS. Consistent with the observation above, the distribution of selection coefficients is accurately inferred when selfing rates are below 0.8 (Supplementary Figure 2) but remains inaccurate at extremely high selfing rates (0.95-0.99; Figure 1D; Supplementary Figure 2). That is, the inferred DFE (in terms of the selection coefficients) tends to have both more strongly deleterious mutations and nearly neutral mutations and results in a more platykurtic than the simulated distribution (Figure 1D; Supplementary Figure 2). This suggests that a simple rescaling of the effective population size can correct for the misinference when selfing rates are low/moderate (when the population is likely experiencing classical BGS) but not when rates are high (when the population is likely in the interference selection regime). This effect is especially substantial when a higher proportion of the DFE is composed of weakly and moderately deleterious mutations (*e.g.* DFE1 and DFE2), which are more likely to experience HRI(Figure 1D; Supplementary Figure 2).

The simulated DFEs were accurately estimated from single-locus simulations with no linkage even in highly selfing populations (Supplementary Figure 3), despite a significant reduction in the total number of segregating sites at high selfing (Supplementary Table 3). Concordantly, the observed SFSs at selected and neutral sites were highly similar across different selfing levels, confirming that selfing does not drastically influence the proportions of allele frequencies in a population without linkage (Supplementary Figure 4), assuming that deleterious mutations are additive. Importantly, as high rates of selfing increase the levels of homozygosity, the site frequency spectrum (SFS) obtained from a random sample of diploid *individuals* deviated starkly from one obtained by a random sampling of *genomes* (an example shown in Supplementary Figure 5A). The inferred DFEs were very similar when we sampled individuals *vs*. genomes (Supplementary Figure 5B) and thus all results that follow were obtained by sampling genomes.

The effects of linkage on DFE inference in regions of low recombination

HRI is more likely in genomic regions of low recombination and may similarly bias DFE inference. With decreasing rates of recombination, the extent of mis-inference of the DFE increased (Figure 2A, B). As before, while the DFE accounting for BGS explained the estimated DFEs quite well for higher recombination rates, at very low recombination rates, it did not match the inferred DFE (Figure 2C). The inferred distribution of selection coefficients tended to overestimate the proportion of strongly deleterious and nearly neutral mutations and underestimated the proportion of mildly deleterious mutations (Figure 2D; Supplementary Figure 6). As with high selfing, the estimated distribution of selection coefficients at low recombination was observed to be more platykurtic than that simulated, and mis-inference was much stronger at the lowest recombination rates, even for the most strongly deleterious DFE (Supplementary Figure 7). This again reflects the fact that a simple rescaling effect of BGS (*i.e*., the decrease in the rate of coalescence) is unlikely to explain mis-inference observed in regions of very low recombination due to HRI. Note that the relative decrease in nucleotide diversity ($B = \frac{\pi}{\pi_0}$) due to background selection, measured in simulations of regions with low recombination ($B \sim 0.05 - 0.92$) captured the range of B values measured in the simulations with selfing and linkage ($B \sim 0.08 - 0.95$).

505 **Parameters that modulate the extent of HRI**

506 Population-scaled parameters such as NU, NR, and Ns all influence the extent of interference
507 between selected alleles (Good et al. 2014). When the ratio of mutation to recombination is
508 sufficiently high and the strength of purifying selection is low, interference between selected
509 mutations becomes sufficiently common to cause them to diverge from the predictions of single
510 site models. To investigate whether these parameters similarly determine the extent of DFE
511 misinference, we explored how $\frac{U_d}{R}$ and $\frac{U_d}{R_{self}}$ relates to the degree of misinference of s and β
512 (Figure 3A) in the simulations with low recombination and selfing respectively, where U_d is the
513 genome-wide deleterious mutation rate, R is the map length of the simulated chromosome
514 (assuming that recombination scales linearly with distance), and $R_{self} = R \times (1 - F)$, where
515 $F = P_{self}/(2 - P_{self})$ (Nordborg 2000). We found that error is relatively small at low $\frac{U_d}{R}$ ratios,
516 but when $\frac{U_d}{R}$ is greater than ~5, error began to rapidly increase, with the largest error present in
517 the DFE with predominantly weakly deleterious mutations. Interestingly, we found that the
518 extent of BGS, as measured by B, was by itself a good predictor of the extent of this error,
519 finding that as B decreased, the error in both $\bar{s}_d$ and β increased, and that the relationship
520 between B and error was very similar in the low recombination and selfing simulations (Figure
521 3B). Although this might help determine when inference could be biased, it is difficult to obtain
522 true values of B from empirical data especially if the genome-wide rate of recombination is low.
523

524 **The quantification of HRI using summary statistics**

525 Much theoretical and computational work on HRI has suggested that the decrease in the efficacy
526 of selection results in a decrease in the nucleotide diversity at selected and linked neutral sites as
527 well as an increase in divergence at selected sites due to the increased fixation of deleterious
528 mutations (Comeron et al. 1999; McVean and Charlesworth 2000). Moreover, the site frequency
529 spectrum for selected and neutral sites is expected to be skewed towards low-frequency variants
530 as the strength of BGS and HRI increases (mimicking the genealogy of an expanding population;
531 Zeng and Charlesworth 2011; Walczak *et al.* 2012; Nicolaisen and Desai 2013; Good *et al.*
532 2014), and the nucleotide diversity and site frequency spectrum of selected mutations are
533 expected to become more similar to those of neutral mutations (Comeron and Kreitman 2002;
534 Kaiser and Charlesworth 2009; O'Fallon et al. 2010; Seger et al. 2010; Nicolaisen and Desai

535 2013). Because interference results in a gene genealogy with longer external branches than
536 expected under a standard neutral coalescent (Walczak *et al.* 2012; Nicolaisen and Desai 2013),
537 and consistent with a skew towards low-frequency alleles, new mutations are more likely to
538 occur on separate branches of the genealogy, generating negative LD. Thus signed measures of
539 linkage disequilibrium between selected mutations and nearby neutral sequences become more
540 negative as HRI becomes stronger (Hill and Robertson 1966; McVean and Charlesworth 2000;
541 Comeron and Kreitman 2002; Garcia and Lohmueller 2021). In addition, in populations with
542 pervasive HRI, the SFS has been observed to show non-monotonic behavior at high frequencies,
543 resulting in a U-shape, which deviates from the predictions of the classical BGS theory (Seger et
544 al. 2010; Neher and Hallatschek 2013; Good et al. 2014; Zeng and Corcoran 2015; Cvijović et al.
545 2018).

546 In our simulations, the SFSs of neutral and selected sites shifted towards lower frequency
547 mutations and became more similar at 90% selfing and above (Figure 4A, Supplementary
548 Figures 8A & 9A), which is consistent with the extent of DFE mis-inference and with previously
549 simulated results in highly selfing populations (Charlesworth *et al.* 1993). In addition, the SFS at
550 high frequency alleles showed non-monotonic (U-shaped) behavior (Figure 4B, Supplementary
551 Figures 8B & 9B). Note that the SFS of neutral sites at 0% selfing was very similar to the
552 unlinked neutral SFS (Supplementary Figure 4), consistent with high B values. Trends in $\Delta\theta_w$, a
553 measure of the skewness of the SFS (with positive values indicating a relative increase in rare
554 alleles), were concordant with the patterns in the SFSs, with $\Delta\theta_w$ values for neutral and selected
555 sites sharply increasing and converging towards each other at 90% selfing and above (Figure 5).
556 Values of $\Delta\theta_w$ at neutral sites nearly converge with values at selected sites at 99% selfing,
557 reflecting the reduced efficacy of selection and almost complete linkage. Similar patterns were
558 observed in the simulations with low recombination, with values of $\Delta\theta_w$ increasing sharply and
559 converging at low recombination rates (Supplementary Figure 10).

560 For selfing rates between 80% and 95%, D' tended to become closer to 0 at both selected
561 and neutral sites (Figure 4B). This is similar to an effect observed in simulations by Kamran-
562 Disfani and Agarwal (2014), where partially selfing populations with intermediate selfing rates
563 showed increases in linkage disequilibria. This phenomenon is expected at higher selfing levels
564 if the efficacy of selection is not overwhelmed by HRI, because of correlations in homozygosity
565 at different loci across the genome (Roze and Lenormand 2005). In contrast, D' remained

566 relatively flat for simulations with intermediate recombination rates (Supplementary Figure 10).
567 At 99% selfing and at very low recombination rates, D' values became considerably more
568 negative for selected and neutral sites, consistent with a population experiencing pervasive HRI.
569 To understand how common summary statistics relate to errors in DFE misinference, we
570 investigated how nucleotide diversity (π), θ_H (Fay and Wu 2000) , singleton density ($sing$),
571 haplotype diversity ($hapdiv$), and two LD statistics (r^2 and D) compared with the errors ($\varepsilon =$
572 $\left|\frac{inferred-true}{true}\right|$) of the inferred parameters of the DFE ($2N\bar{s}_d$ and β). In general, we found that
573 SFS-based statistics as well as $hapdiv$ at nonsynonymous sites divided by synonymous sites
574 positively correlated with error in DFE inference (Supplementary Figure 11). On the other hand,
575 LD-based statistics were not found to be particularly informative of the extent of misinference.
576 However, we found that the values for each statistic vary depending on the DFE, suggesting that
577 the value of any one summary statistic cannot be used to determine if pervasive interference is
578 occurring in a population. Moreover, other factors such as assumptions about the fitness model,
579 epistasis, and non-equilibrium demography will also affect the LD statistics (discussed in Johri
580 and Charlesworth 2024), masking the effect of HRI.
581
582 **Simulation rescaling alters the effects of HRI**
583 Due to computational time constraints, it was necessary to rescale the parameters $N\mu$, Nr, and
584 Ns for most simulations in this study by lowering N and increasing μ, r, and s by the rescaling
585 factor $Q = 100$. While equivalent equilibria are expected according to diffusion theory if the
586 population-scaled parameters are held constant (Hill and Robertson 1966; Crow and Kimura, M.
587 1970; Ewens 1979; Li 1987), it has previously been observed that high levels of rescaling can
588 increase the effects of HRI (Comeron and Kreitman 2002). To understand the effects of rescaling
589 at high selfing rates, we once again simulated *C. elegans*-like populations with 500 genes and
590 selfing rates of 95% and 99% and the three deleterious DFEs, with $Q = 50$, 20, and 10, though
591 at $Q = 10$ only a limited number of simulations were able to be completed within a reasonable
592 timeframe. We find that as Q decreases from the original value of 100, the effects of background
593 selection and HRI decrease (Supplementary Figure 12). While the extent of DFE mis-inference
594 decreases as Q is lowered, the DFEs estimated at low Q values and 99% selfing were still mis-
595 inferred, especially the DFEs with more weakly and moderately deleterious mutations. The SFS
596 at higher selfing rates and low Q was still skewed towards lower frequency mutations and U-

shaped, though less than at high Q (Supplementary Figures 13-14). Thus, it is likely that fully unscaled simulations ($Q = 1$) would have even less HRI effects, especially for the strongly deleterious DFE, though it is not unrealistic to expect significant effects of BGS and interference between selected mutations based on the trends observed here. For instance, we observed substantially more mis-inference of the DFE when larger genomic regions were simulated (Supplementary Figure 15), suggesting that full length chromosomes simulated at $Q = 1$ will likely have more pervasive linked effects of selection. Indeed, Gilbert *et al.* (2022) conducted unscaled simulations of the entire genome, including all full-length chromosomes and a reduced recombination rate in chromosome centers, with *C. elegans*-like parameters and found a drastic decrease in population size due to background selection (see figure 4 of Gilbert *et al.*), so exploration of our scaled simulations with pervasive HRI is still relevant to highly selfing populations.

Extent of mis-inference does not depend on coding density

The effects of HRI are expected to increase when there is a higher density of selected sites, and gene density varies along the *C. elegans* chromosomes, with higher gene densities found in the chromosome centers than in the chromosome arms (*C. elegans* Sequencing Consortium 1998). Moreover, the rate of recombination in *C. elegans* is higher in the gene-poor chromosome arms than in the gene-rich cores (Rockman and Kruglyak 2009). We however observed no obvious changes in the extent of DFE inference when coding density was 2× and 6× higher (Supplementary Figure 16), although local gene densities could increase more than we simulated.

The impact of dominance on DFE inference

Dominance coefficients of new deleterious mutations vary considerably and are partially recessive on average, with strongly deleterious mutations tending to be highly recessive (Simmons and Crow 1977; Agrawal and Whitlock 2011; Manna et al. 2011). Most DFE inference methods assume that new mutations are semidominant and thus provide estimates of the joint distribution of the selection and dominance coefficients, "$s_d h$". A recent study by Wade *et al*. (2023) suggests that, if there are recessive lethal mutations, current DFE inference approaches can lead to underestimating the true proportion of strongly deleterious mutations, as

628 more strongly deleterious mutations are likely to persist in the population if they are recessive.
629 Furthermore, since selfing increases the levels of homozygosity in the genome, the efficacy of
630 selection against large effect and highly recessive deleterious mutations is expected to be greater
631 (Charlesworth and Charlesworth 1998), leading to more efficient purging of deleterious
632 mutations. Thus, with higher rates of selfing one might instead expect to observe a decrease in
633 the allele frequencies of mildly and moderately deleterious mutations, leading to the false
634 inference of the presence of more strongly deleterious mutations in the population.

635 At 0% selfing, as new deleterious mutations became more recessive (especially when
636 $h = 0.1$), the inferred distribution of the population-scaled product of selection and dominance
637 coefficients slightly underestimated the proportion of strongly deleterious mutations
638 (Supplementary Figure 17, Supplementary Table 5), consistent with Wade *et al.* (2023).
639 Additionally, the frequency of the nearly neutral class of mutations was underestimated in all
640 three DFEs. In contrast, when more dominant mutations were simulated, DFE inference resulted
641 in mis-inference towards both weakly and strongly deleterious mutations, though this effect was
642 fairly small. Mis-inference was stronger when the true DFE was skewed towards mildly
643 deleterious mutations, as these mutations are more likely to be present as homozygotes in the
644 population.

645 As selfing increases homozygosity, the dominance coefficient is a less important factor
646 for the efficacy of selection in highly selfing populations (Caballero and Hill 1992; Charlesworth
647 1992). Thus, at 50% selfing, the DFE was inferred more accurately (Supplementary Figure 18,
648 Supplementary Table 5) and the dominance coefficient played a negligible role in DFE inference
649 when the selfing rate was 99% (Supplementary Figure 17). Thus, at high rates of selfing, HRI
650 effects were found to be primarily responsible for DFE mis-inference.

651 Increased purging of recessive deleterious mutations has been hypothesized to reduce
652 their average allele frequencies, leading to DFE mis-inference (Arunkumar et al. 2015; Gilbert et
653 al. 2022). However, observable effects of purging are likely to occur only when mutations are
654 highly recessive (Nei 1968) and strongly deleterious (Glémin 2003). Concordantly, we observed
655 that the distribution of allele frequencies of partially recessive ($h = 0.25$) mutations at
656 intermediate selfing levels was the same as those of semidominant mutations (Supplementary
657 Figure 19), suggesting that increased purging of recessive deleterious alleles did not have a
658 substantial effect on the average allele frequencies in a population sample at equilibrium.

659

660 **Inference of the full DFE of new deleterious and beneficial mutations**

661 Both BGS and HRI lead to a decrease in the efficacy of selection at linked selected sites, thus
662 reducing the probability of fixation of beneficial mutations while increasing the probability of
663 fixation of deleterious mutations (Charlesworth 1992; Kamran-Disfani and Agrawal 2014). It is
664 therefore likely that the proportion of fixed mutations at selected sites that are beneficial (α) is
665 mis-estimated when effective recombination rates are low. We conducted simulations with
666 selfing, where 0.1% and 1% of new mutations in exons were beneficial, following an exponential
667 distribution with $2N\overline{s_a} = 200$. Due to recurrent selective sweeps in this scenario as well as BGS,
668 there is likely to be a substantial decrease in effective population size experienced by selected
669 alleles (and thus a reduced $2N_e s_d$). Concordantly, the population-scaled selection coefficients of
670 deleterious mutations were estimated to be heavily skewed towards mildly deleterious mutations
671 even at much lower selfing rates (Supplementary Figures 20 and 21). When 0.1% of new exonic
672 mutations were beneficial, and selfing rates were above 90%, the estimated distributions of
673 selection coefficients were biased towards higher proportions of nearly neutral and strongly
674 deleterious mutations, as observed previously (Figure 6A). However, the inferred distributions
675 were skewed more towards strongly deleterious mutations compared to the simulations with only
676 deleterious mutations. Mis-inference of selection coefficients was particularly substantial when
677 the simulated deleterious DFE consisted of more weakly deleterious mutations, suggesting that
678 HRI effects might cause mis-inference even at moderate levels of selfing if beneficial mutations
679 are reasonably prevalent. The selected SFSs resembled the neutral SFSs in simulations with DFE
680 mis-inference (Supplementary Figure 22). With a high rate of beneficial mutations entering the
681 population, hitchhiking can reduce the efficacy of selection on weakly deleterious alleles
682 (Campos and Charlesworth 2019), leading to the mis-inference of the DFE for the more weakly
683 deleterious DFEs. In addition, the failure of DFE inference programs to fully correct for the
684 presence of mildly beneficial alleles in the SFS could also have contributed to the observed mis-
685 inference (Tataru et al. 2017).

686 As the folded SFS might provide better estimates of the deleterious DFE when beneficial
687 mutations are segregating at high frequencies (Keightley and Eyre-Walker 2007; Eyre-Walker
688 and Keightley 2009), we also tested the inference using the folded SFS. Overall, the deleterious
689 DFE inferred by GRAPES was comparable when using the unfolded and folded SFS

690 (Supplementary Figures 23A & 24A). However, the DFEs estimated by DFE-alpha using the
691 folded SFS were biased towards weakly deleterious mutations even with no selfing, with much
692 larger uncertainty in the estimated DFE at high selfing levels, especially when 1% of all new
693 selected mutations were beneficial. This indicates that folding the SFS is inadequate to correct
694 for the mis-inference of the deleterious DFE when the rate of new beneficial mutations is
695 extremely high.

696 As expected, the true fraction of beneficial substitutions (α) decreased as the selfing rate
697 increased (Figure 6B, Supplementary Figure 20B). Changes in this parameter were driven by
698 both increases in the number of deleterious substitutions ($\sim 2 - 4 \times$ higher at 99% selfing
699 relative to 0% selfing) as well as the decreases in the number of beneficial substitutions ($\sim 3 \times$
700 lower at 99% selfing relative to 0% selfing; Supplementary Table 6). In simulations with both
701 0.1% beneficial mutations and 1% beneficial mutations, α tended to be overestimated for the
702 weakly deleterious DFE at all selfing levels, with mis-inference increasing steadily as the selfing
703 rate increased. For the moderately and strongly deleterious DFEs, α was only overestimated at
704 high selfing levels, with the strongly deleterious DFE corresponding with the most accurate
705 inference of α. This is consistent with the expectation that a decrease in the efficacy of selection
706 will increase the fixation of weakly deleterious alleles, which will be misinterpreted as beneficial
707 fixations by GRAPES, leading to an overestimation of α at high selfing levels. Very similar
708 trends were observed when the folded SFS was used to estimate α (Supplementary Figures 23B
709 & 24B). Overall, at high selfing levels, α values were substantially overestimated by GRAPES.
710

711 **Effects of population structure and sampling on the accuracy of inference**

712 While selfing organisms tend to have highly structured populations, DFE inference in the context
713 of population structure has been largely unexplored, though the effects of cryptic structure
714 (without migration) were tested in Kim *et al.* (2017). Here, we simulated an island model, with
715 five demes that exchanged migrants at a total rate m each generation. Multiple values of m were
716 used to vary the degree of isolation between demes in this model, and the number of individuals
717 in each deme (N_{deme}) was varied so that the effective size of the metapopulation (N_{meta}) was
718 equivalent to 500,000 individuals (Supplementary Table 7). Under strict neutrality and while
719 selfing was taken into account (see Methods), the neutral nucleotide diversity of the entire

720 metapopulation ($2T_T\mu$), of individual subpopulations ($2T_S\mu$), and F_{ST} was equal to theoretical
721 expectations (equations 2-4, Supplementary Table 8).
722 Population structure by itself did not result in mis-inference of the DFE when the rate of
723 migration was sufficiently high (*i.e.*, $N_{deme}m = 2, 1,$ and 0.5). High selfing rates with
724 population structure again led to inferring a DFE (as population-scaled selection coefficients)
725 skewed almost entirely towards mildly deleterious mutations, thus producing a very similar
726 extent of mis-inference as that observed in a panmictic population (Supplementary Figure 25 A,
727 B, and C, respectively). However, at low rates of migration between demes ($N_{deme}m$ of 0.1), the
728 DFE was mis-inferred even at 0% selfing, with a bias towards inferring a lower efficacy of
729 selection than the simulated DFE (Figure 7; Supplementary Figure 25D). This was largely
730 because the relative increase in intermediate frequency alleles due to population structure as
731 opposed to panmixia (Supplementary Figures 26-27) was falsely inferred as a bottleneck (mean
732 fold change = 0.45-0.50; similar to Chikhi *et al.* 2010) by DFE-alpha, leading to incorrect
733 estimates of the DFE. As expected, these distortions of intermediate frequency alleles in the SFS
734 caused by population structure were observed to increase at higher selfing levels and at lower
735 migration rates, with particularly large deviations from panmixia observed at $N_{deme}m = 0.1$.
736 Empirical studies that draw from worldwide population samples may knowingly or
737 unknowingly sample unevenly from structured populations when performing DFE inference. To
738 investigate if this has unintended consequences on DFE inference, we repeated our experiments
739 with population structure, altering our sampling strategy to primarily draw genomes from one
740 deme (60%) or two demes (35% from each), with the remaining demes contributing only 10% of
741 the sampled genomes each. As expected, the site frequency spectra from both unevenly sampled
742 populations were observed to be even more distorted at intermediate frequencies than the evenly
743 sampled populations with low migration rates (Supplementary Figures 28-31). For the sampling
744 strategy primarily drawing from one deme, some DFE mis-inference towards nearly neutral and
745 strongly deleterious mutations was observed at 0% and 50% selfing even for $N_{deme}m = 1$ and
746 more strongly at $N_{deme}m = 0.5$, and this effect was stronger at the DFE with predominantly
747 weakly deleterious mutations (Supplementary Figure 32). This effect was also observed for the
748 sampling strategy primarily drawing from two demes, but to a lesser extent (Supplementary
749 Figure 33). At the lowest migration rate, the inferred DFEs for both uneven sampling cases were
750 substantially less deleterious at 0% and 50% selfing than for even sampling, particularly for the

751 DFE with predominantly weakly deleterious mutations (Figure 7). At higher selfing levels, the
752 inferred DFEs for all sampling schemes falsely inferred a larger proportion of weakly deleterious
753 mutations than predicted by the DFE corrected for BGS (Figure 7), likely due to a combination
754 of HRI and uneven sampling. The BGS-corrected DFE was unable to correct for the mis-
755 inference of the DFE for all selfing levels at the lowest migration rate, reflecting the fact that
756 DFE mis-inference is likely driven by changes in the SFS caused by population structure rather
757 than changes in the level of BGS.
758 Overall, these results indicate both DFE inference approaches are fairly robust to
759 population structure in an island model, even with uneven sampling, until the populations
760 become extremely isolated from each other, or individuals are mostly drawn from one deme,
761 especially when the true DFE has a significant proportion of mildly deleterious mutations.
762 Additionally, both low rates of migration and highly uneven sampling result in the inference of a
763 DFE even more skewed towards weakly deleterious mutations than simulated. Testing DFE
764 inference with more models of population structure and additional sampling strategies might be
765 necessary to interpret empirically estimated DFEs from natural populations.
766
767
768 **DISCUSSION**
769 Inference of the distribution of fitness effects (DFE) of new mutations is a critical step in
770 understanding the forces that shape genetic variation in a population. Population genetic methods
771 to infer the DFE that account for nonequilibrium demography usually assume independent
772 segregation of putatively neutral and selected sites (Eyre-Walker and Keightley 2007; Keightley
773 and Eyre-Walker 2007; Galtier 2016; Tataru et al. 2017). However, organisms that have little/ no
774 recombination, for instance, those that undergo high rates of selfing or asexual reproduction, are
775 likely to violate this assumption. A major consequence of strong linkage is the increase in HRI
776 effects that lower the efficacy of selection. When the regime of classical BGS and sweeps is
777 predominant, inferred population-scaled selection coefficients are biased, but accounting for the
778 relative decrease in the rate of coalescence can provide reasonably accurate estimates of the
779 selection coefficients. However, when interference between selected alleles is pervasive, the
780 estimation of the distribution of selection coefficients is also severely mis-inferred. We also find
781 that while purging of partially recessive deleterious mutations does not lead to mis-inference, the

presence of cryptic population structure where there is a low rate of migration between subpopulations and/or sampling from predominantly one subpopulation leads to inferring a DFE (in terms of the population-scaled coefficients) skewed towards effectively neutral/mildly deleterious class of mutations. Moreover, the proportion of beneficial substitutions (α) is substantially overestimated in highly selfing species, suggesting caution when performing inference in species or genomic regions with little/no recombination.

Why is the DFE estimated from *C. elegans* populations not skewed towards mildly deleterious mutations?

While our study suggests that DFE inference in highly selfing species should yield population-scaled selection coefficients skewed towards weakly/moderately deleterious mutations, surprisingly, the previous empirical estimate of the *C. elegans* DFE using DFE-alpha is heavily skewed towards the class of strongly deleterious mutations ($2N_e\overline{s_d} > 10{,}000$, Gilbert *et al.* 2022). One explanation of this discrepancy is that the mean $2N_e\overline{s_d}$ of the population is even greater than 10,000. Interestingly, direct measurements of fitness-related traits in mutation accumulation lines suggest that *C. elegans* has a highly deleterious DFE, with estimates of the mean deleterious selection coefficient ranging from -0.09 to -0.46 (Vassilieva et al. 2000; Baer et al. 2005; Katju et al. 2015). Thus, using previously calculated *C. elegans* N_e ranging from 5,000 to 80,000 (Table 4 in Teterina *et al.* 2023), the expected $2NB\overline{s_d}$ would range from 900 to 72,000, consistent with this explanation. However, there are a few major caveats to these observations. (a) The experimental estimates of selection coefficients are likely biased towards more deleterious selection coefficients due to the difficulty of measuring small fitness changes in experimental lines (Davies et al. 1999; Eyre-Walker and Keightley 2007), and might not reflect fitness effects in the wild. (b) It is unclear whether previous estimates of the population sizes of *C. elegans* populations using neutral nucleotide diversity (Barrière and Félix 2005; Cutter 2006; Rockman and Kruglyak 2009; Teterina et al. 2023) are accurate due to the joint effects of selfing, HRI, and demography (c) Empirical estimates of the deleterious DFE in *C. elegans* (Gilbert *et al.* 2022) were obtained by sampling worldwide rather than from local populations, and thus other factors such as complex demographic history and population structure could play a role as well. For instance, selfing populations are likely to follow extinction-recolonization dynamics

812 (Charlesworth and Wright 2001; Ingvarsson 2002; Wright et al. 2013) and such models remain
813 understudied.
814 A second explanation for the discrepancy between the expected and observed DFE in *C.*
815 *elegans* is that the true selfing rate in wild *C. elegans* might be lower than 99%, thus reducing
816 linked effects of selection. Though selfing rate estimates from unique populations range from
817 80% to ~100% using various methods (Barrière and Félix 2005; Sivasundar and Hey 2005;
818 Teterina et al. 2023), in general, the high LD in *C. elegans* populations (haplotype blocks of 2.5
819 Mb on average; Cutter 2006) along with low frequency of males in wild specimens (Barrière and
820 Félix 2005; Richaud et al. 2018) suggest the outcrossing rate is very low in most populations. A
821 recent study using whole-genome sequencing data focusing on Hawaiian *C. elegans* estimated a
822 relatively lower selfing rate of 93%, suggesting that selfing rate can vary across populations
823 (Teterina et al. 2023). Importantly, as the samples used in Gilbert *et al.* (2022) were unevenly
824 sampled worldwide (with many samples from Hawaiian populations), variation in selfing rate
825 across populations or through time could additionally influence DFE inference results.
826 A third possibility relates to the difficulty in obtaining the SFS using highly inbred
827 strains. The SNP-calling pipeline used to obtain *C. elegans* population-genetic data converted
828 heterozygous sites into homozygous reference or alternate alleles depending on if the mutant was
829 above or below 50% (Cook et al. 2017). This method of SNP processing could lead to the
830 inference of a more deleterious DFE if the heterozygote frequency is higher at neutral sites than
831 selected sites by skewing the neutral SFS towards higher frequencies and the selected SFS
832 towards lower frequencies, though the low frequency of heterozygotes in highly selfing
833 populations makes this unlikely to be a large issue. Future studies working with inbred strains
834 should evaluate the effect of employing such SNP processing approaches on population genomic
835 inference.
836 Finally, we have only examined a population under equilibrium in the current study,
837 whereas a recent population expansion/ contraction could decrease the observed effects of
838 interference between selected alleles at multiple loci, allowing for a correct inference of selection
839 coefficients. HRI effects in non-equilibrium populations remain to be studied more thoroughly.
840 Unfortunately, as linked effects of selection will also lead to falsely inferring recent population
841 growth (Supplementary Table 1; Ewing and Jensen 2016; Schrider *et al.* 2016; Johri *et al.* 2021),
842 there is no straightforward solution to accounting for the effects of the true demography (Johri,

843 Eyre-Walker, et al. 2022). Thus performing a joint inference of demography and the DFE as
844 employed by Johri *et al.* (2020) is likely to be the most promising approach to circumvent this
845 challenge.
846
847 **How broadly do our results apply**?
848 Our results have implications for the population genetics of other highly selfing
849 organisms, many of which could fall into a parameter space where linked effects of selection are
850 pervasive. A key factor that determines the extent of HRI is the number (U_d) of new deleterious
851 mutations per diploid genome per generation, with higher values of NU_d relative to NR causing
852 more interference. Thus, the extent of HRI across species would likely differ due to differences
853 in outcrossing rates, population sizes, mutation and recombination rates, and genome architecture
854 (McVean and Charlesworth 2000; Comeron and Kreitman 2002; Kaiser and Charlesworth 2009;
855 Good et al. 2014). Our Figure 3 suggests that the extent of background selection (measured by B)
856 is a good predictor of the possible extent of HRI and that $B < 0.5$ could result in substantial
857 misinference. Interestingly, a number of highly selfing species may have reasonably low B
858 values (Table 2). In addition to *C. elegans*, a variety of species such as *C. briggsae*, *A. tauschii*,
859 *A. thaliana*, *C. bursa-pastoris*, *C. orientalis,* and *S. lycopersicon* have their lowest B value
860 estimates below 0.25, with *C. elegans, C. briggsae,* and *S. lycopersicon* also exhibiting values of
861 $U_d/R_{self} > 5$. Interestingly, *C. elegans* has been observed to have a U-shaped SFS in many
862 samples (Freund et al. 2023), consistent with HRI, though in empirical data a variety of
863 explanations such as ancestral allele misorientation, positive selection, and various demographic
864 effects could explain a U-shaped SFS (Freund et al. 2023). This could pose problems for
865 methods that infer the dominance coefficients of mutations by comparing the DFEs of closely
866 related selfing and obligate outcrossing species, such as a recent study of *Arabidopsis* (Huber et
867 al. 2018), and thus efforts to quantify the levels of HRI in highly selfing species merits additional
868 investigations. In addition to selfing organisms, pathogenic species like *Plasmodium* ($U_d = 0.25$;
869 Lynch *et al.* 2016) that have variable rates of sexual reproduction between genetically identical
870 clones (and thus experience reduced rates of recombination), seem to have nearly identical
871 neutral and selected site frequency spectra (Figure 3 in Parobek *et al.* 2016), suggesting that HRI
872 effects might play an important role in shaping variation across their genomes. We therefore also
873 expect DFE inference to be biased due to HRI in asexual organisms, mitochondrial genomes, and

the Y chromosome, all of which have low effective recombination rates (Barton and Charlesworth 1998; Charlesworth and Charlesworth 2000; Weinreich and Rand 2000). Importantly, as structural variants (Adrion et al. 2017; Abel et al. 2020) and mutations in noncoding regions (Racimo and Schraiber 2014) are a significant source of deleterious mutations accounting for the input of other mutation types is likely to increase the estimated value of U_d, making HRI more likely in populations with little/no recombination.

Considerations for inferring the DFE in highly selfing organisms

Given our observations, we here provide a few points to consider when inferring the DFE of new mutations in organisms with little/no recombination, where effects of BGS, selective sweeps, or HRI might be pervasive:

(1) The DFE of new deleterious mutations estimated using the two-step population-genetic methods is most closely explained by the distribution of $2NBs_d$, which is equivalent to $2N_{emp}(1+F)s_d$ in partially selfing populations. Here N_{emp} represents the effective population size estimated using neutral nucleotide diversity , which includes the effects of BGS and is what is usually estimated using demographic inference approaches that do not account for linked effects of selection. Thus, if there exist experimentally validated estimates of selfing rates, it is possible to accurately infer the distribution of selection coefficients in populations with moderate levels of selfing. However, in many organisms selfing rates are inferred using allele frequencies and those estimates are likely to be biased by population history and effects of selection at linked sites. Moreover, this raises the question of how one can accurately simulate an estimated DFE (in terms of population-scaled selection coefficients) when multiple linked selected sites are to be simulated, which will be especially important to determine the extent of HRI effects in populations with little/no recombination.

(2) Different models of population structure and the effects of demographic changes need to be considered to fully understand the robustness of DFE inference. For instance, it is known that local populations of selfing organisms are prone to recurrent extinction and recolonization events (Pannell and Charlesworth 1999; Ingvarsson 2002) which may bias DFE inference further. Indeed, recent field studies of *C. elegans* populations suggest that 3-10 individuals colonize a food source and quickly reproduce to census sizes of up to 10,000 individuals before

905 dispersing in search of new food sources (Barrière and Félix 2005; Richaud et al. 2018). When
906 sampling across many demes, we suggest also inferring the DFE in isolated populations to
907 minimize biases due to cryptic population structure or uneven sampling and to downsample the
908 number of genomes such that sampling is as even as possible across demes. Sampling strategies
909 such as a scattered sampling scheme may be useful in removing such bias (Wakeley 1999;
910 Städler et al. 2009), though the reduction in sample size may reduce the ability to accurately infer
911 the moderate and deleterious portions of the DFE (Kim et al. 2017).
912 (3) If possible, it could be helpful to infer the DFE in closely related non-selfing species
913 or in different populations of the same species with known differences in selfing rates. For
914 instance, *C. elegans* and *A. thaliana* populations vary in the estimated rates of selfing by ~10%,
915 and the mostly outcrossing *A. lyrata* has several populations that have evolved partial selfing
916 (Mable et al. 2005; Bomblies et al. 2010; Teterina et al. 2023). Though differences such as
917 population structure and demography need to be carefully accounted for, statistical comparisons
918 across populations/species with flexible DFE inference frameworks (Sendrowski and Bataillon
919 2024) could also be used to approximate the extent of HRI in a selfing species.
920 (4) Finally, in the cases where HRI is determined to be extensive, joint inference of
921 demography and the DFE as employed by Johri *et al.* in *D. melanogaster* (2020) and human
922 (2022) populations could be especially useful for DFE inference. They employed an approximate
923 Bayesian computation (Beaumont et al. 2002) framework combined with forward simulations to
924 jointly infer parameters of the DFE of new deleterious mutations and an arbitrary size change,
925 while accounting for the effects of selection at linked sites. While highly successful, such an
926 approach has been limited to a relatively simple demographic model of a single size change in
927 one population due to the large number of parameters required to be jointly estimated. In
928 addition, our work here indicates that simulation rescaling may have to be limited to accurately
929 capture the dynamics of Hill-Robertson interference, which will further increase the
930 computational burden of simulations. However, if computationally feasible, such an approach
931 could yield the most likely distribution of selection coefficients, especially because, the
932 distortions of the SFS from a neutral model caused by interference cannot be explained by any
933 constant N_e (see discussion in Neher 2013; Good *et al.* 2014; Melissa *et al.* 2022). Thus, until
934 theoretical models can accurately estimate the effects of HRI in organisms with little/no
935 recombination with complex DFEs, simulation-based approaches will be the most helpful in

inferring the DFE of new mutations in such populations, as well as obtaining the fixation probability of new mutations, which will be altered by HRI.

ACKNOWLEDGEMENTS

We thank Brian Charlesworth for many helpful discussions related to the project and for providing suggestions and comments that improved the manuscript. We are also thankful to Matthew Hartfield for providing helpful comments to improve the manuscript and to Matt Rockman for many helpful discussions and for pointing us to relevant resources available for *C. elegans*. We thank an anonymous reviewer and Thomas Batallion for their helpful suggestions and for improving the manuscript. The research in this study was conducted using computational resources provided by ITS Research Computing at the University of North Carolina at Chapel Hill. A.T.D. received support from NIGMS predoctoral training grant 5T32 GM067553. Research reported in this publication was supported by the National Institute of General Medical Sciences of the National Institutes of Health under award number R35GM154969 to P.J. The authors declare no conflicts of interests.

DATA AVAILABILITY

The following data are publicly available on https://github.com/JohriLab/DFESelfing: (1) Data and scripts to reproduce figures; (2) Config files used for DFE inference; (3) Simulation outputs in SLiM format; (4) templates and example scripts for launching SLiM simulations.

REFERENCES

Abel HJ, Larson DE, Regier AA, Chiang C, Das I, Kanchi KL, Layer RM, Neale BM, Salerno WJ, Reeves C, et al. 2020. Mapping and characterization of structural variation in 17,795 human genomes. Nature. 583(7814):83–89. doi:10.1038/s41586-020-2371-0.

Adrion JR, Song MJ, Schrider DR, Hahn MW, Schaack S. 2017. Genome-wide estimates of transposable element insertion and deletion rates in Drosophila melanogaster. Genome biology and evolution. 9(5):1329–1340. doi:10.1093/gbe/evx050.

Agrawal AF, Whitlock MC. 2011. Inferences about the distribution of dominance drawn from Yeast gene knockout data. Genetics. 187(2):553–566. doi:10.1534/genetics.110.124560.

Ågren JA, Wang W, Koenig D, Neuffer B, Weigel D, Wright SI. 2014. Mating system shifts and transposable element evolution in the plant genus *Capsella*. BMC Genom. 15(1):602. doi:10.1186/1471-2164-15-602.

Anderson JL, Morran LT, Phillips PC. 2010. Outcrossing and the maintenance of males within *C. elegans* populations. J Hered. 101(Suppl 1):S62–S74. doi:10.1093/jhered/esq003.

Arunkumar R, Ness RW, Wright SI, Barrett SCH. 2015. The evolution of selfing is accompanied by reduced efficacy of selection and purging of deleterious mutations. Genetics. 199(3):817–829. doi:10.1534/genetics.114.172809.

Baer CF, Shaw F, Steding C, Baumgartner M, Hawkins A, Houppert A, Mason N, Reed M, Simonelic K, Woodard W, et al. 2005. Comparative evolutionary genetics of spontaneous mutations affecting fitness in rhabditid nematodes. Proc Natl Acad Sci USA. 102(16):5785–5790. doi:10.1073/pnas.0406056102.

Bah S, van der Merwe R, Labuschagne MT. 2017. Estimation of outcrossing rates in intraspecific (*Oryza sativa*) and interspecific (*Oryza sativa* × *Oryza glaberrima*) rice under field conditions using agro-morphological markers. Euphytica. 213(4):81. doi:10.1007/s10681-017-1872-x.

Bank C, Ewing GB, Ferrer-Admettla A, Foll M, Jensen JD. 2014. Thinking too positive? Revisiting current methods of population genetic selection inference. Trends Genet. 30(12):540–546. doi:10.1016/j.tig.2014.09.010.

Barrière A, Félix M-A. 2005. High local genetic diversity and low outcrossing rate in *Caenorhabditis elegans* natural populations. Curr Biol. 15(13):1176–1184. doi:10.1016/j.cub.2005.06.022.

Barrière A, Félix M-A. 2007. Temporal dynamics and linkage disequilibrium in natural *Caenorhabditis elegans* populations. Genetics. 176(2):999–1011. doi:10.1534/genetics.106.067223.

Barton NH, Charlesworth B. 1998. Why sex and recombination? Science. 281(5385):1986–1990. doi:10.1126/science.281.5385.1986.

Beaumont MA, Zhang W, Balding DJ. 2002. Approximate Bayesian computation in population genetics. Genetics. 162(4):2025–2035. doi:10.1093/genetics/162.4.2025.

Becher H, Jackson BC, Charlesworth B. 2020. Patterns of genetic variability in genomic regions with low rates of recombination. Curr Biol. 30(1):94-100.e3. doi:10.1016/j.cub.2019.10.047.

Bomblies K, Yant L, Laitinen RA, Kim S-T, Hollister JD, Warthmann N, Fitz J, Weigel D. 2010. Local-scale patterns of genetic variability, outcrossing, and spatial structure in natural stands of *Arabidopsis thaliana*. PLoS Genet. 6(3):e1000890. doi:10.1371/journal.pgen.1000890.

1016 Burgarella C, Brémaud M-F, Von Hirschheydt G, Viader V, Ardisson M, Santoni S, Ranwez V,
1017 de Navascués M, David J, Glémin S. 2024. Mating systems and recombination landscape
1018 strongly shape genetic diversity and selection in wheat relatives. Evolution
1019 Letters.:qrae039. doi:10.1093/evlett/qrae039.
1020 *C. elegans* Sequencing Consortium. 1998. Genome sequence of the nematode *C. elegans*: a
1021 platform for investigating biology. Science. 282(5396):2012–8.
1022 doi:10.1126/science.282.5396.2012.
1023 Caballero A, Hill WG. 1992. Effects of partial inbreeding on fixation rates and variation of
1024 mutant genes. Genetics. 131(2):493–507.
1025 Caballero A, Keightley PD, Hill WG. 1991. Strategies for increasing fixation probabilities of
1026 recessive mutations. Genet Res. 58(2):129–138. doi:10.1017/S0016672300029785.
1027 Campos JL, Charlesworth B. 2019. The effects on neutral variability of recurrent selective
1028 sweeps and background selection. Genetics. 212(1):287–303.
1029 doi:10.1534/genetics.119.301951.
1030 Charlesworth B. 1992. Evolutionary rates in partially self-fertilizing species. Am Nat.
1031 140(1):126–148. doi:10.1086/285406.
1032 Charlesworth B. 1994. The effect of background selection against deleterious mutations on
1033 weakly selected, linked variants. Genet Res. 63(3):213–227.
1034 doi:10.1017/S0016672300032365.
1035 Charlesworth B, Charlesworth D. 1998. Some evolutionary consequences of deleterious
1036 mutations. Genetica. 102(0):3–19. doi:10.1023/A:1017066304739.
1037 Charlesworth B, Charlesworth D. 2000. The degeneration of Y chromosomes. Philos Trans R
1038 Soc Lond B Biol Sci. 355(1403):1563–1572.
1039 Charlesworth B, Charlesworth D. 2010. Elements of Evolutionary Genetics. Greenwoord
1040 Village, Colorado, USA: Roberts and Company. [accessed 2023 Dec 10].
1041 https://www.research.ed.ac.uk/en/publications/elements-of-evolutionary-genetics.
1042 Charlesworth B, Jensen JD. 2021. Effects of selection at linked sites on patterns of genetic
1043 variability. Annu Rev Ecol Syst. 52:177–197. doi:10.1146/annurev-ecolsys-010621-
1044 044528.
1045 Charlesworth B, Morgan MT, Charlesworth D. 1993. The effect of deleterious mutations on
1046 neutral molecular variation. Genetics. 134(4):1289–1303.
1047 doi:10.1093/genetics/134.4.1289.
1048 Charlesworth D. 2003. Effects of inbreeding on the genetic diversity of populations. Philos Trans
1049 R Soc Lond B Biol Sci. 358(1434):1051–1070. doi:10.1098/rstb.2003.1296.
1050 Charlesworth D, Charlesworth B. 1987. Inbreeding depression and its evolutionary
1051 consequences. Annu Rev Ecol Syst. 18(1):237–268.
1052 doi:10.1146/annurev.es.18.110187.001321.
1053 Charlesworth D, Wright SI. 2001. Breeding systems and genome evolution. Curr Opin Genet
1054 Dev. 11(6):685–690. doi:10.1016/s0959-437x(00)00254-9.
1055 Cheng C-Y, Krishnakumar V, Chan AP, Thibaud-Nissen F, Schobel S, Town CD. 2017.
1056 Araport11: a complete reannotation of the *Arabidopsis thaliana* reference genome. Plant
1057 J. 89(4):789–804. doi:10.1111/tpj.13415.
1058 Chikhi L, Sousa VC, Luisi P, Goossens B, Beaumont MA. 2010. The confounding effects of
1059 population structure, genetic diversity and the sampling scheme on the detection and
1060 quantification of population size changes. Genetics. 186(3):983–995.
1061 doi:10.1534/genetics.110.118661.

1062 Comeron JM, Kreitman M. 2002. Population, evolutionary and genomic consequences of
1063 interference selection. Genetics. 161(1):389–410. doi:10.1093/genetics/161.1.389.
1064 Comeron JM, Kreitman M, Aguadé M. 1999. Natural selection on synonymous sites is correlated
1065 with gene length and recombination in *Drosophila*. Genetics. 151(1):239–249.
1066 doi:10.1093/genetics/151.1.239.
1067 Cook DE, Zdraljevic S, Roberts JP, Andersen EC. 2017. CeNDR, the *Caenorhabditis elegans*
1068 natural diversity resource. Nucleic Acids Res. 45(D1):D650–D657.
1069 doi:10.1093/nar/gkw893.
1070 Crow JF, Kimura, M. 1970. An Introduction to Population Genetics Theory. New York, NY:
1071 Harper & Row.
1072 Cutter AD. 2006. Nucleotide polymorphism and linkage disequilibrium in wild populations of
1073 the partial selfer *Caenorhabditis elegans*. Genetics. 172(1):171–184.
1074 doi:10.1534/genetics.105.048207.
1075 Cvijović I, Good BH, Desai MM. 2018. The effect of strong purifying selection on genetic
1076 diversity. Genetics. 209(4):1235–1278. doi:10.1534/genetics.118.301058.
1077 Davies EK, Peters AD, Keightley PD. 1999. High frequency of cryptic deleterious mutations in
1078 *Caenorhabditis elegans*. Science. 285(5434):1748–1751.
1079 doi:10.1126/science.285.5434.1748.
1080 De Leon TB, Linscombe S, Subudhi PK. 2016. Molecular dissection of seedling salinity
1081 tolerance in rice (*Oryza sativa L.*) using a high-density GBS-based SNP linkage map.
1082 Rice. 9(1):52. doi:10.1186/s12284-016-0125-2.
1083 Denver DR, Morris K, Lynch M, Thomas WK. 2004. High mutation rate and predominance of
1084 insertions in the *Caenorhabditis elegans* nuclear genome. Nature. 430(7000):679–682.
1085 doi:10.1038/nature02697.
1086 Estes S, Phillips PC, Denver DR, Thomas WK, Lynch M. 2004. Mutation accumulation in
1087 populations of varying size: The distribution of mutational effects for fitness correlates in
1088 *Caenorhabditis elegans*. Genetics. 166(3):1269–1279. doi:10.1534/genetics.166.3.1269.
1089 Ewens WJ. 1979. Mathematical Population Genetics. Berlin: Springer (Antman SS, Marsden JE,
1090 Sirovich L, Wiggins S, editors. Interdisciplinary Applied Mathematics). [accessed 2024
1091 Apr 14]. http://link.springer.com/10.1007/978-0-387-21822-9.
1092 Ewing GB, Jensen JD. 2016. The consequences of not accounting for background selection in
1093 demographic inference. Mol Ecol. 25(1):135–141. doi:10.1111/mec.13390.
1094 Eyre-Walker A, Keightley PD. 2007. The distribution of fitness effects of new mutations. Nat
1095 Rev Genet. 8(8):610–618. doi:10.1038/nrg2146.
1096 Eyre-Walker A, Keightley PD. 2009. Estimating the rate of adaptive molecular evolution in the
1097 presence of slightly deleterious mutations and population size change. Mol Biol Evol.
1098 26(9):2097–2108. doi:10.1093/molbev/msp119.
1099 Eyre-Walker A, Woolfit M, Phelps T. 2006. The distribution of fitness effects of new deleterious
1100 amino acid mutations in humans. Genetics. 173(2):891–900.
1101 doi:10.1534/genetics.106.057570.
1102 Fay JC, Wu C-I. Hitchhiking Under Positive Darwinian Selection. :9.
1103 doi:10.1093/genetics/155.3.1405.
1104 Felsenstein J. 1974. The evolutionary advantage of recombination. Genetics. 78(2):737–756.
1105 doi:10.1093/genetics/78.2.737.

Ferrer-Admetlla A, Liang M, Korneliussen T, Nielsen R. 2014. On detecting incomplete soft or hard selective sweeps using haplotype structure. MBE. 31(5):1275–1291. doi:10.1093/molbev/msu077.

Freund F, Kerdoncuff E, Matuszewski S, Lapierre M, Hildebrandt M, Jensen JD, Ferretti L, Lambert A, Sackton TB, Achaz G. 2023. Interpreting the pervasive observation of U-shaped Site Frequency Spectra. PLoS Genet. 19(3):e1010677. doi:10.1371/journal.pgen.1010677.

Galtier N. 2016. Adaptive protein evolution in animals and the effective population size hypothesis. PLoS Genet. 12(1):e1005774. doi:10.1371/journal.pgen.1005774.

Garcia JA, Lohmueller KE. 2021. Negative linkage disequilibrium between amino acid changing variants reveals interference among deleterious mutations in the human genome. PLoS Genet. 17(7):e1009676. doi:10.1371/journal.pgen.1009676.

Gilbert KJ, Zdraljevic S, Cook DE, Cutter AD, Andersen EC, Baer CF. 2022. The distribution of mutational effects on fitness in *Caenorhabditis elegans* inferred from standing genetic variation. Moyle L, editor. Genetics. 220(1):iyab166. doi:10.1093/genetics/iyab166.

Glémin S. 2003. How are deleterious mutations purged? Drift versus nonrandom mating. Evolution. 57(12):2678–2687. doi:10.1111/j.0014-3820.2003.tb01512.x.

Good BH, Walczak AM, Neher RA, Desai MM. 2014. Genetic diversity in the interference selection limit. PLoS Genet. 10(3):e1004222. doi:10.1371/journal.pgen.1004222.

Goodwillie C, Kalisz S, Eckert CG. 2005. The evolutionary enigma of mixed mating systems in plants: Occurrence, theoretical explanations, and empirical evidence. Annu Rev Ecol Syst. 36(1):47–79. doi:10.1146/annurev.ecolsys.36.091704.175539.

Gorton AJ, Heath KD, Pilet-Nayel M-L, Baranger A, Stinchcombe JR. 2012. Mapping the genetic basis of symbiotic variation in legume-rhizobium interactions in *Medicago truncatula*. G3. 2(11):1291–1303. doi:10.1534/g3.112.003269.

Haller BC, Messer PW. 2023. SLiM 4: Multispecies eco-evolutionary modeling. Am Nat. 201(5):E127–E139. doi:10.1086/723601.

Hartfield M, Bataillon T. 2020. Selective sweeps under dominance and inbreeding. G3. 10(3):1063–1075. doi:10.1534/g3.119.400919.

Hartfield M, Glémin S. 2014. Hitchhiking of deleterious alleles and the cost of adaptation in partially selfing species. Genetics. 196(1):281–293. doi:10.1534/genetics.113.158196.

Hartfield M, Glémin S. 2016. Limits to adaptation in partially selfing species. Genetics. 203(2):959–974. doi:10.1534/genetics.116.188821.

Hedrick PW. 1980. Hitchhiking: a comparison of linkage and partial selfing. Genetics. 94(3):791–808. doi:10.1093/genetics/94.3.791.

Hill WG, Robertson A. 1966. The effect of linkage on limits to artificial selection. Genet Res. 8(3):269–294. doi:10.1017/S0016672300010156.

Hill WG, Robertson A. 1968. Linkage disequilibrium in finite populations. Theoret Appl Genetics. 38(6):226–231. doi:10.1007/BF01245622.

Hodgkin J. 1983. Male phenotypes and mating efficiency in *Caenorhabditis elegans*. Genetics. 103(1):43–64. doi:10.1093/genetics/103.1.43.

Horneburg B, Becker HC. 2018. Spontaneous outcrossing in tomato depends on cultivar and environment and varies between individual flowers. Plant Breed. 137(4):638–643. doi:10.1111/pbr.12600.

1150 Huang X, Fortier AL, Coffman AJ, Struck TJ, Irby MN, James JE, León-Burguete JE, Ragsdale
1151 AP, Gutenkunst RN. 2021. Inferring genome-wide correlations of mutation fitness effects
1152 between populations. Mol Biol Evol. 38(10):4588–4602. doi:10.1093/molbev/msab162.
1153 Huber CD, Kim BY, Marsden CD, Lohmueller KE. 2017. Determining the factors driving
1154 selective effects of new nonsynonymous mutations. Proc Natl Acad Sci USA.
1155 114(17):4465–4470. doi:10.1073/pnas.1619508114.
1156 Ingvarsson PK. 2002. A metapopulation perspective on genetic diversity and differentiation in
1157 partially self-fertilizing plants. Evolution. 56(12):2368–2373. doi:10.1111/j.0014-
1158 3820.2002.tb00162.x.
1159 Jarne P, Auld JR. 2006. Animals mix it up too: the distribution of self-fertilization among
1160 hermaphroditic animals. Evolution. 60(9):1816–1824. doi:10.1111/j.0014-
1161 3820.2006.tb00525.x.
1162 Johri P, Aquadro CF, Beaumont M, Charlesworth B, Excoffier L, Eyre-Walker A, Keightley PD,
1163 Lynch M, McVean G, Payseur BA, et al. 2022. Recommendations for improving
1164 statistical inference in population genomics. PLoS Biol. 20(5):e3001669.
1165 doi:10.1371/journal.pbio.3001669.
1166 Johri P, Charlesworth B. 2024. A gene-based model of fitness and its implications for genetic
1167 variation. :2024.09.12.612686. doi:10.1101/2024.09.12.612686. [accessed 2024 Sep 18].
1168 https://www.biorxiv.org/content/10.1101/2024.09.12.612686v1.
1169 Johri P, Charlesworth B, Jensen JD. 2020. Toward an evolutionarily appropriate null model:
1170 jointly inferring demography and purifying selection. Genetics. 215(1):173–192.
1171 doi:10.1534/genetics.119.303002.
1172 Johri P, Eyre-Walker A, Gutenkunst RN, Lohmueller KE, Jensen JD. 2022. On the prospect of
1173 achieving accurate joint estimation of selection with population history. Genome Biol
1174 Evol. 14(7):evac088. doi:10.1093/gbe/evac088.
1175 Johri P, Riall K, Becher H, Excoffier L, Charlesworth B, Jensen JD. 2021. The impact of
1176 purifying and background selection on the inference of population history: problems and
1177 prospects. Mol Biol Evol. 38(7):2986–3003. doi:10.1093/molbev/msab050.
1178 Jullien M, Ronfort J, Gay L. 2021. How and when does outcrossing occur in the predominantly
1179 selfing species *Medicago truncatula*? Front Plant Sci. 12:619154.
1180 doi:10.3389/fpls.2021.619154.
1181 Kaiser VB, Charlesworth B. 2009. The effects of deleterious mutations on evolution in non-
1182 recombining genomes. Trends Genet. 25(1):9–12. doi:10.1016/j.tig.2008.10.009.
1183 Kamran-Disfani A, Agrawal AF. 2014. Selfing, adaptation and background selection in finite
1184 populations. J Evol Biol. 27(7):1360–1371. doi:10.1111/jeb.12343.
1185 Katju V, Packard LB, Bu L, Keightley PD, Bergthorsson U. 2015. Fitness decline in spontaneous
1186 mutation accumulation lines of *Caenorhabditis elegans* with varying effective population
1187 sizes. Evolution. 69(1):104–16. doi:10.1111/evo.12554.
1188 Keightley PD, Eyre-Walker A. 2007. Joint inference of the distribution of fitness effects of
1189 deleterious mutations and population demography based on nucleotide polymorphism
1190 frequencies. Genetics. 177(4):2251–2261. doi:10.1534/genetics.107.080663.
1191 Kim BY, Huber CD, Lohmueller KE. 2017. Inference of the distribution of selection coefficients
1192 for new nonsynonymous mutations using large samples. Genetics. 206(1):345–361.
1193 doi:10.1534/genetics.116.197145.

1194 Konrad A, Brady MJ, Bergthorsson U, Katju V. 2019. Mutational landscape of spontaneous base
1195 substitutions and small indels in experimental *Caenorhabditis elegans* populations of
1196 differing size. Genetics. 212(3):837–854. doi:10.1534/genetics.119.302054.
1197 Kousathanas A, Keightley PD. 2013. A comparison of models to infer the distribution of fitness
1198 effects of new mutations. Genetics. 193(4):1197–1208. doi:10.1534/genetics.112.148023.
1199 Lewontin RC. 1964. The interaction of selection and linkage. I. general considerations; heterotic
1200 models. Genetics. 49(1):49–67. doi:10.1093/genetics/49.1.49.
1201 Lewontin RC. 1988. On measures of gametic disequilibrium. Genetics. 120(3):849–852.
1202 doi:10.1093/genetics/120.3.849.
1203 Li W-H. 1987. Models of nearly neutral mutations with particular implications for nonrandom
1204 usage of synonymous codons. J Mol Evol. 24(4):337–345. doi:10.1007/BF02134132.
1205 Linde M, Diel S, Neuffer B. 2001. Flowering ecotypes of *Capsella bursa-pastoris*(L.) Medik.
1206 (Brassicaceae) analysed by a cosegregation of phenotypic characters (QTL) and
1207 molecular markers. Ann Bot. 87(1):91–99. doi:10.1006/anbo.2000.1308.
1208 Ling H-Q, Ma B, Shi X, Liu H, Dong L, Sun H, Cao Y, Gao Q, Zheng S, Li Ye, et al. 2018.
1209 Genome sequence of the progenitor of wheat A subgenome *Triticum urartu*. Nature.
1210 557(7705):424–428. doi:10.1038/s41586-018-0108-0.
1211 Luo M-C, Gu YQ, You FM, Deal KR, Ma Y, Hu Y, Huo N, Wang Y, Wang J, Chen S, et al.
1212 2013. A 4-gigabase physical map unlocks the structure and evolution of the complex
1213 genome of *Aegilops tauschii*, the wheat D-genome progenitor. Proc Natl Acad Sci USA.
1214 110(19):7940–7945. doi:10.1073/pnas.1219082110.
1215 Mable BK, Robertson AV, Dart S, Di Berardo C, Witham L. 2005. Breakdown of self-
1216 incompatibility in the perennial *Arabidopsis lyrata* (*Brassicaceae*) and its genetic
1217 consequences. Evolution. 59(7):1437–1448.
1218 Manna F, Martin G, Lenormand T. 2011. Fitness landscapes: An alternative theory for the
1219 dominance of mutation. Genetics. 189(3):923–937. doi:10.1534/genetics.111.132944.
1220 Maruyama T. 1970. Effective number of alleles in a subdivided population. Theor Popul Biol.
1221 1(3):273–306. doi:10.1016/0040-5809(70)90047-X.
1222 Maureira-Butler IJ, Pfeil BE, Muangprom A, Osborn TC, Doyle JJ. 2008. The reticulate history
1223 of *Medicago* (*Fabaceae*). Syst Biol. 57(3):466–482. doi:10.1080/10635150802172168.
1224 McVean GA, Charlesworth B. 2000. The effects of Hill-Robertson interference between weakly
1225 selected mutations on patterns of molecular evolution and variation. Genetics.
1226 155(2):929–944.
1227 Melissa MJ, Good BH, Fisher DS, Desai MM. 2022. Population genetics of polymorphism and
1228 divergence in rapidly evolving populations. Genetics. 221(4):iyac053.
1229 doi:10.1093/genetics/iyac053.
1230 Neher RA. 2013. Genetic draft, selective interference, and population genetics of rapid
1231 adaptation. Annu Rev Ecol Syst. 44(1):195–215. doi:10.1146/annurev-ecolsys-110512-
1232 135920.
1233 Neher RA, Hallatschek O. 2013. Genealogies of rapidly adapting populations. Proc Natl Acad
1234 Sci USA. 110(2):437–442. doi:10.1073/pnas.1213113110.
1235 Nei M. 1968. The frequency distribution of lethal chromosomes in finite populations. Proc Natl
1236 Acad Sci USA. 60(2):517–524. doi:10.1073/pnas.60.2.517.
1237 Nei M. 1973. Analysis of gene diversity in subdivided populations. Proc Natl Acad Sci USA.
1238 70(12):3321–3323. doi:10.1073/pnas.70.12.3321.

1239 Nei M, Tajima F. 1981. DNA polymorphism detectable by restriction endonucleases. Genetics.
1240 97(1):145–163. doi:10.1093/genetics/97.1.145.
1241 Nicolaisen LE, Desai MM. 2013. Distortions in genealogies due to purifying selection and
1242 recombination. Genetics. 195(1):221–230. doi:10.1534/genetics.113.152983.
1243 Nordborg M. 2000. Linkage disequilibrium, gene trees and selfing: an ancestral recombination
1244 graph with partial self-fertilization. Genetics. 154(2):923–929.
1245 doi:10.1093/genetics/154.2.923.
1246 O'Fallon BD, Seger J, Adler FR. 2010. A continuous-state coalescent and the impact of weak
1247 selection on the structure of gene genealogies. Mol Biol Evol. 27(5):1162–1172.
1248 doi:10.1093/molbev/msq006.
1249 Ossowski S, Schneeberger K, Lucas-Lledó JI, Warthmann N, Clark RM, Shaw RG, Weigel D,
1250 Lynch M. 2010. The rate and molecular spectrum of spontaneous mutations in
1251 Arabidopsis thaliana. Science. 327(5961):92–94. doi:10.1126/science.1180677.
1252 Pannell JR, Charlesworth B. 1999. Neutral genetic diversity in a metapopulation with recurrent
1253 local extinction and recolonization. Evolution. 53(3):664–676. doi:10.1111/j.1558-
1254 5646.1999.tb05362.x.
1255 Parobek CM, Lin JT, Saunders DL, Barnett EJ, Lon C, Lanteri CA, Balasubramanian S, Brazeau
1256 N, DeConti DK, Garba DL, et al. 2016. Selective sweep suggests transcriptional
1257 regulation may underlie *Plasmodium vivax* resilience to malaria control measures in
1258 Cambodia. Proc Natl Acad Sci USA. 113(50):E8096–E8105.
1259 doi:10.1073/pnas.1608828113.
1260 Penin AA, Kasianov AS, Klepikova AV, Omelchenko DO, Makarenko MS, Logacheva MD.
1261 2024. Origin and diversity of *Capsella bursa-pastoris* from the genomic point of view.
1262 BMC Biology. 22(1):52. doi:10.1186/s12915-024-01832-1.
1263 Pollak E. 1987. On the theory of partially inbreeding finite populations. I. Partial selfing.
1264 Genetics. 117(2):353–360. doi:10.1093/genetics/117.2.353.
1265 Pruitt KD, Brown GR, Hiatt SM, Thibaud-Nissen F, Astashyn A, Ermolaeva O, Farrell CM, Hart
1266 J, Landrum MJ, McGarvey KM, et al. 2014. RefSeq: an update on mammalian reference
1267 sequences. Nucleic Acids Res. 42(Database issue):D756-763. doi:10.1093/nar/gkt1114.
1268 Racimo F, Schraiber JG. 2014. Approximation to the distribution of fitness effects across
1269 functional categories in human segregating polymorphisms. PLoS Genet.
1270 10(11):e1004697. doi:10.1371/journal.pgen.1004697.
1271 Richaud A, Zhang G, Lee D, Lee J, Félix M-A. 2018. The Local Coexistence Pattern of Selfing
1272 Genotypes in Caenorhabditis elegans Natural Metapopulations. Genetics. 208(2):807–
1273 821. doi:10.1534/genetics.117.300564.
1274 Rockman MV, Kruglyak L. 2009. Recombinational landscape and population genomics of
1275 *Caenorhabditis elegans*. PLoS Genet. 5(3):e1000419. doi:10.1371/journal.pgen.1000419.
1276 Roselius K, Stephan W, Städler T. 2005. The relationship of nucleotide polymorphism,
1277 recombination rate and selection in wild tomato species. Genetics. 171(2):753–763.
1278 doi:10.1534/genetics.105.043877.
1279 Roze D, Lenormand T. 2005. Self-fertilization and the evolution of recombination. Genetics.
1280 170(2):841–857. doi:10.1534/genetics.104.036384.
1281 Sanjuán R, Moya A, Elena SF. 2004. The distribution of fitness effects caused by single-
1282 nucleotide substitutions in an RNA virus. Proc Natl Acad Sci USA. 101(22):8396–8401.
1283 doi:10.1073/pnas.0400146101.

Saxena AS, Salomon MP, Matsuba C, Yeh S-D, Baer CF. 2019. Evolution of the mutational process under relaxed selection in *Caenorhabditis elegans*. Mol Biol Evol. 36(2):239–251. doi:10.1093/molbev/msy213.

Schrider DR, Shanku AG, Kern AD. 2016. Effects of linked selective sweeps on demographic inference and model selection. Genetics. 204(3):1207–1223. doi:10.1534/genetics.116.190223.

Seger J, Smith WA, Perry JJ, Hunn J, Kaliszewska ZA, Sala LL, Pozzi L, Rowntree VJ, Adler FR. 2010. Gene genealogies strongly distorted by weakly interfering mutations in constant environments. Genetics. 184(2):529–545. doi:10.1534/genetics.109.103556.

Sendrowski J, Bataillon T. 2024. fastDFE: Fast and flexible inference of the distribution of fitness effects. Mol Biol Evol. 41(5):msae070. doi:10.1093/molbev/msae070.

Sicard A, Lenhard M. 2011. The selfing syndrome: a model for studying the genetic and evolutionary basis of morphological adaptation in plants. Ann Bot. 107(9):1433–1443. doi:10.1093/aob/mcr023.

Simmons MJ, Crow JF. 1977. Mutations affecting fitness in *Drosophila* populations. Ann Rev Genet. 11(1):49–78. doi:10.1146/annurev.ge.11.120177.000405.

Singer T, Fan Y, Chang H-S, Zhu T, Hazen SP, Briggs SP. 2006. A high-resolution map of *Arabidopsis* recombinant inbred lines by whole-genome exon array hybridization. PLoS Genet. 2(9):e144. doi:10.1371/journal.pgen.0020144.

Sivasundar A, Hey J. 2005. Sampling from natural populations with RNAI reveals high outcrossing and population structure in Caenorhabditis elegans. Curr Biol. 15(17):1598–1602. doi:10.1016/j.cub.2005.08.034.

Slatkin M, Voelm L. 1991. F_{ST} in a hierarchical island model. Genetics. 127(3):627–629. doi:10.1093/genetics/127.3.627.

Snape JW, Lawrence MJ. 1971. The breeding system of *Arabidopsis thaliana*. Heredity. 27(2):299–302. doi:10.1038/hdy.1971.91.

Städler T, Haubold B, Merino C, Stephan W, Pfaffelhuber P. 2009. The impact of sampling schemes on the site frequency spectrum in nonequilibrium subdivided populations. Genetics. 182(1):205–216. doi:10.1534/genetics.108.094904.

Su X, Wang B, Geng X, Du Y, Yang Q, Liang B, Meng G, Gao Q, Yang W, Zhu Y, et al. 2021. A high-continuity and annotated tomato reference genome. BMC Genom. 22(1):898. doi:10.1186/s12864-021-08212-x.

Tataru P, Mollion M, Glémin S, Bataillon T. 2017. Inference of distribution of fitness effects and proportion of adaptive substitutions from polymorphism data. Genetics. 207(3):1103–1119. doi:10.1534/genetics.117.300323.

Teterina AA, Willis JH, Lukac M, Jovelin R, Cutter AD, Phillips PC. 2023. Genomic diversity landscapes in outcrossing and selfing *Caenorhabditis* nematodes. PLoS Genet. 19(8):e1010879. doi:10.1371/journal.pgen.1010879.

Thornton K. 2003. libsequence: a C++ class library for evolutionary genetic analysis. Bioinformatics. 19(17):2325–2327. doi:10.1093/bioinformatics/btg316.

Vassilieva LL, Hook AM, Lynch M. 2000. The fitness effects of spontaneous mutations in *Caenorhabditis elegans*. Evolution. 54(4):1234–1246. doi:10.1111/j.0014-3820.2000.tb00557.x.

Víquez-Zamora M, Caro M, Finkers R, Tikunov Y, Bovy A, Visser RG, Bai Y, van Heusden S. 2014. Mapping in the era of sequencing: high density genotyping and its application for

mapping TYLCV resistance in *Solanum pimpinellifolium*. BMC Genom. 15(1):1152. doi:10.1186/1471-2164-15-1152.

Wade EE, Kyriazis CC, Cavassim MIA, Lohmueller KE. 2023. Quantifying the fraction of new mutations that are recessive lethal. Evolution. 77(7):1539–1549. doi:10.1093/evolut/qpad061.

Wakeley J. 1999. Nonequilibrium migration in human history. Genetics. 153(4):1863–1871. doi:10.1093/genetics/153.4.1863.

Walczak AM, Nicolaisen LE, Plotkin JB, Desai MM. 2012. The structure of genealogies in the presence of purifying selection: a fitness-class coalescent. Genetics. 190(2):753–779. doi:10.1534/genetics.111.134544.

Wang L, Zhu T, Rodriguez JC, Deal KR, Dubcovsky J, McGuire PE, Lux T, Spannagl M, Mayer KFX, Baldrich P, et al. 2021. *Aegilops tauschii* genome assembly Aet v5.0 features greater sequence contiguity and improved annotation. G3. 11(12):jkab325. doi:10.1093/g3journal/jkab325.

Watterson GA. 1975. On the number of segregating sites in genetical models without recombination. Theor Popul Biol. 7(2):256–276. doi:10.1016/0040-5809(75)90020-9.

Weinreich DM, Rand DM. 2000. Contrasting patterns of nonneutral evolution in proteins encoded in nuclear and mitochondrial genomes. Genetics. 156(1):385–399. doi:10.1093/genetics/156.1.385.

Wesse C, Welk E, Hurka H, Neuffer B. 2021. Geographical pattern of genetic diversity in *Capsella bursa-pastoris* (Brassicaceae)—A global perspective. Ecol Evol. 11(1):199–213. doi:10.1002/ece3.7010.

Willenborg CJ, Van Acker RC. 2008. The biology and ecology of hexaploid wheat (*Triticum aestivum* L.) and its implications for trait confinement. Can J Plant Sci. 88(5):997–1013. doi:10.4141/CJPS07144.

Williamson SH, Hernandez R, Fledel-Alon A, Zhu L, Nielsen R, Bustamante CD. 2005. Simultaneous inference of selection and population growth from patterns of variation in the human genome. Proc Natl Acad Sci USA. 102(22):7882–7887. doi:10.1073/pnas.0502300102.

Wloch DM, Szafraniec K, Borts RH, Korona R. 2001. Direct estimate of the mutation rate and the distribution of fitness effects in the yeast *Saccharomyces cerevisiae*. Genetics. 159(2):441–452. doi:10.1093/genetics/159.2.441.

Wright SI, Kalisz S, Slotte T. 2013. Evolutionary consequences of self-fertilization in plants. Proc R Soc Lond B. 280(1760):20130133. doi:10.1098/rspb.2013.0133.

Yang S, Wang L, Huang J, Zhang X, Yuan Y, Chen J-Q, Hurst LD, Tian D. 2015. Parent–progeny sequencing indicates higher mutation rates in heterozygotes. Nature. 523(7561):463–467. doi:10.1038/nature14649.

Zeitler L, Gilbert KJ. 2024. Using runs of homozygosity and machine learning to disentangle sources of inbreeding and infer self-fertilization rates. Genome Biol Evol. 16(7):evae139. doi:10.1093/gbe/evae139.

Zeng K, Charlesworth B. 2011. The joint effects of background selection and genetic recombination on local gene genealogies. Genetics. 189(1):251–266. doi:10.1534/genetics.111.130575.

Zeng K, Corcoran P. 2015. The effects of background and interference selection on patterns of genetic variation in subdivided populations. Genetics. 201(4):1539–1554. doi:10.1534/genetics.115.178558.

FIGURES AND TABLES

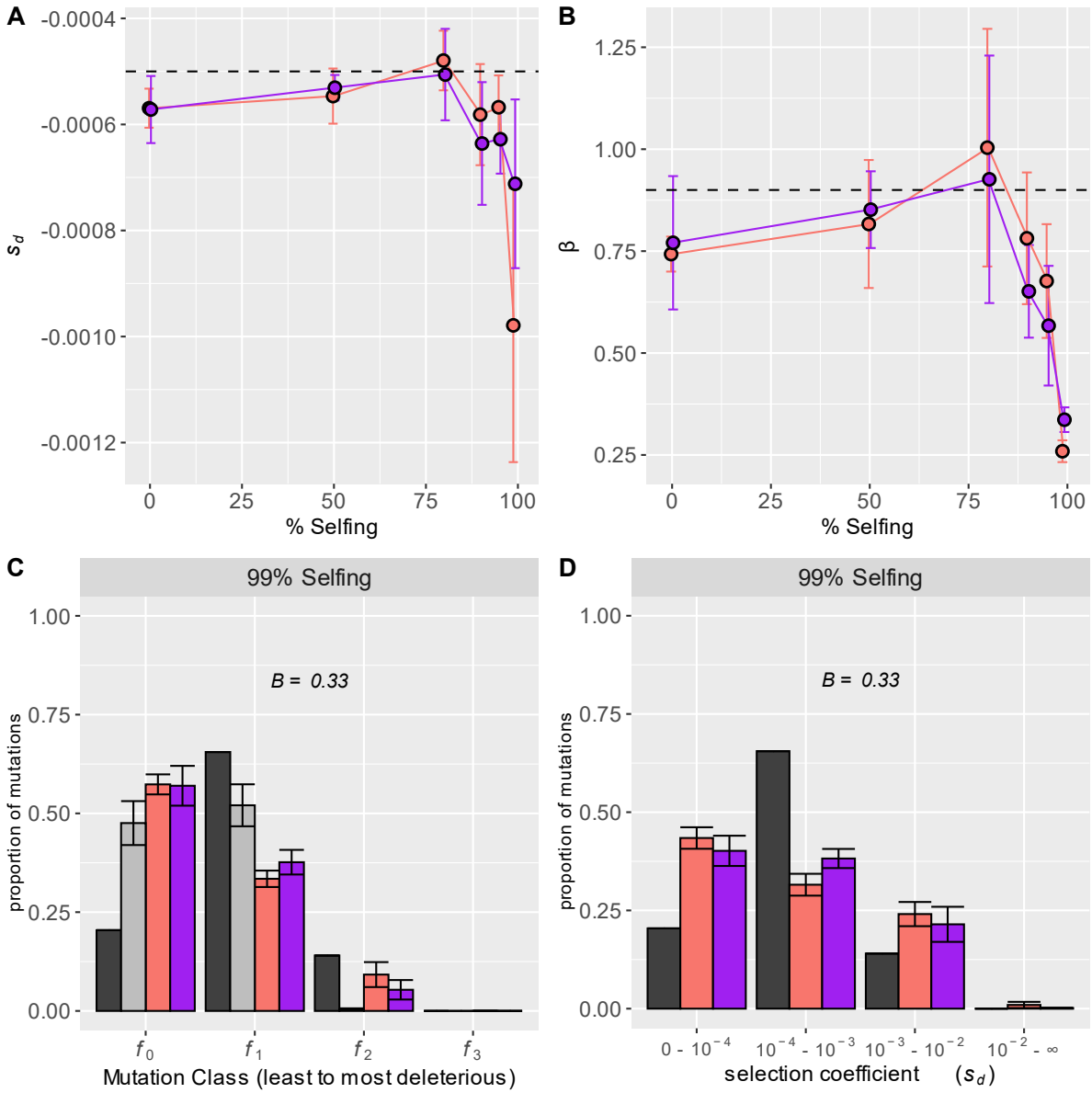

Figure 1: Effects of selfing on the inference of the DFE of new deleterious mutations using DFE-alpha (red bars) and GRAPES (purple bars). (**A**) The mean selection coefficients ($\overline{s_d}$) and (**B**) shape parameters (β) of the inferred gamma distributions for varying selfing rates are shown. (C) A comparison of the simulated and inferred DFE at 99% selfing rate is shown in terms of the proportion of mutations in the effectively neutral (f_0), weakly deleterious (f_1), moderately deleterious (f_2) and strongly deleterious (f_3) classes of mutations. The simulated (black bars) and adjusted (grey bars) DFE represents the distribution of $2Ns_d$ and $2NBs_d$ respectively. (**D**) The simulated and inferred distribution of s_d, which was created by dividing the mean of the gamma distribution ($2N_e\bar{s}_d$) by $2BN$. The nucleotide site diversity with background selection (B) relative to its expectation under strict neutrality is shown in **C** and **D**. In all panels, the error bars denote the standard deviation of proportions estimated from 5 independent replicates.

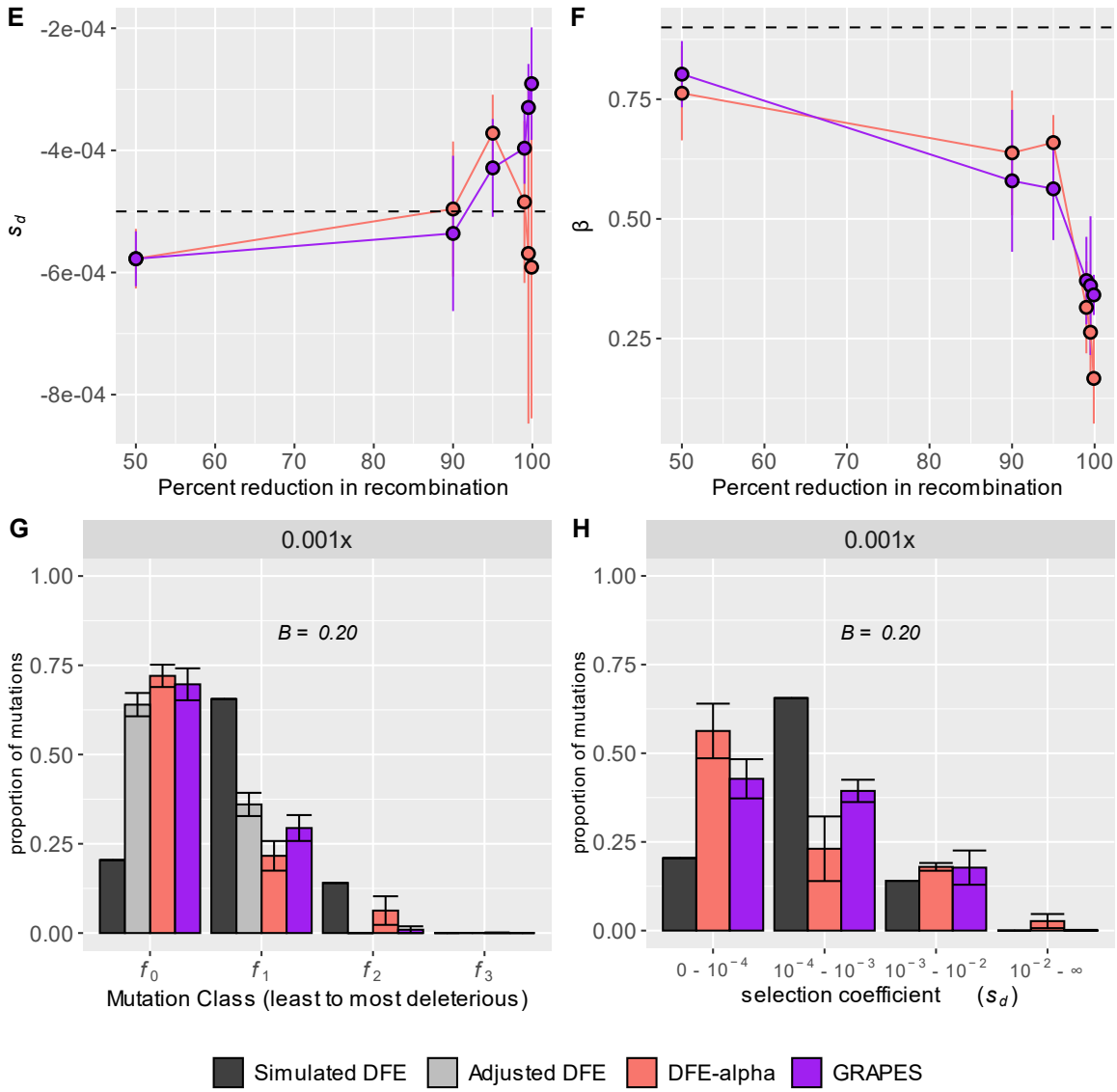

Figure 2: Effects of reduced recombination rates on the inference of the DFE of new deleterious mutations using DFE-alpha (red bars) and GRAPES (purple bars). (**A**) The mean selection coefficients ($\overline{s_d}$) and (**B**) shape parameters (β) of the inferred gamma distributions are plotted for varying recombination rates, reduced from an initial rate of $r = 3.12 \times 10^{-8}$ per site/generation. (**C**) A comparison of the simulated and inferred DFE at a recombination rate reduced by 99.9% is shown in terms of the proportion of mutations in effectively neutral (f_0), weakly deleterious (f_1), moderately deleterious (f_2) and strongly deleterious (f_3) classes of mutations. The simulated (black bars) and adjusted (grey bars) DFE represents the distribution of $2Ns_d$ and $2NBs_d$ respectively. (**D**) The simulated and inferred distribution of s_d, which was created by dividing the mean of the gamma distribution ($2N_e s_d$) by $2BN$. The nucleotide site diversity with background selection (B) relative to its expectation under strict neutrality is shown in **C** and **D**. In all panels, the error bars denote the standard deviation of proportions estimated from 5 independent replicates.

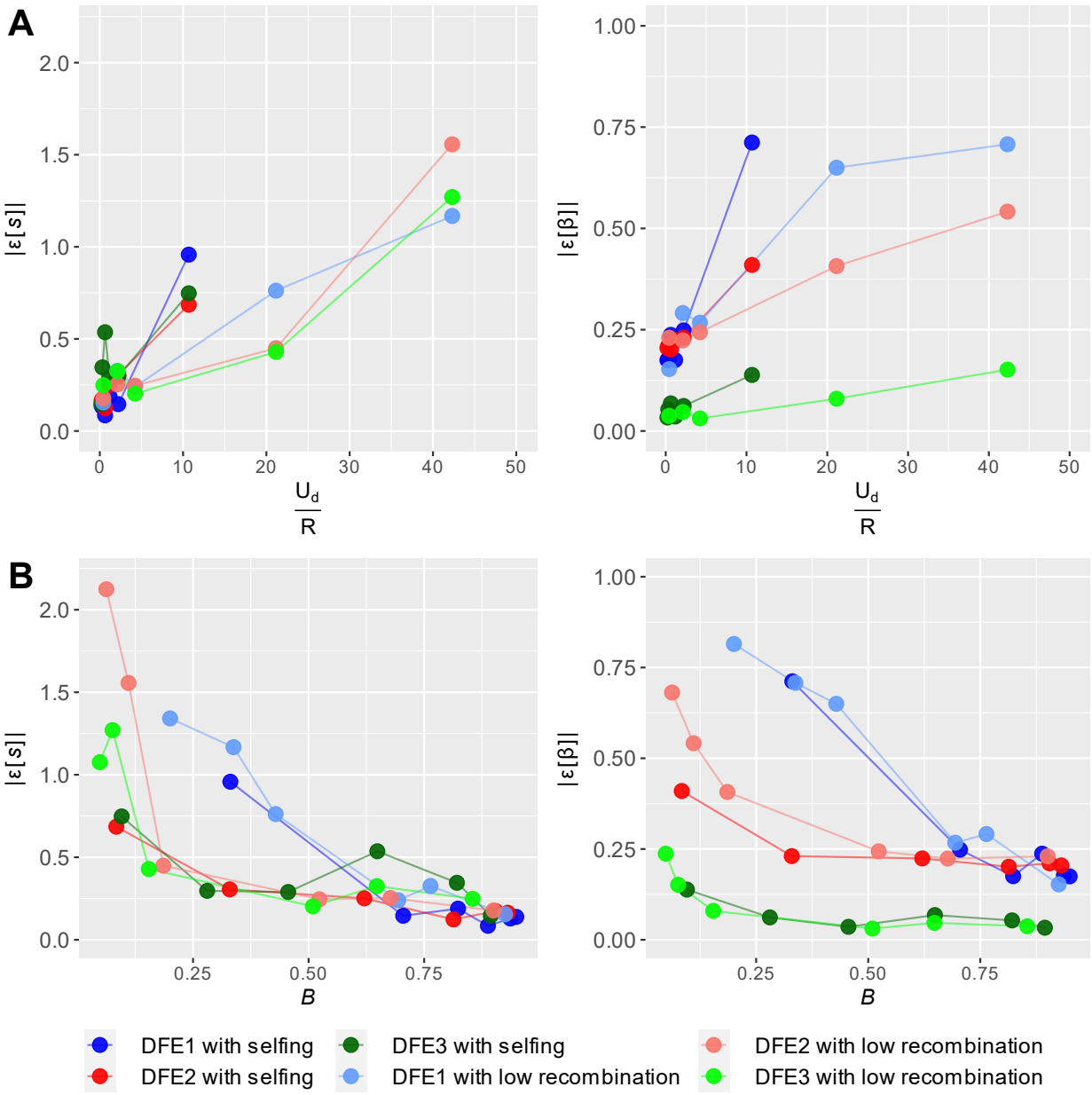

Figure 3: Correlation of error ($\varepsilon = \left|\frac{inferred-true}{true}\right|$) of parameters in DFE inference by DFE-alpha with (**A**) the ratio of number of deleterious mutations per diploid genome per generation (U_d) and number of effective recombination events per individual per generation (R) and (**B**) the neutral nucleotide site diversity (B) with background selection relative to that expected under neutrality (B). Error in the inference of the parameters of the DFE and levels of background selection were averaged over five independent replicates.

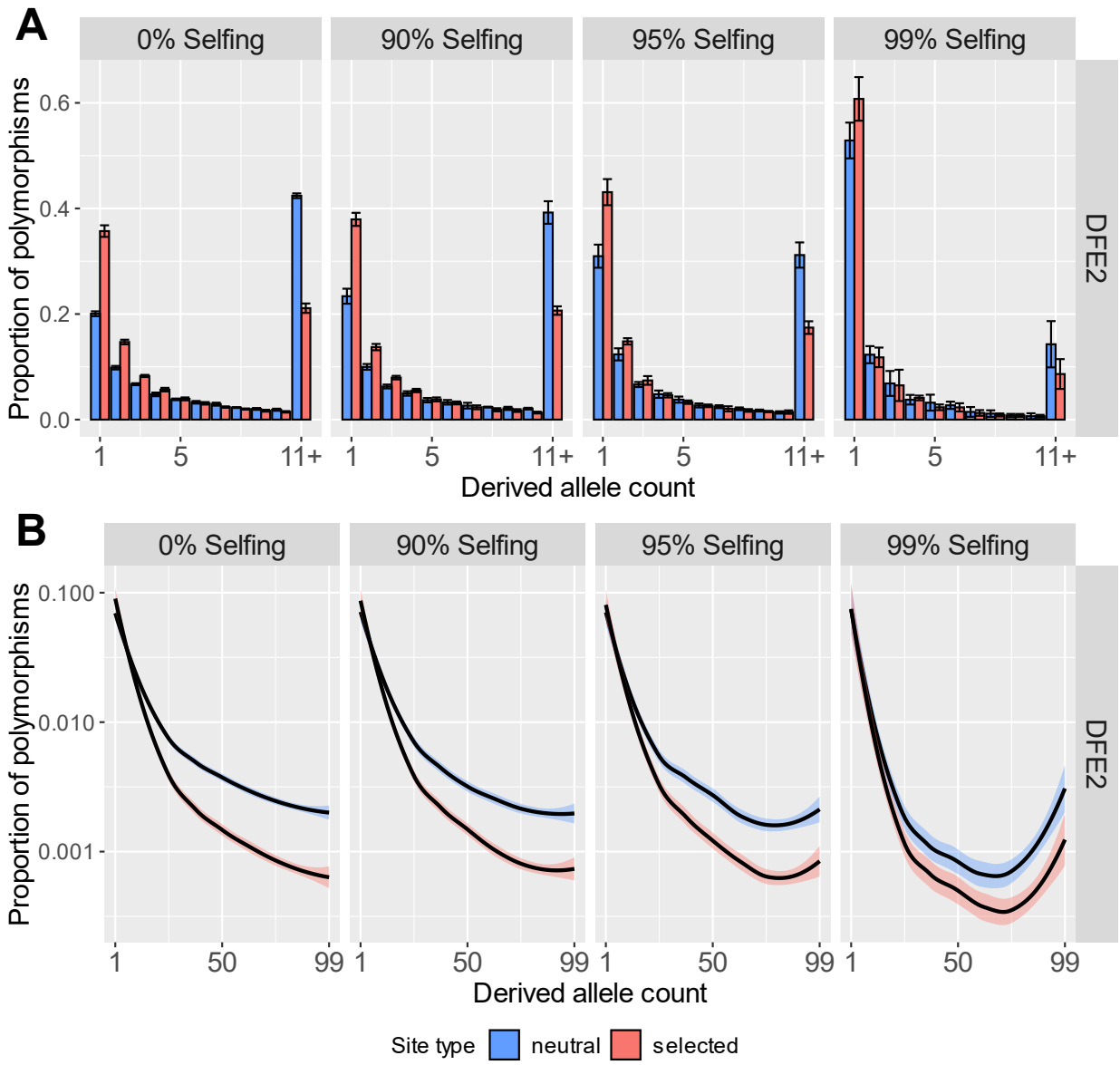

Figure 4: Site frequency spectra of neutral and selected alleles from 100 genomes sampled from simulations where all selected mutations were deleterious, for the moderately deleterious DFE (DFE2). For **(A)** the y-axis represents the proportion of segregating polymorphisms that fall into the given derived allele count. The last class (11+) refers to the derived allele counts 11-99. The error bars denote the standard deviation of proportions estimated from 5 independent replicates. For **(B)** the y-axis is plotted on a log scale, with all derived allele counts displayed. Lines were smoothed with LOESS.

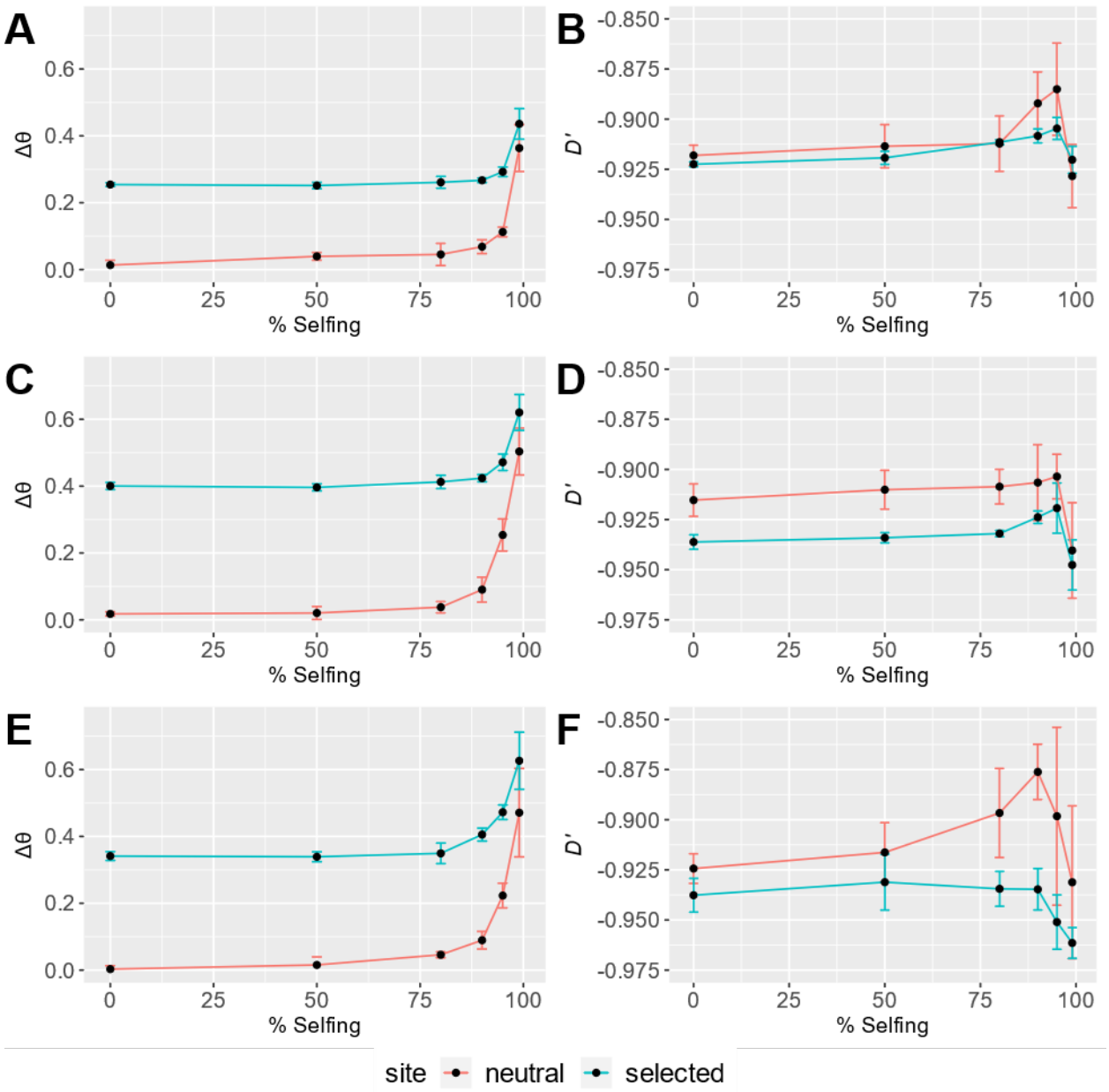

Figure 5: Effects of selfing on the SFS and linkage disequilibrium (LD) at neutral (red lines) and selected (blue lines) sites. The skew in the SFS was quantified using $\Delta\theta$ for DFE1 (**A**), DFE2 (**C**), and DFE3 (**E**), calculated using alleles at all frequencies, while LD was summarized by the statistic D' for DFE1 (**B**), DFE2 (**D**), and DFE3 (**F**), calculated for alleles at frequencies of 1%-5%. The error bars denote the standard deviation of the genome-wide average of each summary statistic estimated from 5 independent replicates.

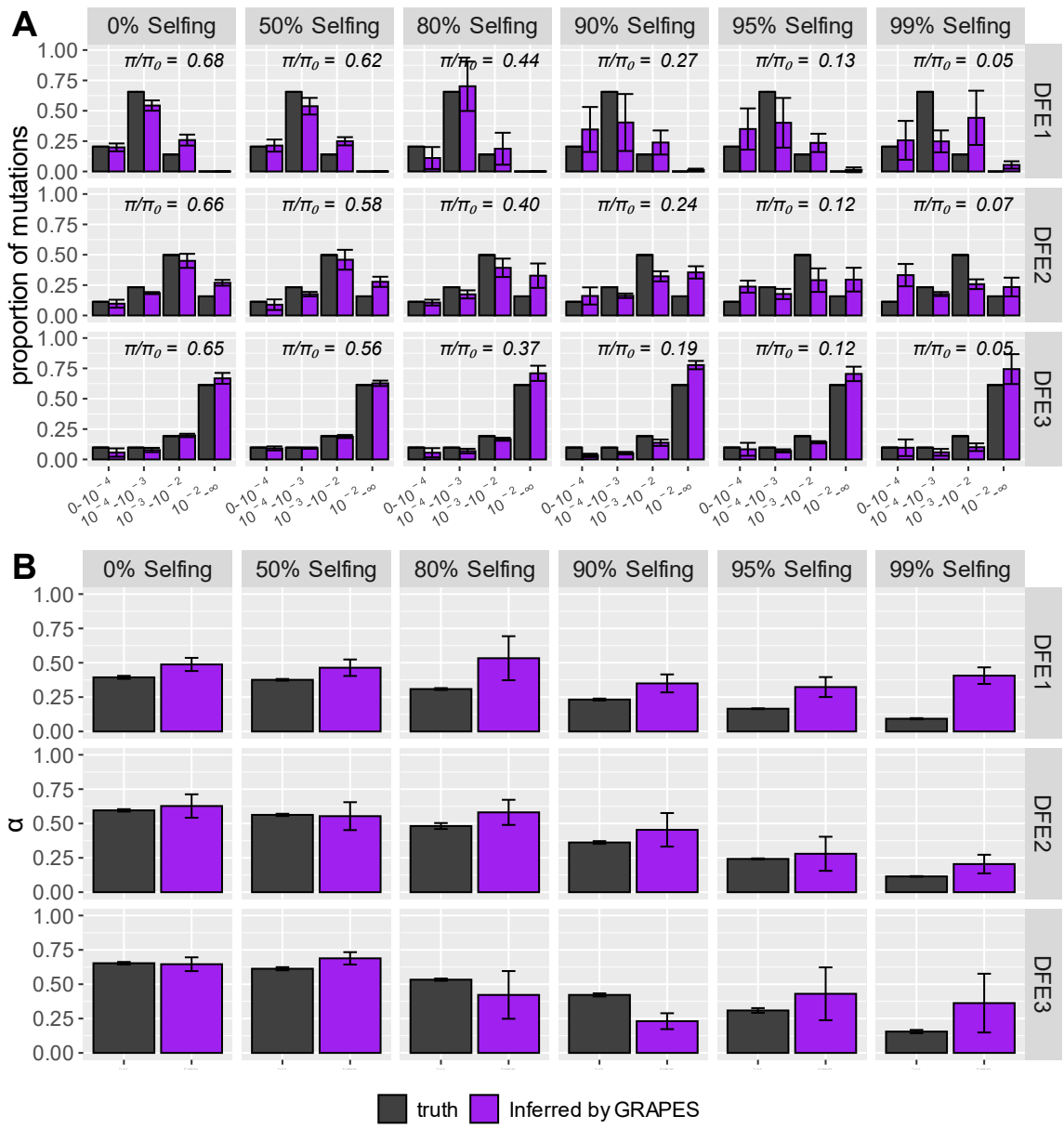

Figure 6: Effects of selfing on the inference of (A) the DFE of new deleterious mutations and (**B**) the proportion of beneficial fixations (α) using GRAPES (shown in purple bars). (**A**) Here the DFE is displayed as the distribution of s_d, which was created by dividing the mean of the gamma distribution ($2N_e s_d$) by $2(\pi_{obs}/\pi_{exp})N$, where π_{obs} is the neutral nucleotide site diversity observed in each scenario and π_{exp} is the neutral nucleotide site diversity expected in a population of size N at strict neutrality. Results are shown in terms of the proportion of mutations in effectively neutral ($0 \leq s_d < 1 \times 10^{-4}$), weakly deleterious ($1 \times 10^{-4} \leq s_d < 1 \times 10^{-3}$), moderately deleterious ($1 \times 10^{-3} \leq s_d < 1 \times 10^{-2}$) and strongly deleterious ($1 \times 10^{-2} \leq s_d < 1$) classes. Selfing rates were varied between 0 and 99 %. π/π_0, the neutral nucleotide diversity with selection relative to that expected under neutrality is shown. For both (**A**) and (**B**), 0.1% of new exonic mutations were beneficial and exponentially distributed with a mean $2Ns_a = 200$. The error bars denote the standard deviation of proportions estimated from 5 independent replicates.

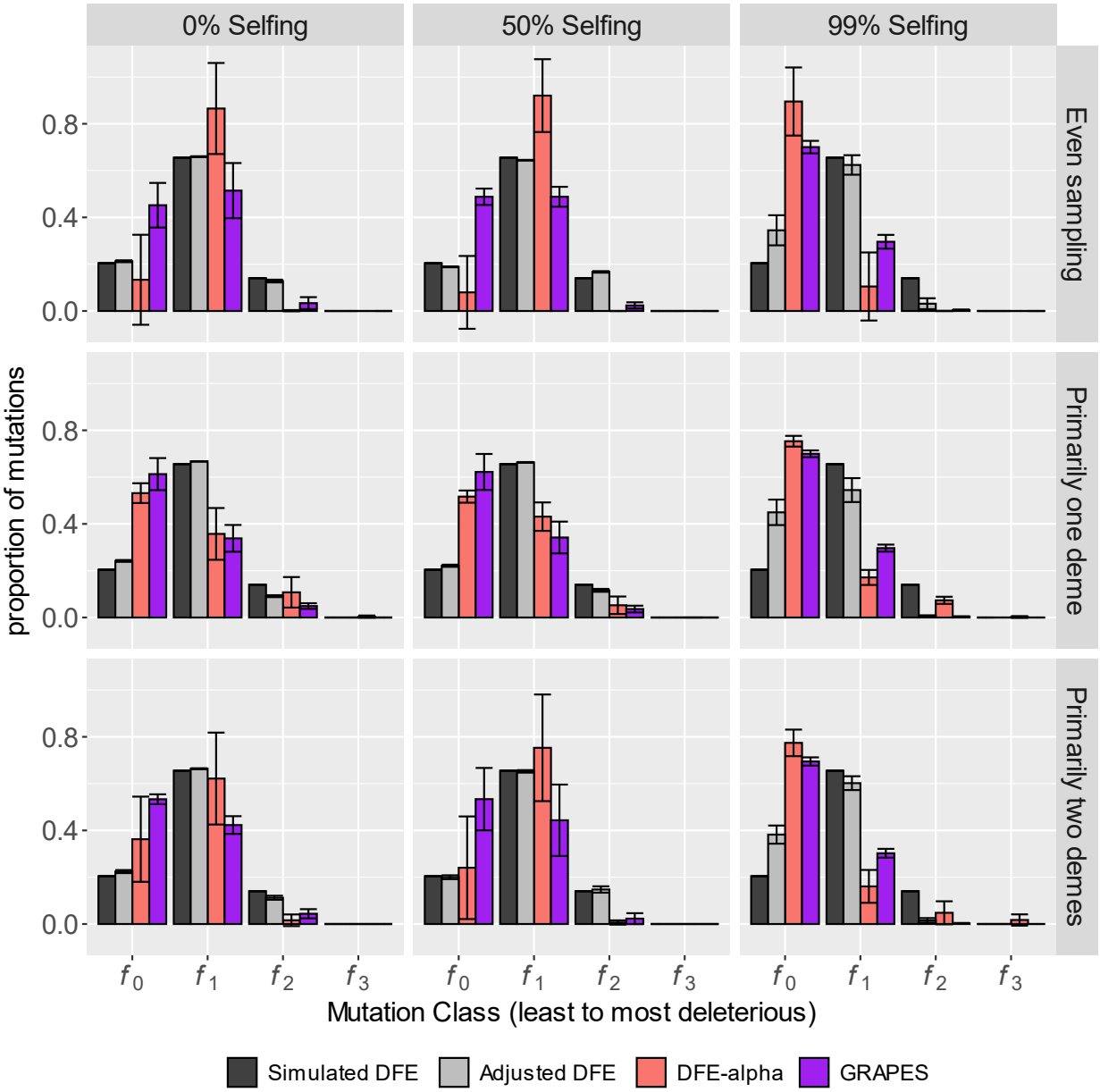

Figure 7: Effects of uneven sampling, population structure, and selfing on the inference of the DFE of new deleterious mutations using DFE-alpha (red bars) and GRAPES (purple bars). Results are shown in terms of the proportion of mutations in effectively neutral (f_0), weakly deleterious (f_1), moderately deleterious (f_2) and strongly deleterious (f_3) classes. Populations were simulated under an island model with five demes such that the metapopulation effective size was equal to 5000 at 0% selfing and $N_{deme}m$ was 0.1. Results are shown for the most weakly deleterious DFE (*i.e.*, DFE1). The error bars denote the standard deviation of proportions estimated from 5 independent replicates. Rows represent the sampling scheme for genomes, where sampling was even, sampling was primarily from one deme, or sampling was primarily from two demes.

1459 **Table 1**: Parameters of the simulated DFEs of deleterious mutations in terms of the proportion of
1460 mutations in effectively neutral (f_0), weakly deleterious (f_1), moderately deleterious (f_2) and
1461 strongly deleterious (f_3) classes. DFEs consisted of predominantly mildly deleterious (DFE1),
1462 moderately deleterious (DFE2), or strongly deleterious (DFE3) mutations.

	β	$2Ns_d$	f_0	f_1	f_2	f_3
DFE1	0.9	5	0.204	0.655	0.140	0.000
DFE2	0.5	50	0.113	0.233	0.497	0.157
DFE3	0.3	1000	0.098	0.097	0.192	0.614

1463

1464 **Table 2:** Estimated levels of background selection (B) in highly selfing species for the range of
1465 previously reported selfing rates. All species are diploid except tetraploid *C. bursa-pastoris*. U_d
1466 is the number of deleterious mutations per diploid genome per generation, while R is the map
1467 length in Morgans for each genome. The strength of BGS was calculated with $B = \exp\left(-\frac{U_d}{R_{self}}\right)$,
1468 where $R_{self} = R \times F$. All mutation rates, recombination rates, and genome annotation
1469 information used to construct this table is present in Supplementary Table 9.

Species	Coding fraction (f_{coding})	$\frac{U_d}{R}$	Selfing rate	$\frac{U_d}{R_{self}}$	Estimated B	References
*Aegilops tauschii**	0.01	0.022	0.90-0.995	0.25-4.45	0.01-0.78	(Willenborg and Van Acker 2008; Luo et al. 2013; Wang et al. 2021; Burgarella et al. 2024)
Arabidopsis thaliana	0.27	0.071	0.97-0.99	1.32-3.89	0.02-0.27	(Snape and Lawrence 1971; Singer et al. 2006; Ossowski et al. 2010; Cheng et al. 2017)
Caenorhabditis briggsae+*	0.22	0.031	0.95-0.999	0.33-15.50	~0-0.72	(Zeitler and Gilbert 2024)
Caenorhabditis elegans	0.3	0.042	0.93-0.999	0.32-21.00	~0-0.73	(*C. elegans* Sequencing Consortium 1998; Denver et al. 2004; Saxena et al. 2019; Teterina et al. 2023)
Capsella bursa-pastoris+	0.21	0.077	0.90-0.99	0.42-3.87	0.02-0.66	(Linde et al. 2001: 200; Wesse et al. 2021; Penin et al. 2024)
Capsella orientalis+	0.24	0.086	0.90-0.99	0.48-4.36	0.01-0.62	(Ågren et al. 2014)
Medicago truncatula	0.13	0.096	0.92-0.95	0.65-1.01	0.36-0.52	(Maureira-Butler et al. 2008; Gorton et al. 2012; Pruitt et al. 2014; Jullien et al. 2021)
Oryza sativa (indica)	0.12	0.017	0.95-0.99	0.17-0.83	0.43-0.84	(Pruitt et al. 2014; Yang et al. 2015: 20; De Leon et al. 2016; Bah et al. 2017)
Solanum lycopersicon	0.06	0.029	0.948-0.999	0.29-14.10	~0-0.75	(Roselius et al. 2005; Víquez-Zamora et al. 2014; Horneburg and Becker 2018; Su et al. 2021)
Triticum urartu+*	0.08	0.026	0.90-0.991	0.14-1.45	0.23-0.87	(Willenborg and Van Acker 2008; Ling et al. 2018; Burgarella et al. 2024)

1470 * mutation rate estimate of closely related species used for calculations (*A. thaliana* for plants, *C.*
1471 *elegans* for *C. briggsae*)
1472 +recombination rate of closely related species used for calculations

SUPPLEMENTARY FIGURES AND TABLES

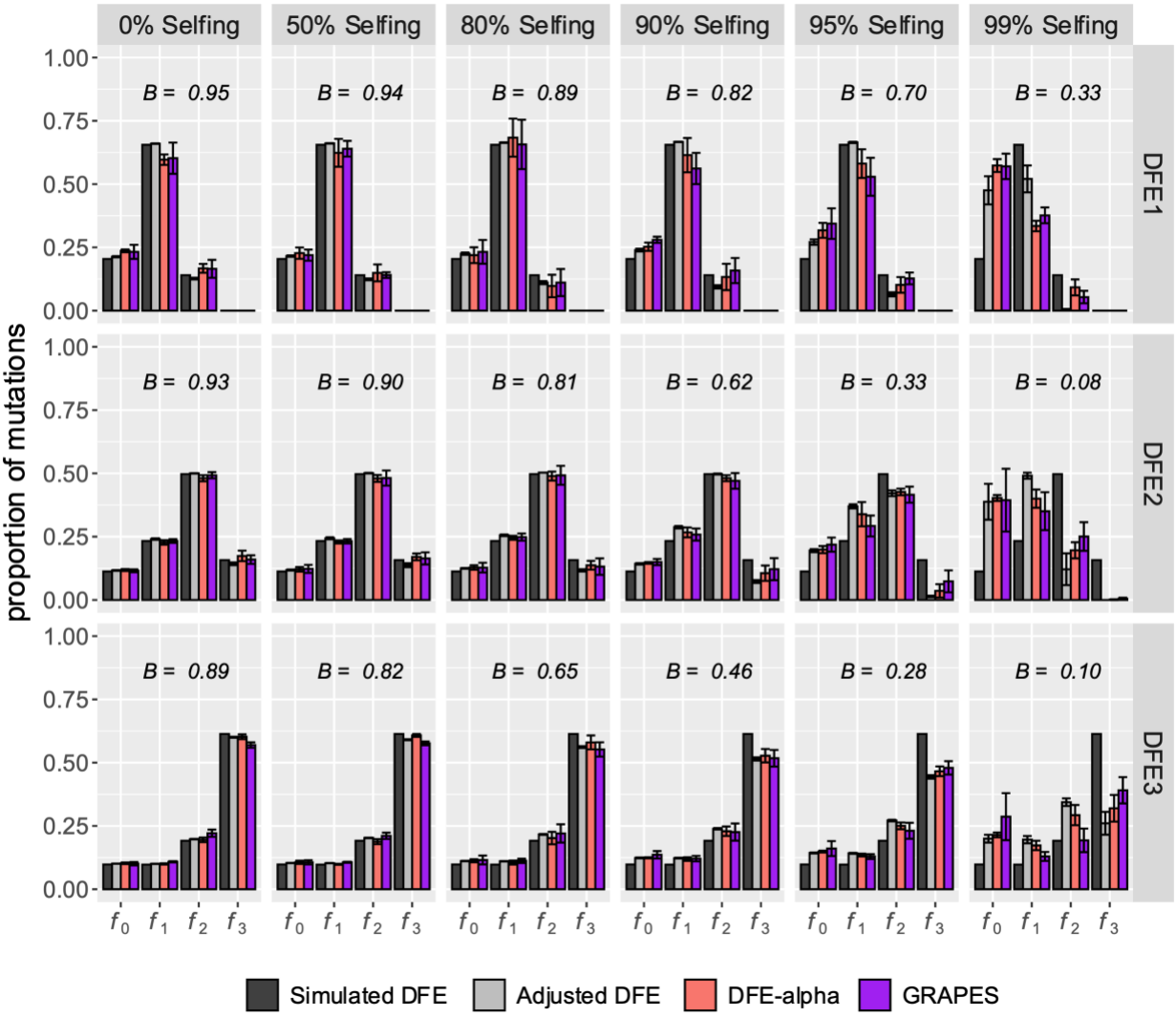

Supplementary Figure 1: Effects of selfing on the inference of the DFE of new deleterious mutations using DFE-alpha (red bars) and GRAPES (purple bars). Results are shown in terms of the proportion of mutations in effectively neutral (f_0), weakly deleterious (f_1), moderately deleterious (f_2) and strongly deleterious (f_3) classes. Selfing rates were varied between 0 and 99 %. The nucleotide site diversity with background selection (B) relative to its expectation under strict neutrality is shown in each panel. The simulated (black bars) and adjusted (grey bars) DFE represents the distribution of $2Ns_d$ and $2NBs_d$ respectively. The error bars denote the standard deviation of proportions estimated from 5 independent replicates.

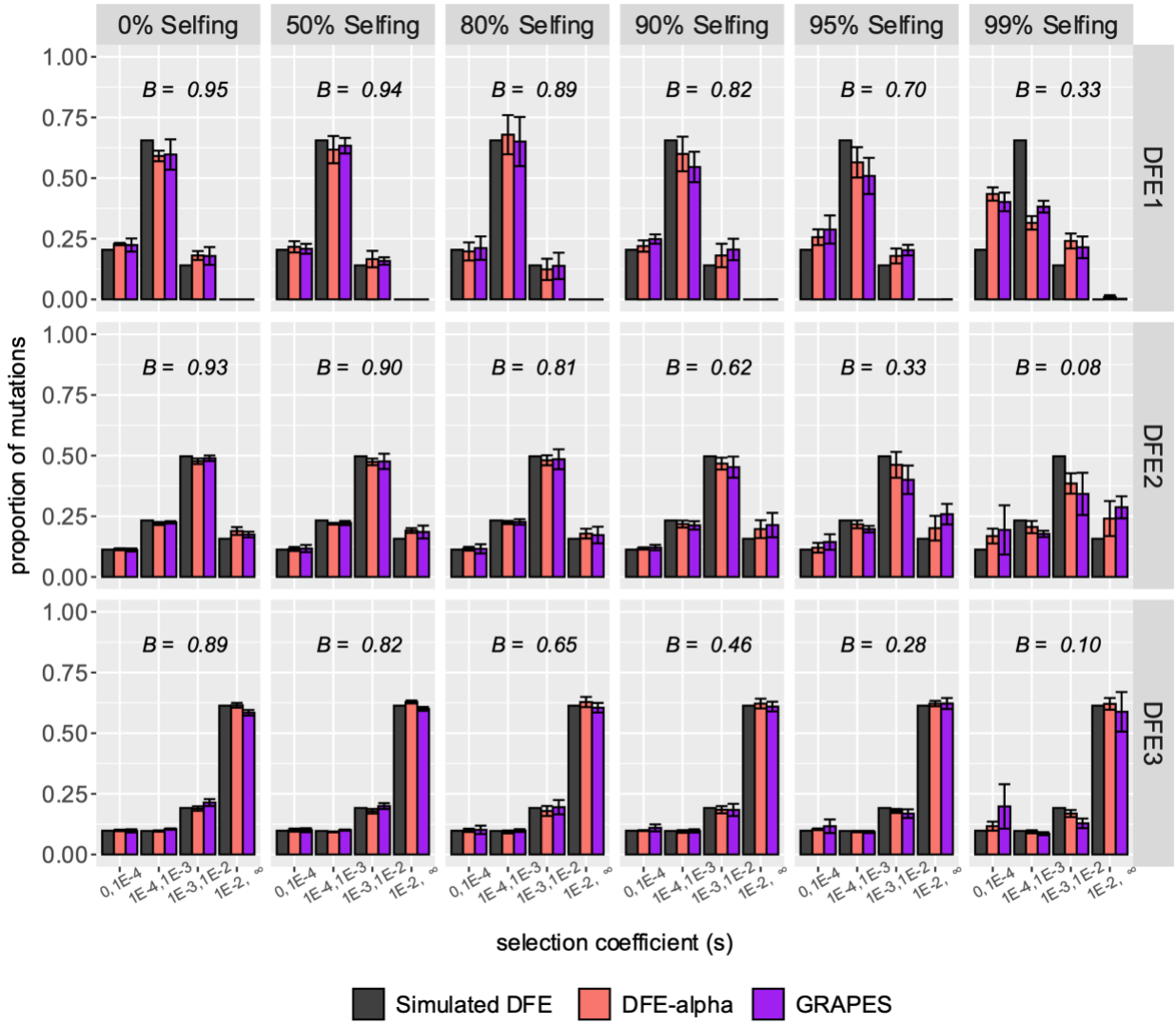

Supplementary Figure 2: Effects of selfing on the inference of the DFE of new deleterious mutations using DFE-alpha (red bars) and GRAPES (purple bars). Here the DFE is displayed as the distribution of s_d, which was created by dividing the mean of the gamma distribution ($2N_e s_d$) by $2BN$. Results are shown in terms of the proportion of mutations in effectively neutral ($0 \leq s_d < 1 \times 10^{-4}$), weakly deleterious ($1 \times 10^{-4} \leq s_d < 1 \times 10^{-3}$), moderately deleterious ($1 \times 10^{-3} \leq s_d < 1 \times 10^{-2}$) and strongly deleterious ($1 \times 10^{-2} \leq s_d < \infty$) classes. Selfing rates were varied between 0 and 99 %. The black bars represent the simulated distribution of s_d. The error bars denote the standard deviation of proportions estimated from 5 independent replicates.

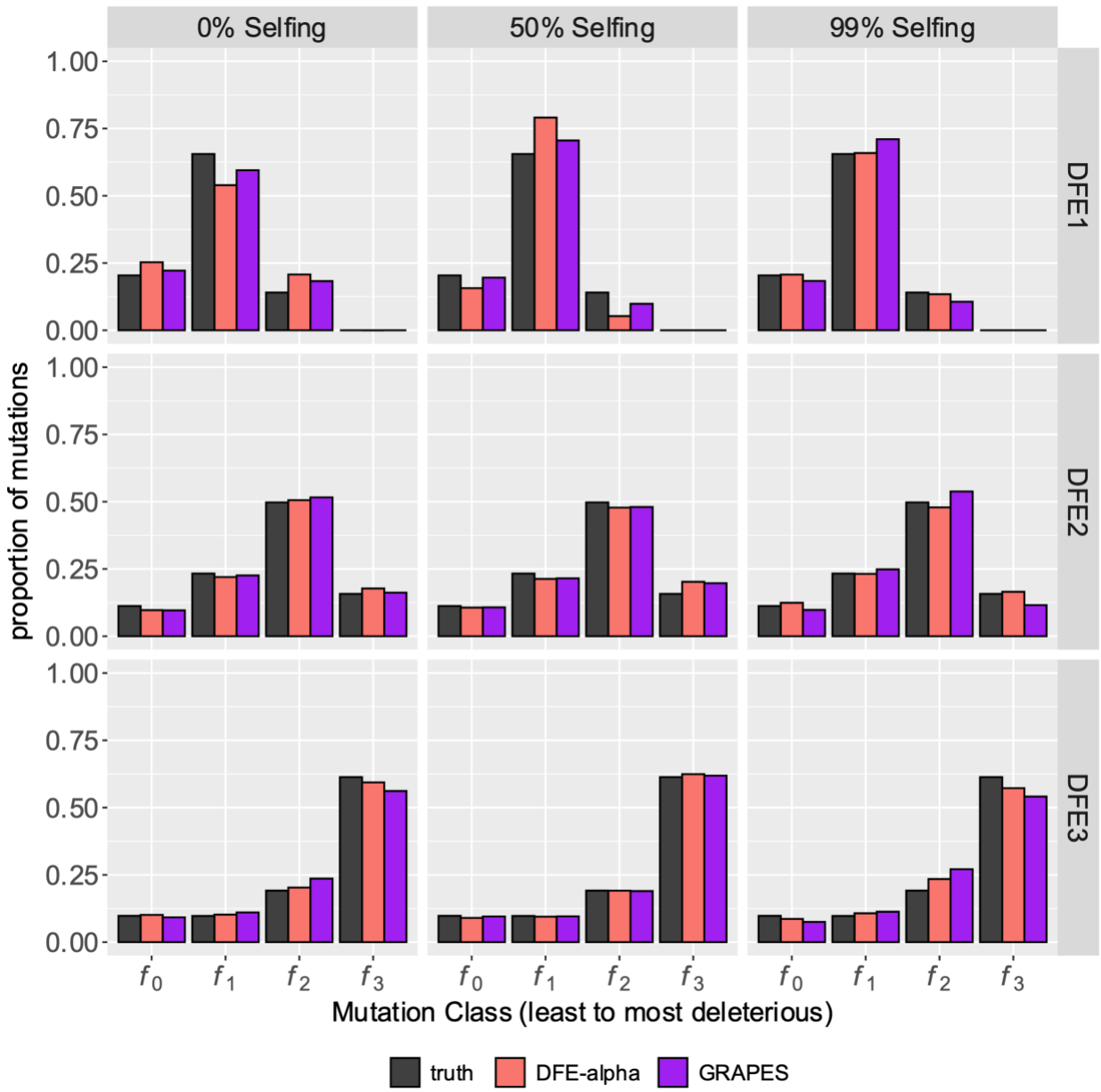

Supplementary Figure 3: Inference of the DFE of new deleterious mutations in partially selfing populations using DFE-alpha and GRAPES for simulations with no linkage. Here, 50,000 selected mutations were simulated individually (as single locus simulations) in various selfing rates without linkage to other selected mutations. Results are shown in terms of the proportion of mutations in effectively neutral (f_0), weakly deleterious (f_1), moderately deleterious (f_2) and strongly deleterious (f_3) classes.

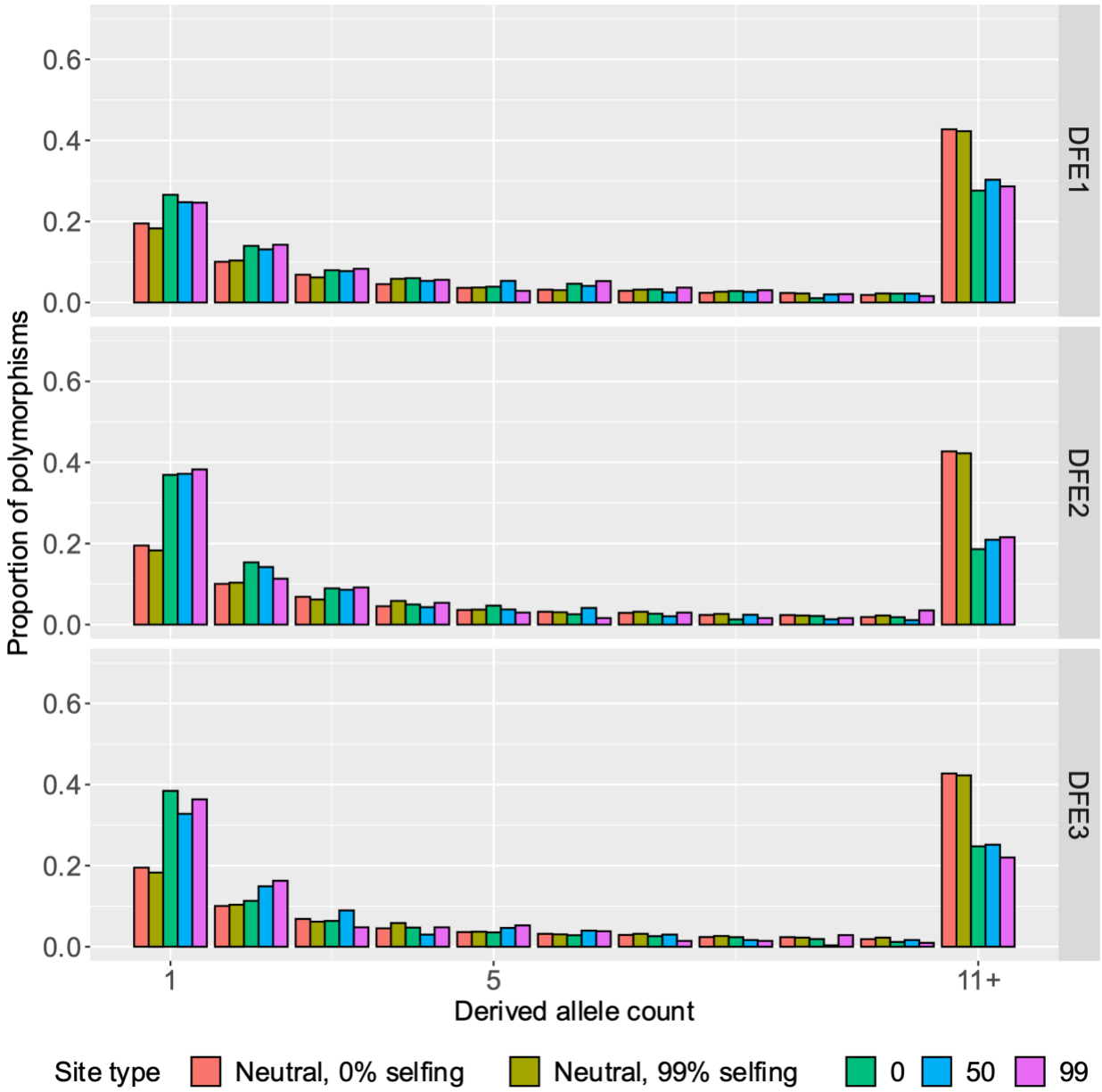

Supplementary Figure 4: Site frequency spectra of neutral and selected alleles in partially selfing populations from single-site simulations. 100 genomes were sampled and all selected mutations were additive and deleterious The *y*-axis represents the proportion of segregating polymorphisms that fall into the given allele-count class. The last class (11+) refers to the derived allele counts 11-100. The SFS of neutral sites is shown in red, while the SFS of selected sites in simulations with 0%, 50%, and 99% selfing are shown as green, blue, and purple bars respectively.

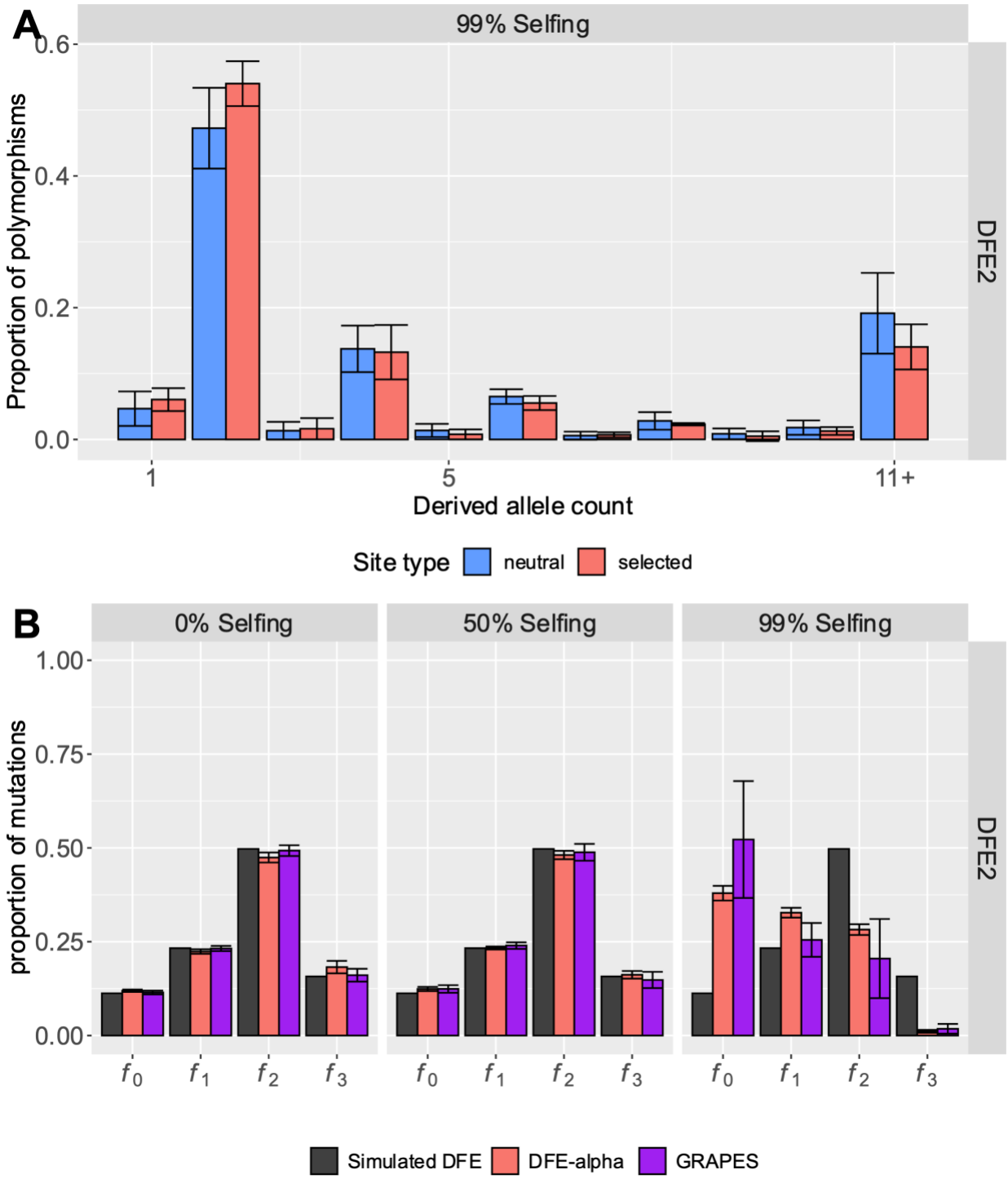

Supplementary Figure 5: (A) The SFS at neutral (blue) and selected (red) sites when 50 diploid individuals are sampled (instead of 100 random genomes). (B) The accuracy of DFE inference when 50 diploid individuals are sampled (instead of 100 random genomes). Results are shown for a predominantly moderately deleterious DFE (DFE2). Results are shown in terms of the proportion of mutations in effectively neutral (f_0), weakly deleterious (f_1), moderately deleterious (f_2) and strongly deleterious (f_3) classes. The error bars denote the standard deviation of proportions estimated from 5 independent replicates.

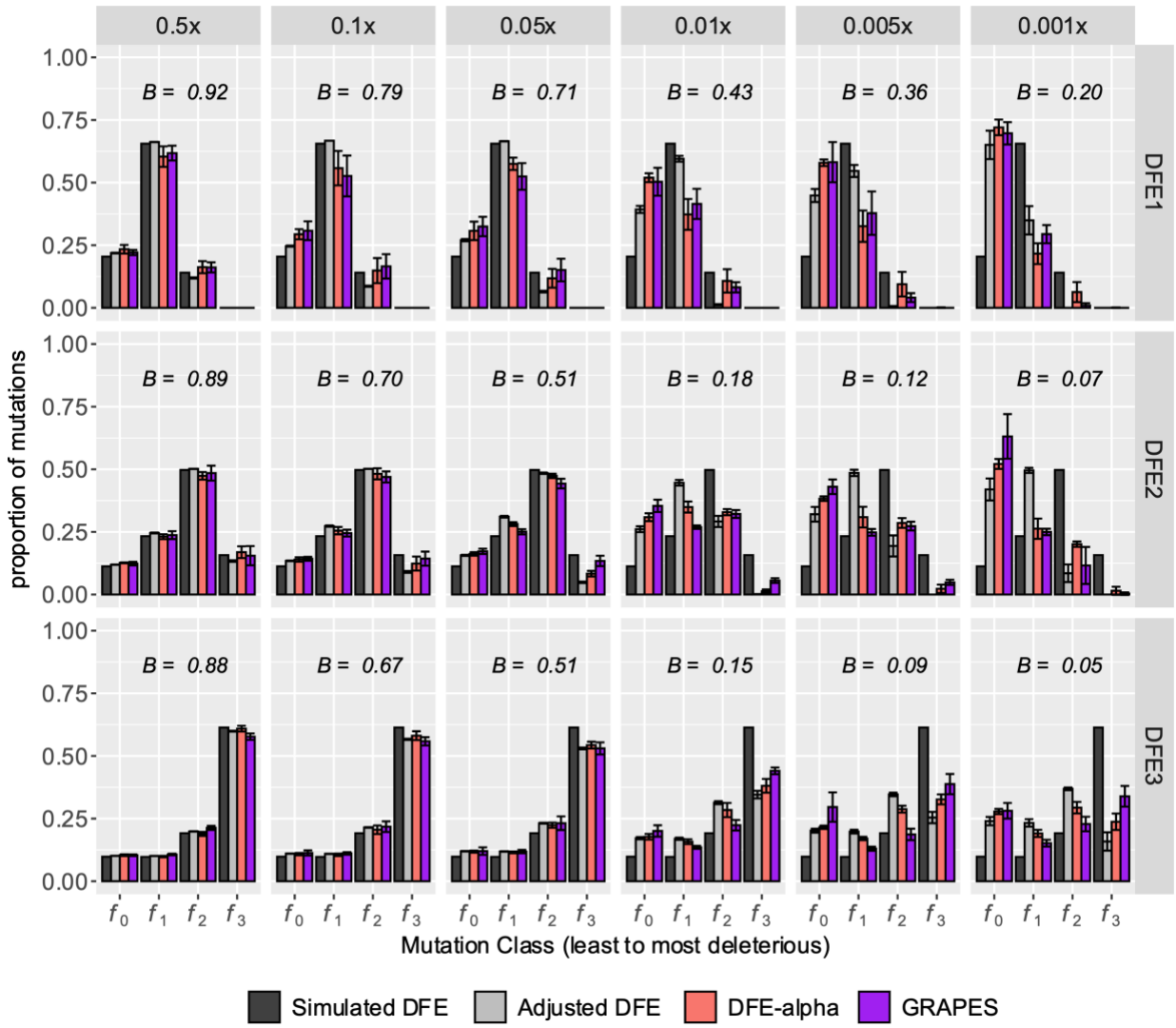

Supplementary Figure 6: Effects of low recombination rate on the inference of the DFE of new deleterious mutations using DFE-alpha (red bars) and GRAPES (purple bars). Results are shown in terms of the proportion of mutations in effectively neutral (f_0), weakly deleterious (f_1), moderately deleterious (f_2) and strongly deleterious (f_3) classes. Recombination rates were varied between 0.5 × mean and 0.001 × mean, where the mean recombination rate was 3.12×10^{-8} per site/generations. The nucleotide site diversity with background selection (B) relative to its expectation under strict neutrality is shown in each panel. The simulated DFE (shown in black) and adjusted DFE (shown in grey) represents the distribution of $2Ns_d$ and $2NBs_d$ respectively. The error bars denote the standard deviation of proportions estimated from 5 independent replicates.

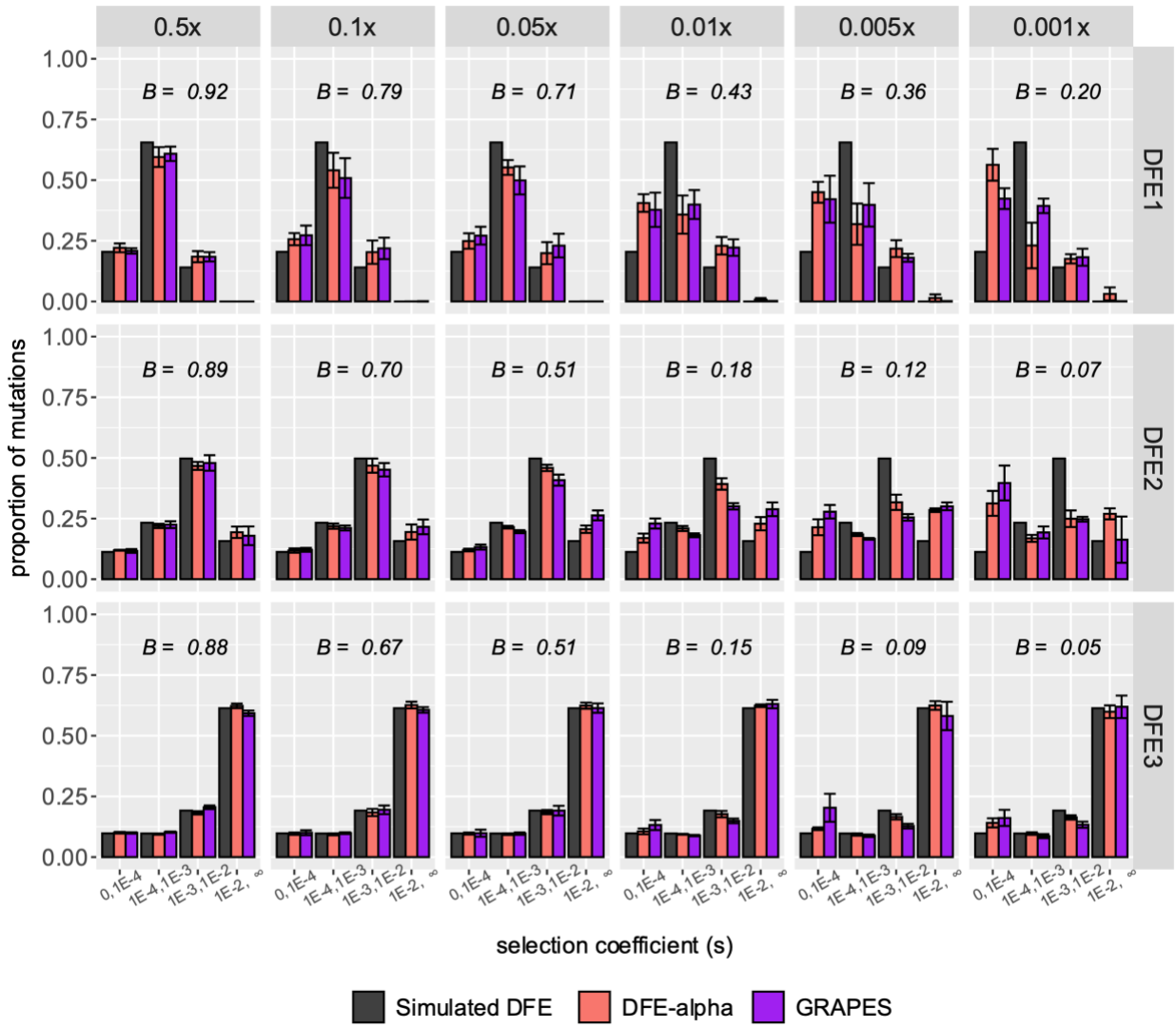

Supplementary Figure 7: Effects of low recombination rate on the inference of the DFE of new deleterious mutations using DFE-alpha (red bars) and GRAPES (purple bars). Here the DFE is displayed as the distribution of s_d, which was created by dividing the mean of the gamma distribution ($2N_e s_d$) by $2BN$. Results are shown in terms of the proportion of mutations in effectively neutral ($0 \leq s_d < 1 \times 10^{-4}$), weakly deleterious ($1 \times 10^{-4} \leq s_d < 1 \times 10^{-3}$), moderately deleterious ($1 \times 10^{-3} \leq s_d < 1 \times 10^{-2}$) and strongly deleterious ($1 \times 10^{-2} \leq s_d < \infty$) classes. Recombination rates were varied between 0.5 × mean and 0.001 × mean, where the mean recombination rate was 3.12×10^{-8} per site/generations. The black bars represent the simulated distribution of s_d. The error bars denote the standard deviation of proportions estimated from 5 independent replicates.

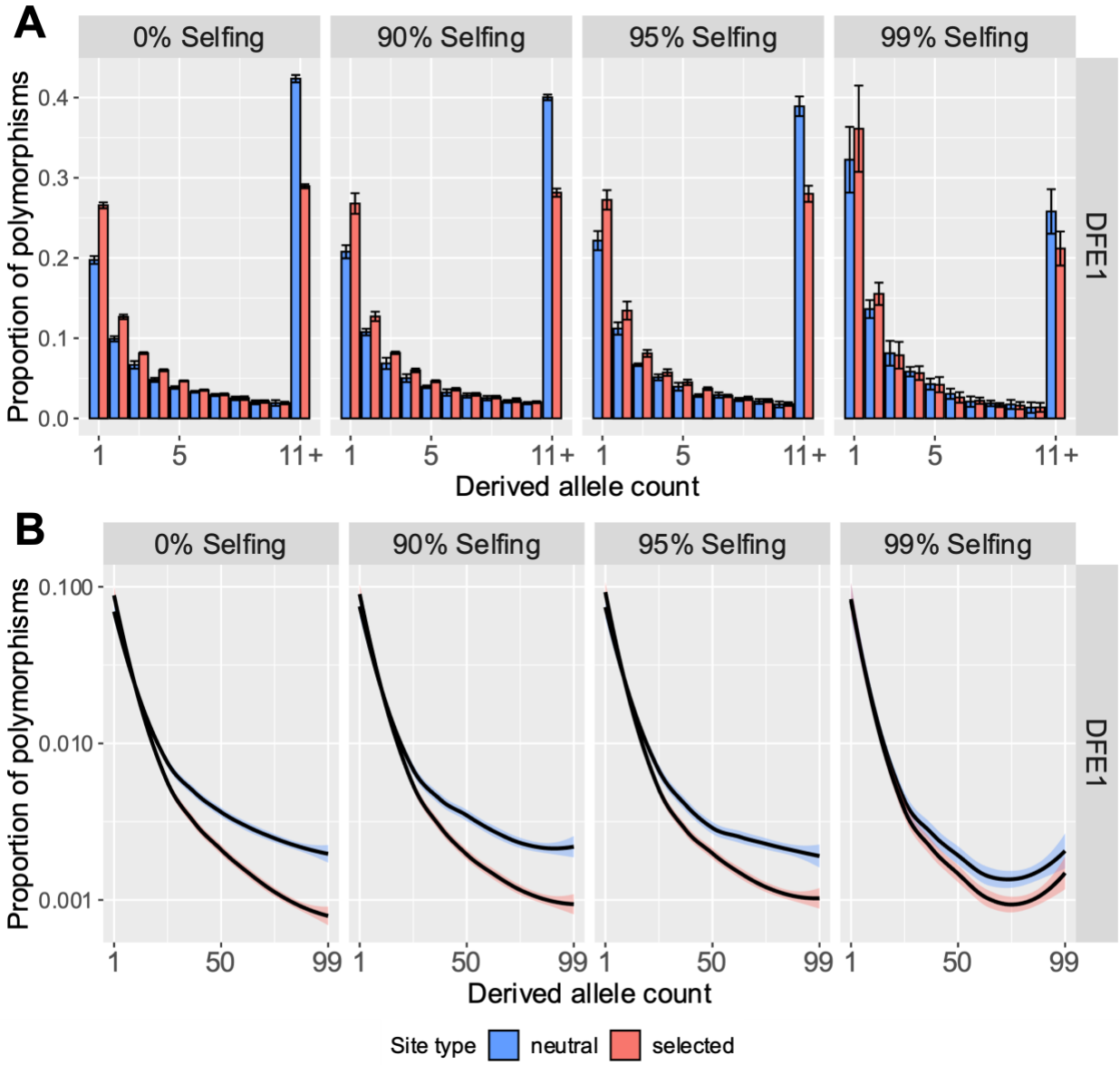

Supplementary Figure 8: Site frequency spectra of neutral and selected alleles from 100 genomes sampled from simulations where all selected mutations were deleterious, for the weakly deleterious DFE. For **(A)** the y-axis represents the proportion of segregating polymorphisms that fall into the given derived allele count. The last class (11+) refers to the derived allele counts 11-99. The error bars denote the standard deviation of proportions estimated from 5 independent replicates. For **(B)** the y-axis is plotted on a log scale, with all derived allele counts displayed. Lines were smoothed with LOESS.

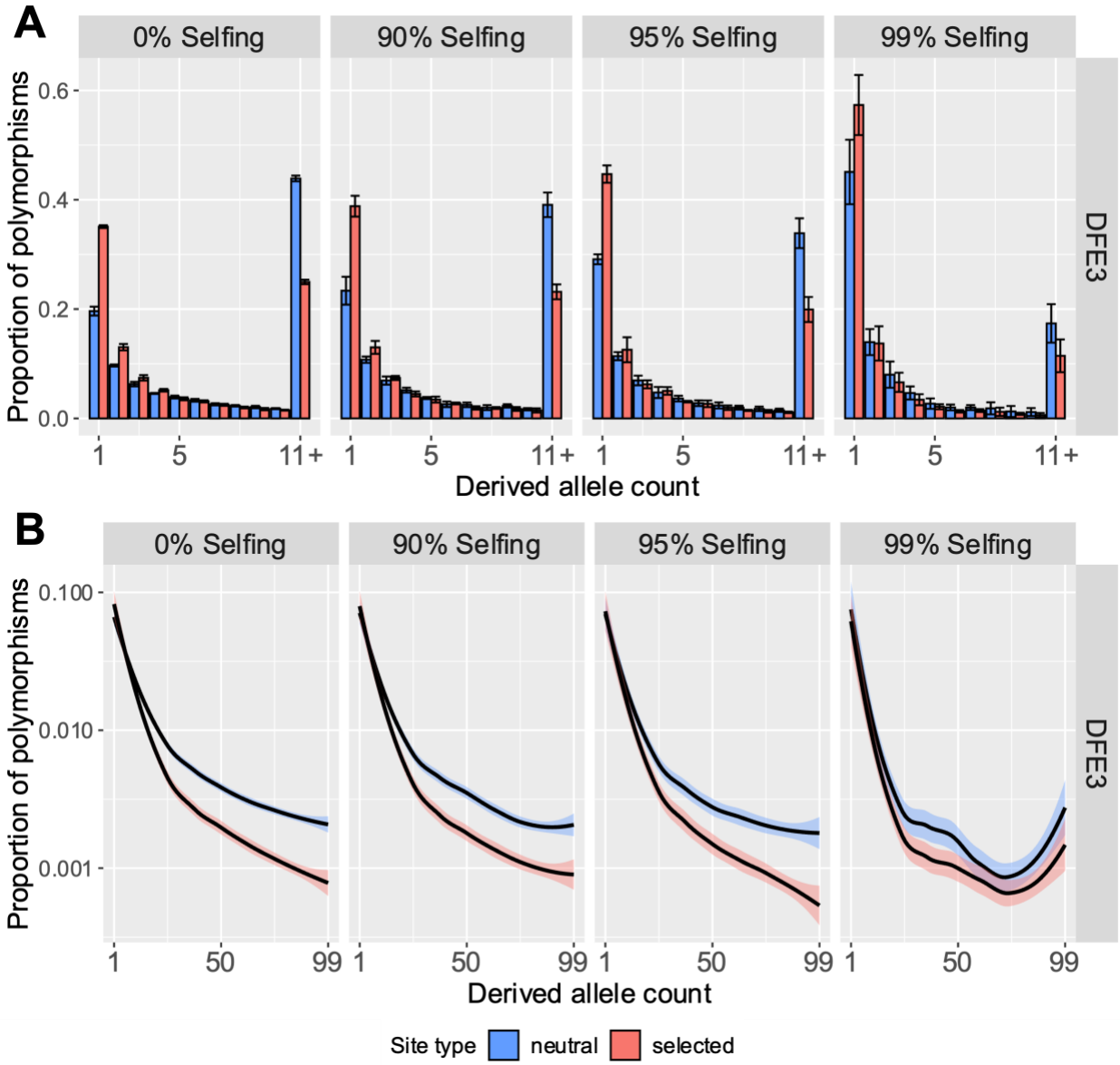

Supplementary Figure 9: Site frequency spectra of neutral and selected alleles from 100 genomes sampled from simulations where all selected mutations were deleterious, for the strongly deleterious DFE. For **(A)** the y-axis represents the proportion of segregating polymorphisms that fall into the given derived allele count. The last class (11+) refers to the derived allele counts 11-99. The error bars denote the standard deviation of proportions estimated from 5 independent replicates. For **(B)** the y-axis is plotted on a log scale, with all derived allele counts displayed. Lines were smoothed with LOESS.

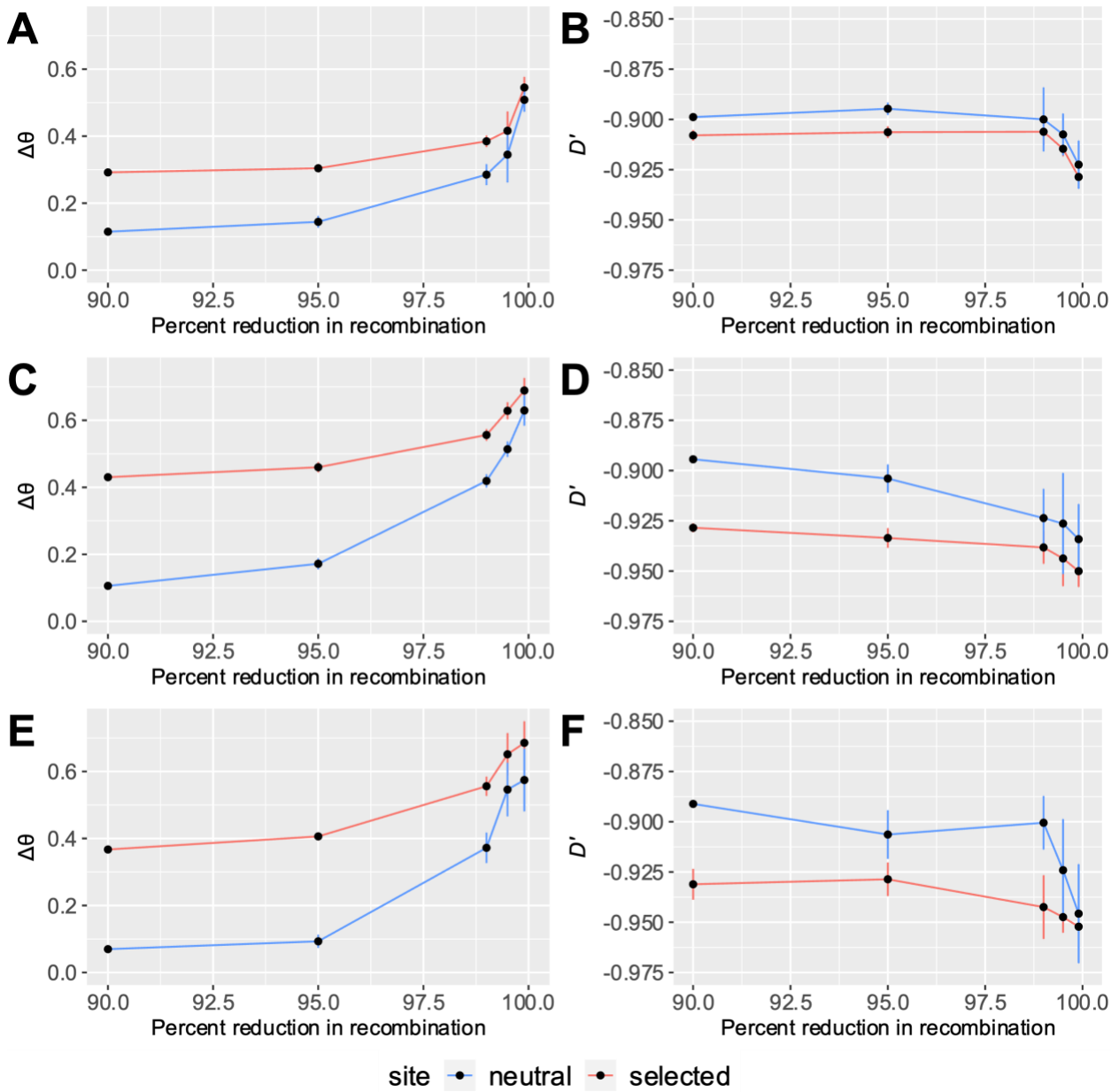

Supplementary Figure 10: Effects of low recombination on the SFS and linkage disequilibrium (LD) at neutral (red lines) and selected (blue lines) sites. The skew in the SFS was quantified using $\Delta\theta$ for DFE1 (**A**), DFE2 (**C**), and DFE3 (**E**), calculated using alleles at all frequencies, while LD was summarized by the statistic D' for DFE1 (**B**), DFE2 (**D**), and DFE3 (**F**), calculated for alleles at frequencies of 1%-5%. The error bars denote the standard deviation of the genome-wide average of each summary statistic estimated from 5 independent replicates.

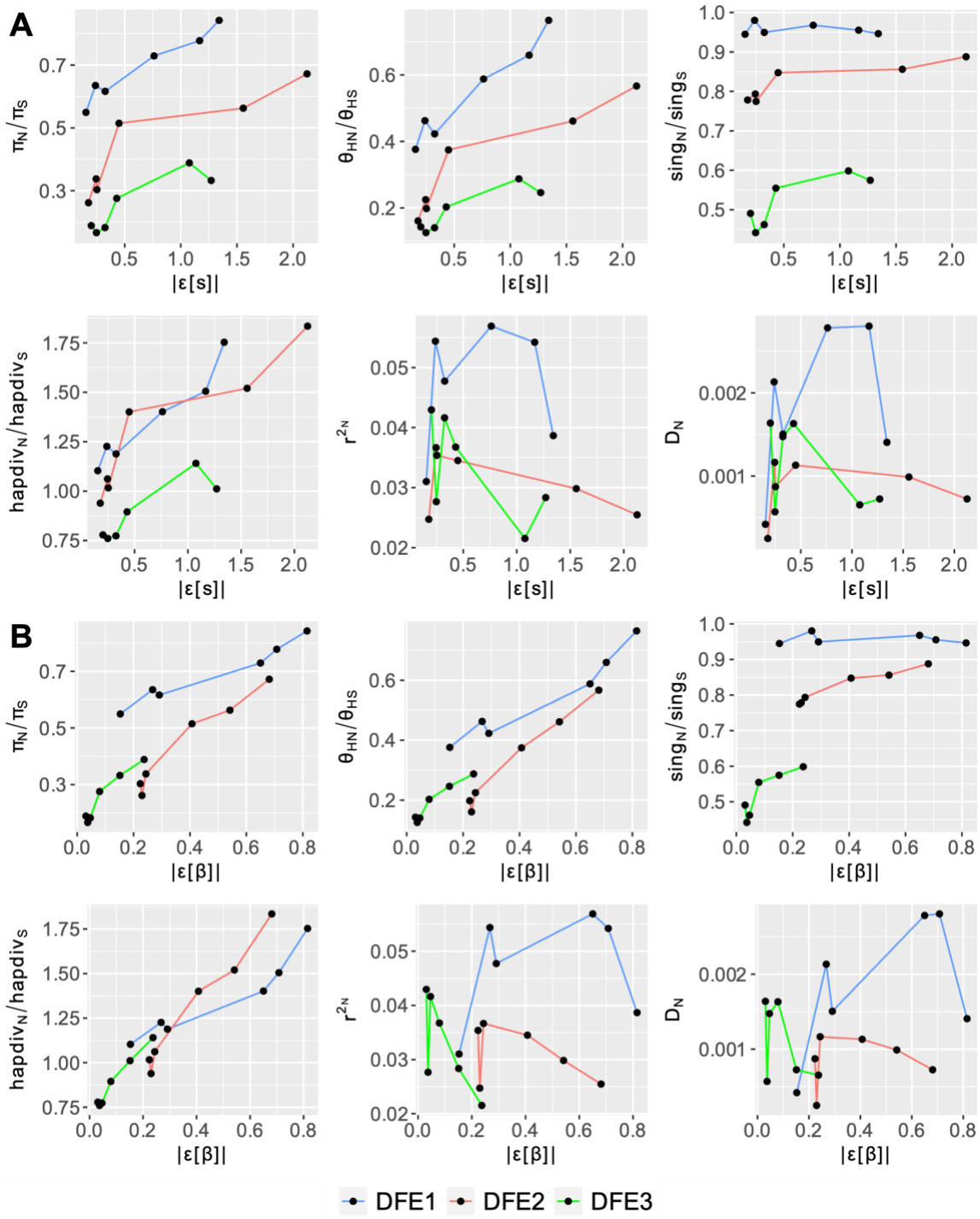

Supplementary Figure 11: Correlation of error in inference of the parameters $2Ns$ (**A**) and β (**B**) by DFE-alpha with various summary statistics calculated by pylibseq. Data points represent the average error and statistic value averaged over five replicates. The skew in the SFS was quantified using π (per site), θ_H (per site), and singleton density ($sing$), while LD was summarized by the statistics haplotype diversity ($hapdiv$), D, and r^2 using minor alleles across the window. Most statistics were calculated in 5000 bp windows for all allele frequencies, and values for nonsynonymous sites were divided by synonymous sites. However, D and r^2 were calculated for only nonsynonymous alleles at frequencies of 1%-5%.

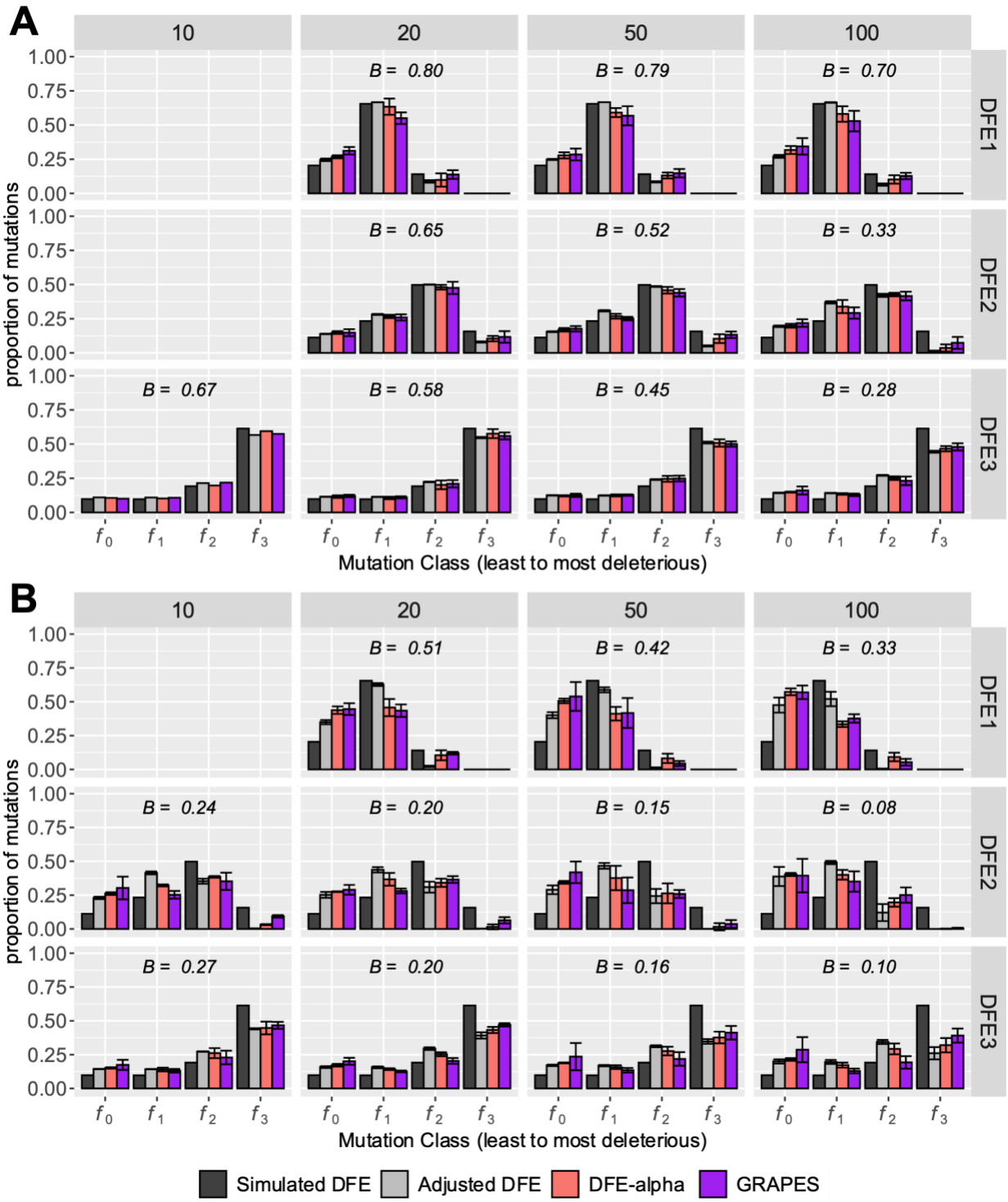

Supplementary Figure 12: Effects of varying the rescaling factor on the estimated DFE of new deleterious mutations in partially selfing organisms using DFE-alpha and GRAPES at selfing rates of (**A**) 95% and (**B**) 99%. The rescaling factors were reduced from the original 100 to 50, 20, and 10 (denoted on top of the columns). The error bars denote the standard deviation of proportions estimated from 5 independent replicates, except for the rescaling factor of 10, where only one replicate of DFE3 at 95% selfing and three replicates each for DFE2 and DFE3 at 99% selfing were completed.

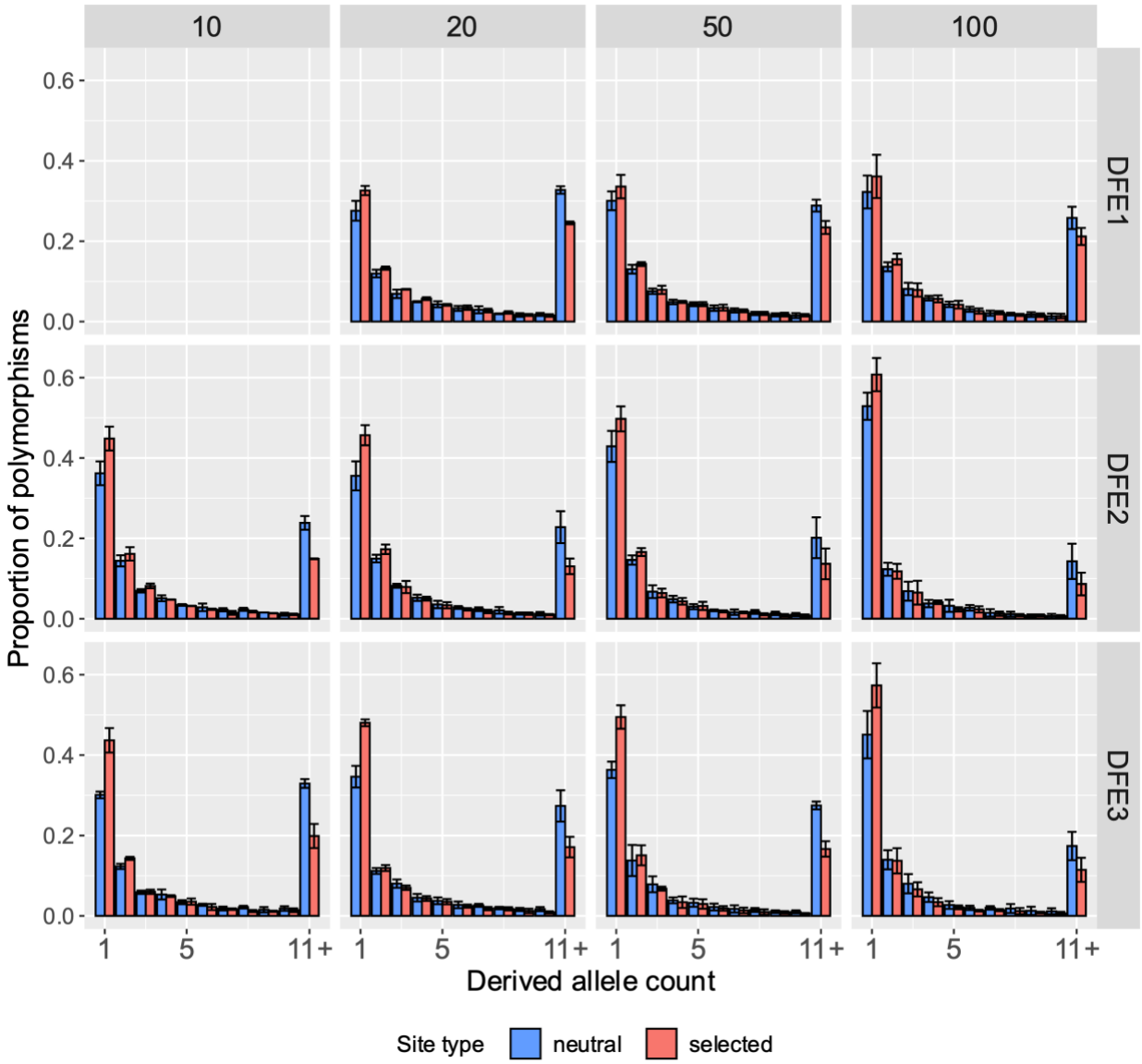

Supplementary Figure 13: Site frequency spectra of neutral and selected alleles from 100 genomes sampled from simulations with 99% selfing where all selected mutations were deleterious, with varying rescaling factors plotted on the x-axis. The y-axis represents the proportion of segregating polymorphisms that fall into the given derived allele count. The last class (11+) refers to the derived allele counts 11-99. The error bars denote the standard deviation of proportions estimated from 5 independent replicates, except for the rescaling factor of 10, where only three replicates each for DFE2 and DFE3 were completed.

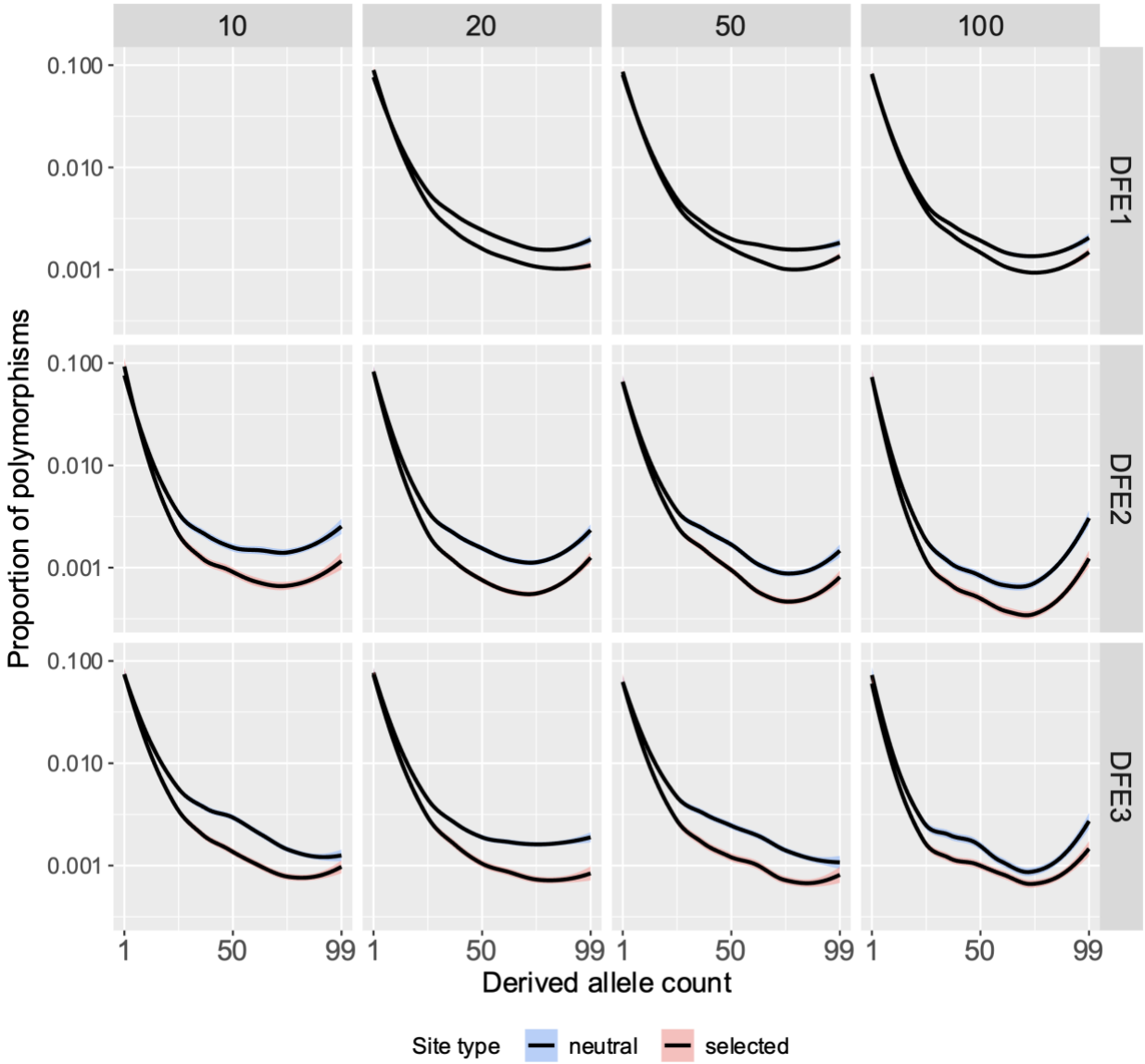

Supplementary Figure 14: Site frequency spectra of neutral and selected alleles from 100 genomes sampled from simulations where all selected mutations were deleterious, with varying rescaling factors plotted on the x-axis. The y-axis is plotted on a log scale, with all derived allele counts (frequencies 1-99) displayed. Lines were smoothed with LOESS.

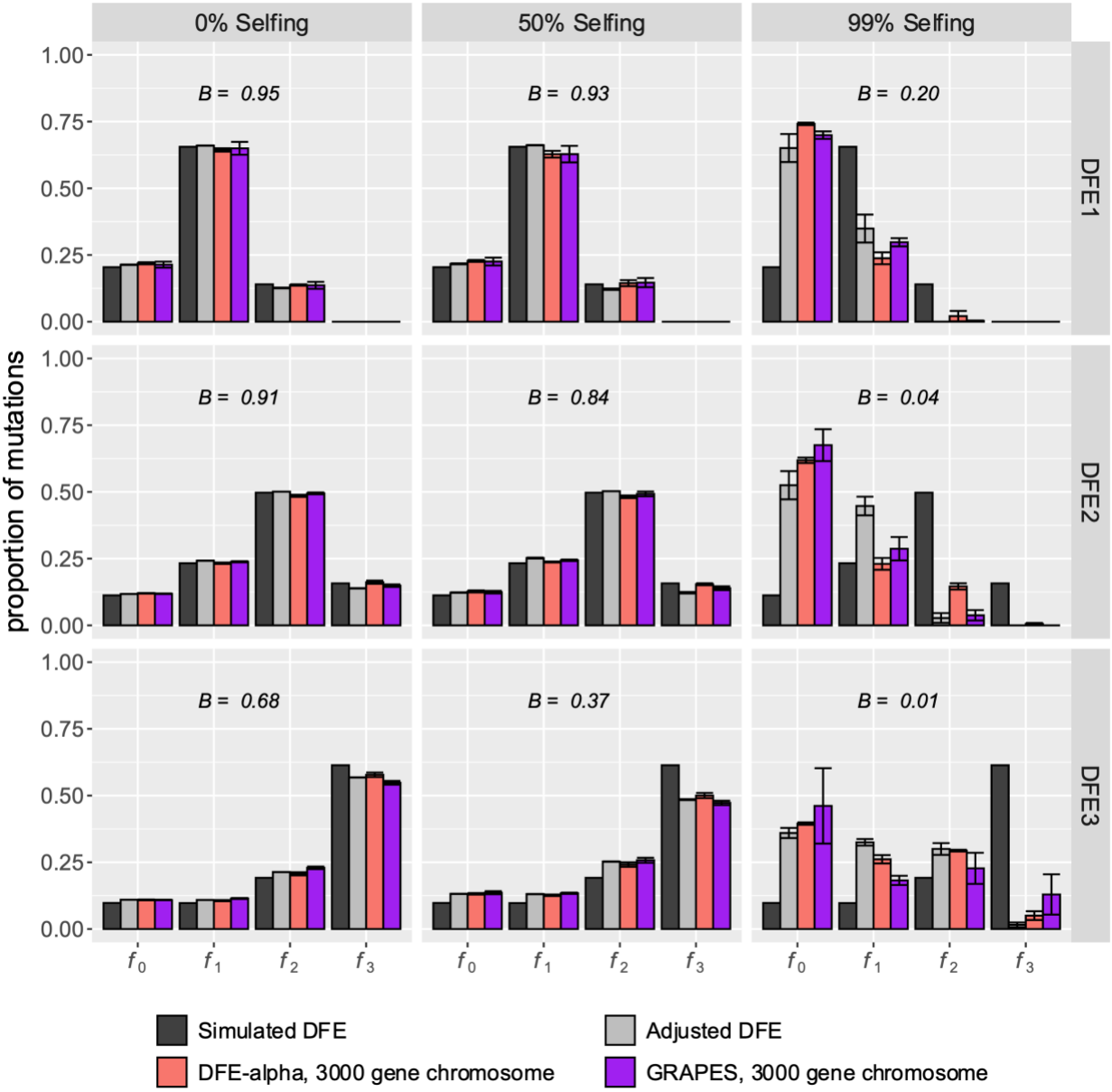

Supplementary Figure 15: The inference of the deleterious DFE when varying chromosome sizes were simulated: a chromosome with 500 genes (shown in darker shades) vs a chromosome with 3000 genes (shown in lighter shades). Results are shown in terms of the proportion of mutations in effectively neutral (f_0), weakly deleterious (f_1), moderately deleterious (f_2) and strongly deleterious (f_3) classes. The nucleotide site diversity with background selection (B) relative to its expectation under strict neutrality is shown in each panel. The adjusted DFE represents the distribution of $2NBs_d$. Inference was performed using DFE-alpha (red bars) and GRAPES purple bars). The error bars denote the standard deviation of proportions estimated from 5 independent replicates.

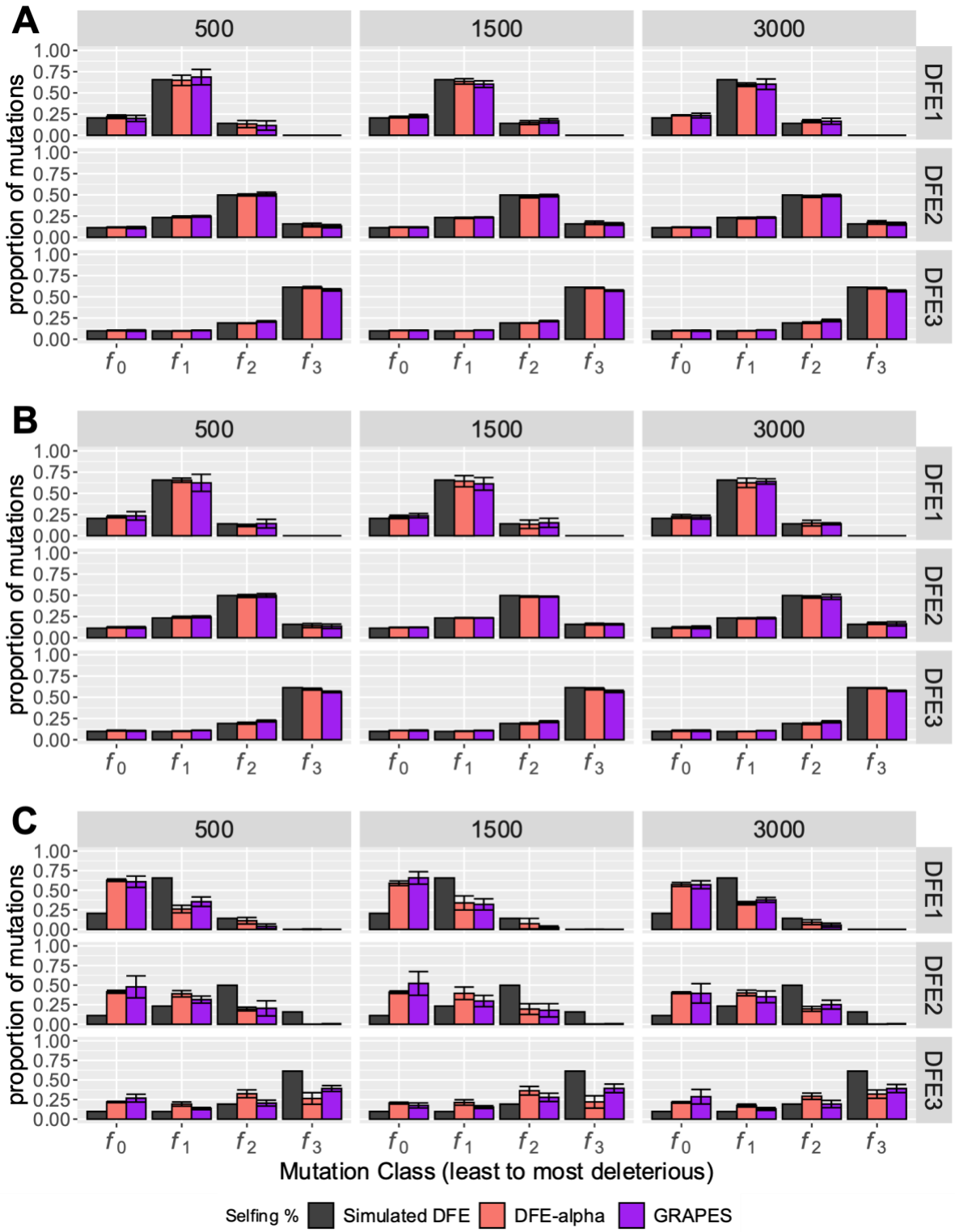

Supplementary Figure 16: Effects of varying the coding density on the estimated DFE of new deleterious mutations in partially selfing organisms using DFE-alpha and GRAPES at selfing rates of (**A**) 0%, (**B**) 50%, and (**C**) 99%. The intergenic regions were reduced from the original 3000 bp to 1500 bp and 500 bp (denoted on top of the columns). The error bars denote the standard deviation of proportions estimated from 5 independent replicates.

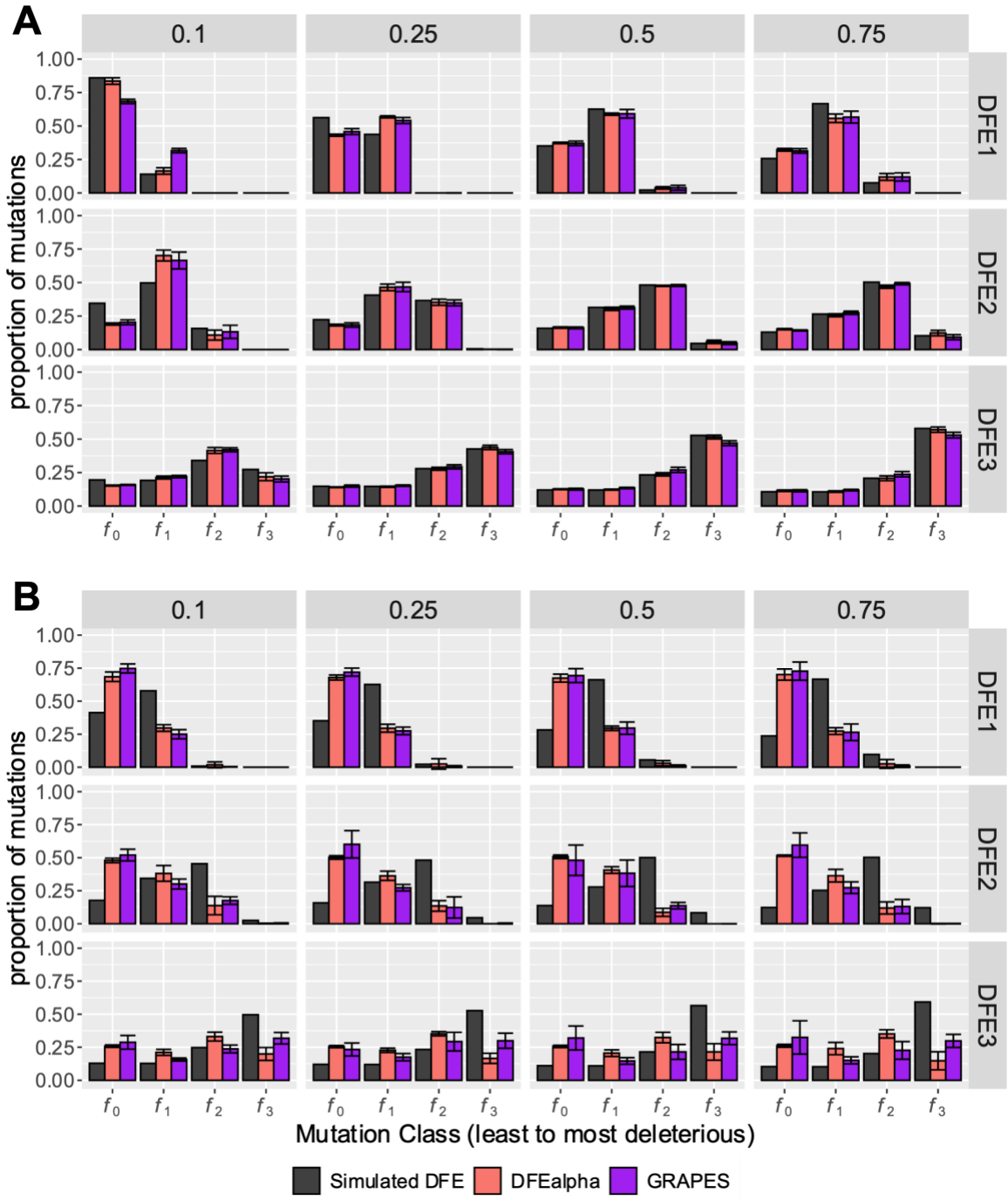

Supplementary Figure 17: Effects of selfing on DFE inference of new deleterious mutations with varying dominance coefficients using DFE-alpha (red bars) and GRAPES (purple bars). The dominance of selected mutations is noted at the top of each column. Results are shown for populations with **(A)** 0% selfing and **(B)** 99% selfing. Here the effectively neutral (f_0), weakly deleterious (f_1), moderately deleterious (f_2) and strongly deleterious (f_3) classes represent $0 < 2N_{self}s_d h_{self} < 1$, $1 < 2N_{self}s_d h_{self} < 10$, $10 < 2N_{self}s_d h_{self} < 100$, and $100 < 2N_{self}s_d h_{self} < 2N_{self}$, respectively. The error bars denote the standard deviation of proportions estimated from 5 independent replicates.

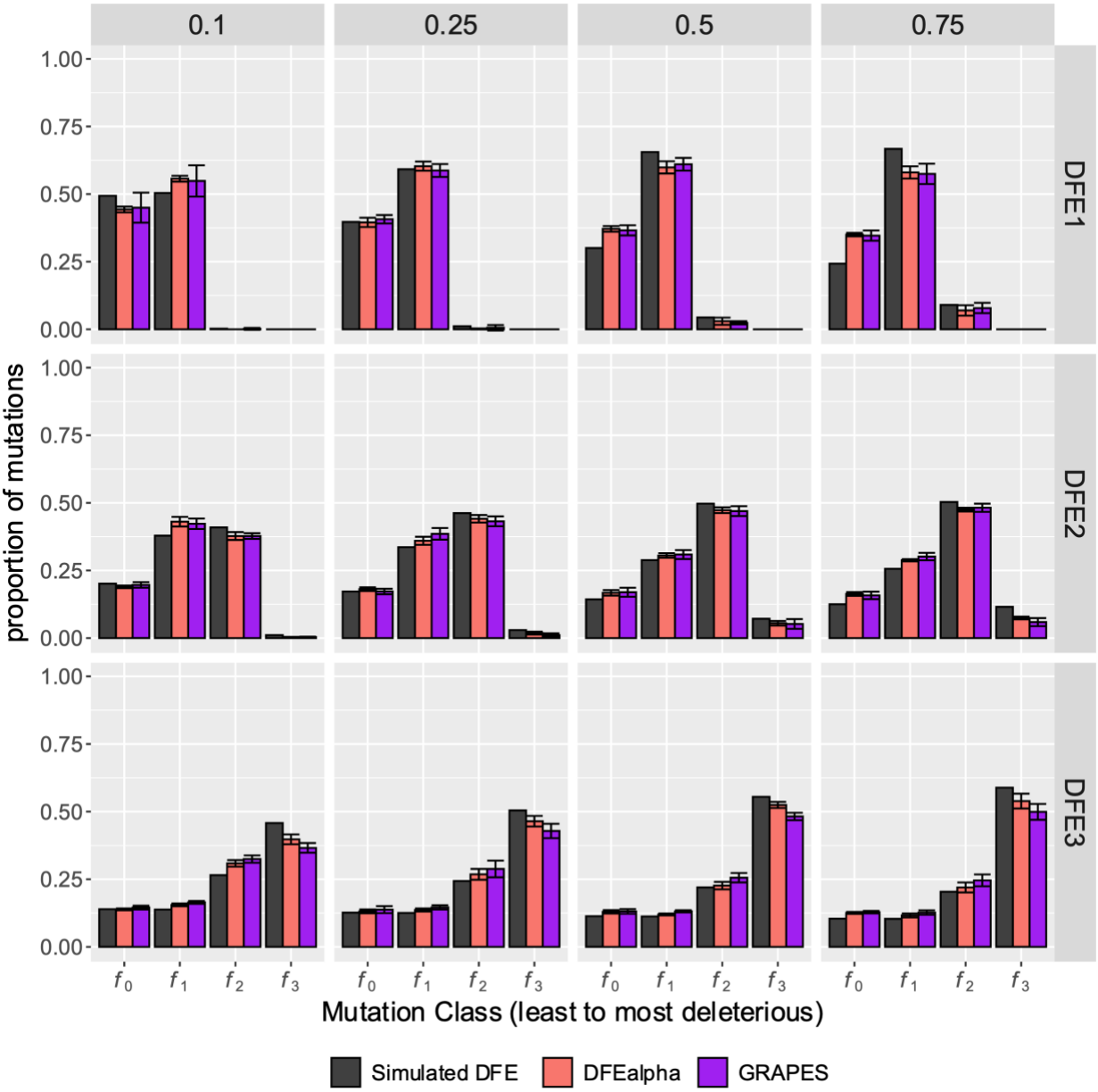

Supplementary Figure 18: Effects of selfing (50%) on the inference of the DFE of new deleterious mutations with varying dominance coefficients using DFE-alpha and GRAPES. The dominance of all new mutations is noted at the top of each column. The error bars denote the standard deviation of proportions estimated from 5 independent replicates.

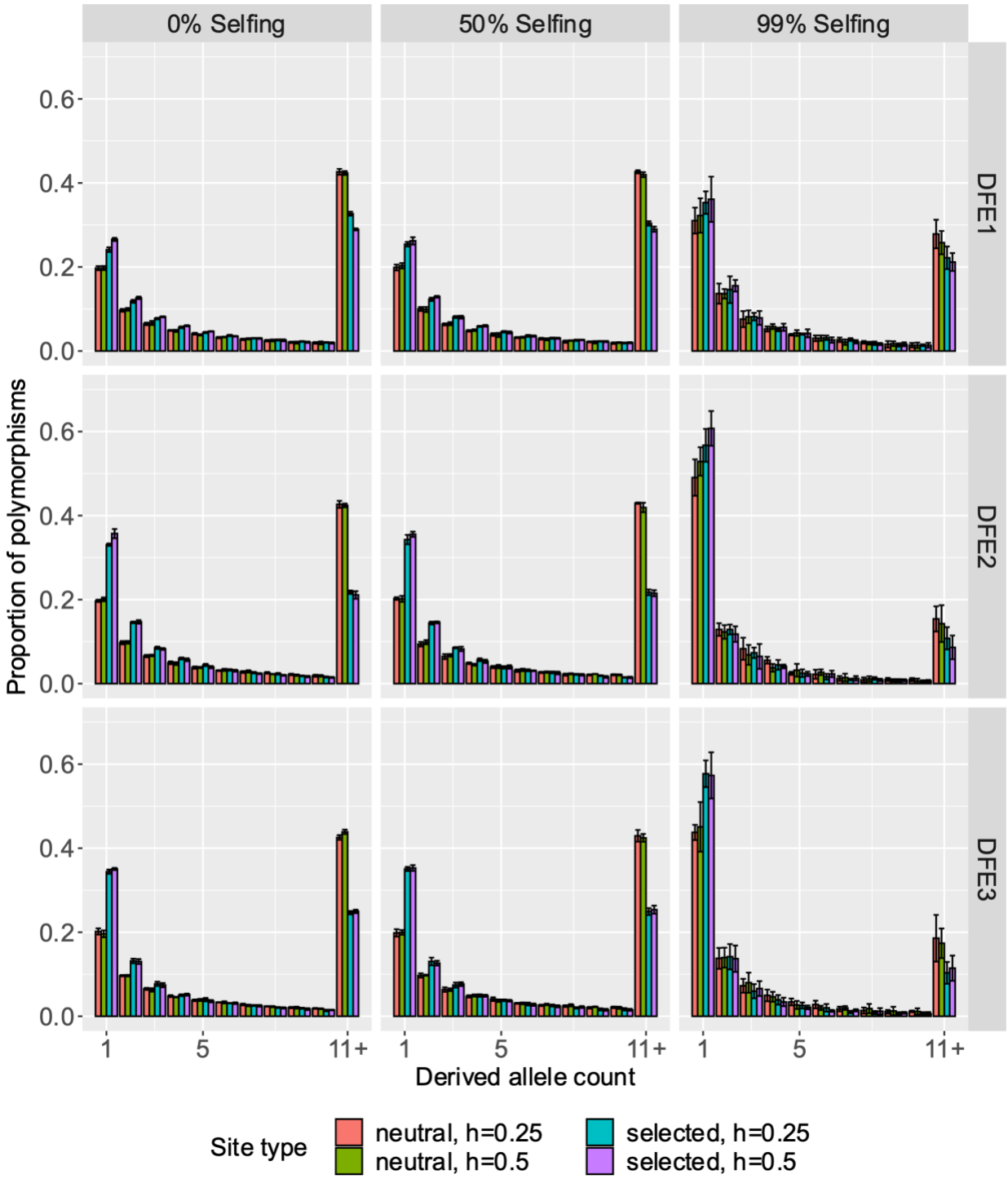

Supplementary Figure 19: Site frequency spectra of neutral and selected alleles for varying rates of selfing, dominance coefficients, and deleterious DFEs. 100 genomes were sampled from simulations. Selected mutations had a dominance coefficient $h = 0.25$ or 0.5.The y-axis represents the proportion of segregating polymorphisms that fall into the given allele-frequency class. The last class (11+) refers to the derived allele counts 11-100.

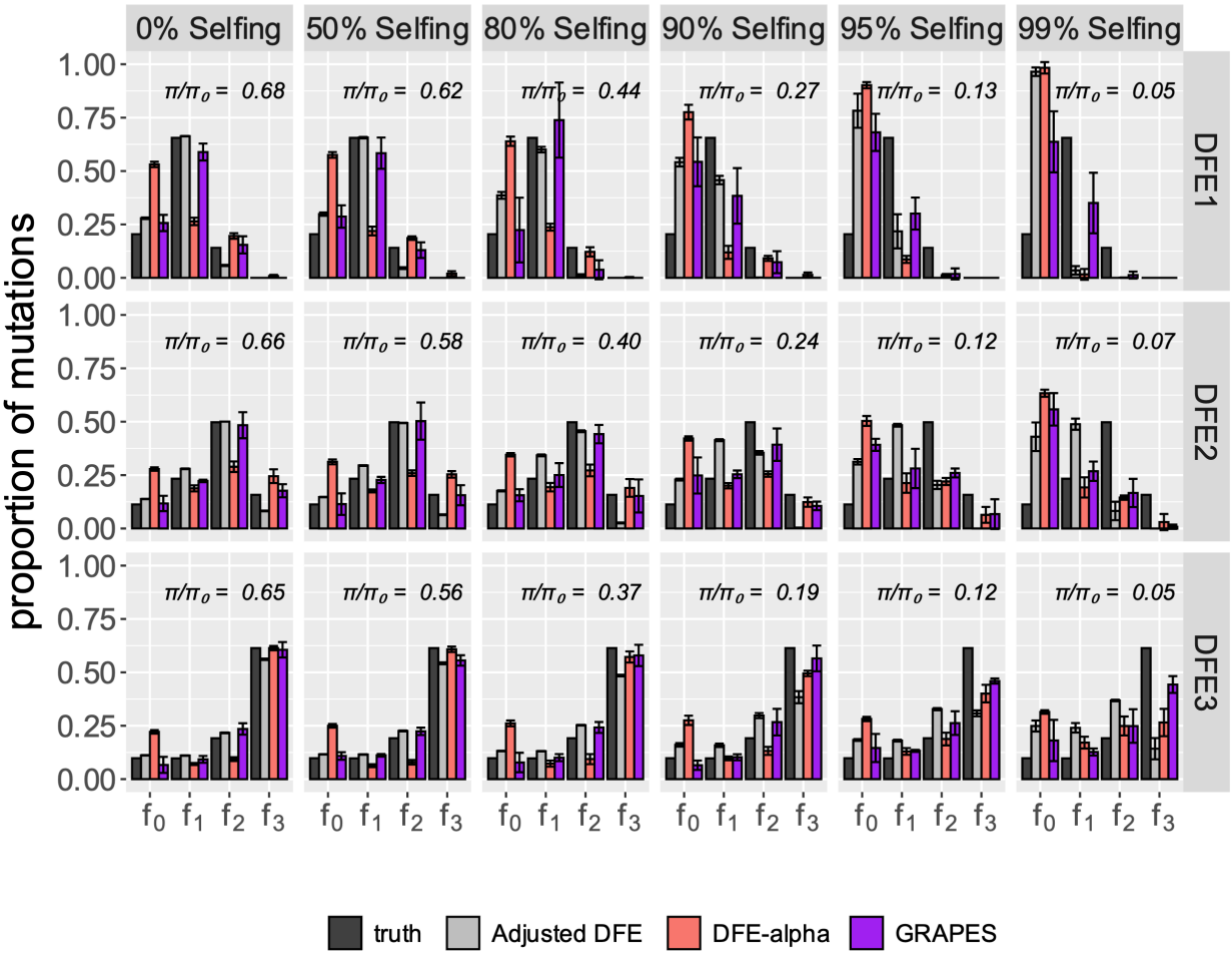

Supplementary Figure 20: Effects of selfing on the inference of the DFE of new deleterious mutations using DFE-alpha and GRAPES (shown in purple bars). Results are shown in terms of the proportion of mutations in effectively neutral (f_0), weakly deleterious (f_1), moderately deleterious (f_2) and strongly deleterious (f_3) classes. The adjusted DFE represents the distribution of $2N(\pi_{obs}/\pi_{exp})s_d$, where π_{obs} is the neutral nucleotide site diversity observed in each scenario and π_{exp} is the neutral nucleotide site diversity expected in a population of size N at strict neutrality. 0.1% of new exonic mutations were beneficial and exponentially distributed with a mean $2Ns_a = 200$. Here, the unfolded SFS was used for inference. The error bars denote the standard deviation of proportions estimated from 5 independent replicates.

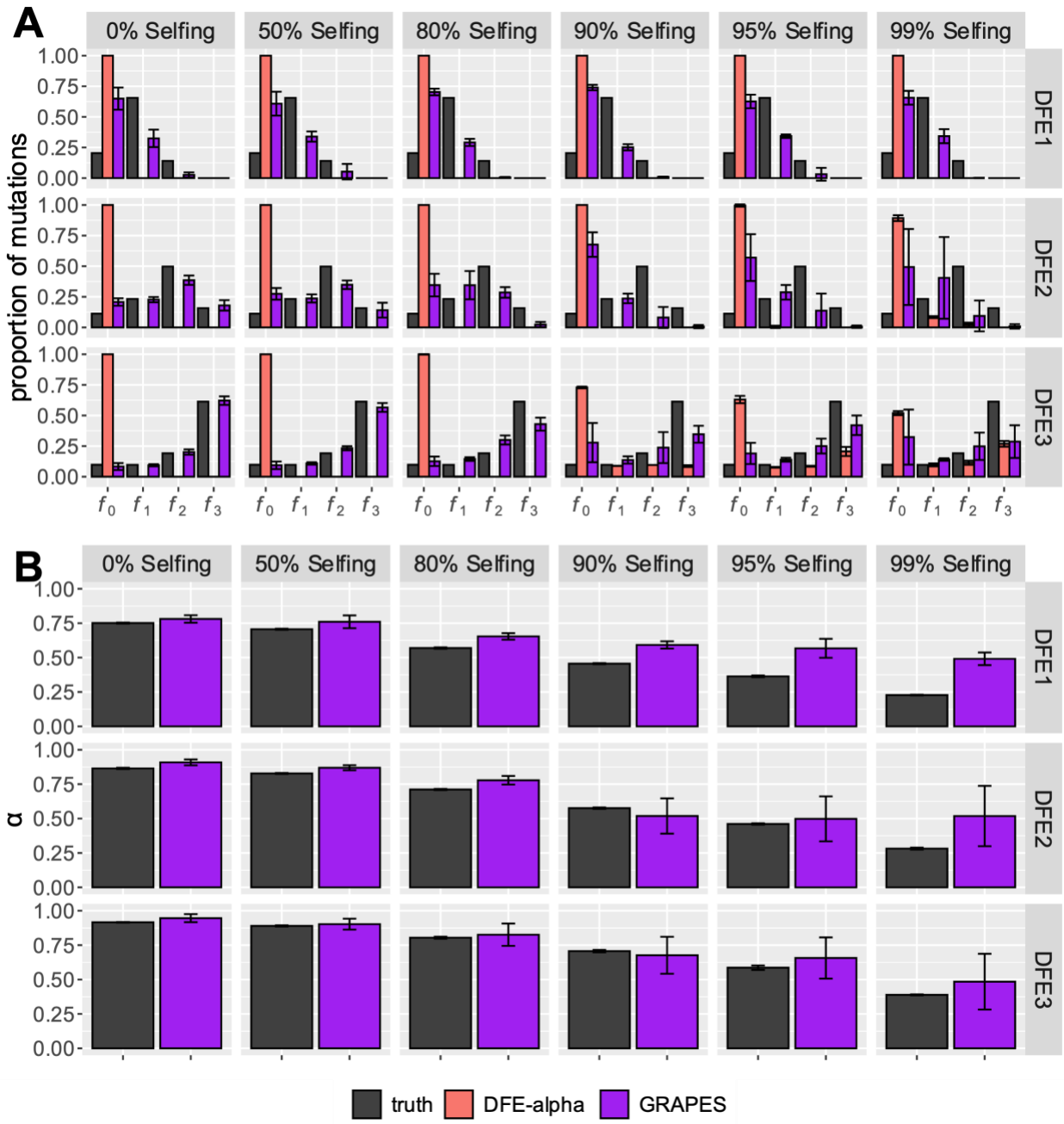

Supplementary Figure 21: Effects of selfing on the inference of (A) the DFE of new deleterious mutations and (B) the proportion of beneficial fixations (α) using DFE-alpha and GRAPES when beneficial mutations are common (1%). Results for A are shown in terms of the proportion of mutations in effectively neutral (f_0), weakly deleterious (f_1), moderately deleterious (f_2) and strongly deleterious (f_3) classes. Here, 1.0% of new exonic mutations were beneficial and exponentially distributed with a mean $2Ns_a = 200$. Here, the unfolded SFS was used for inference. The error bars denote the standard deviation of proportions estimated from 5 independent replicates.

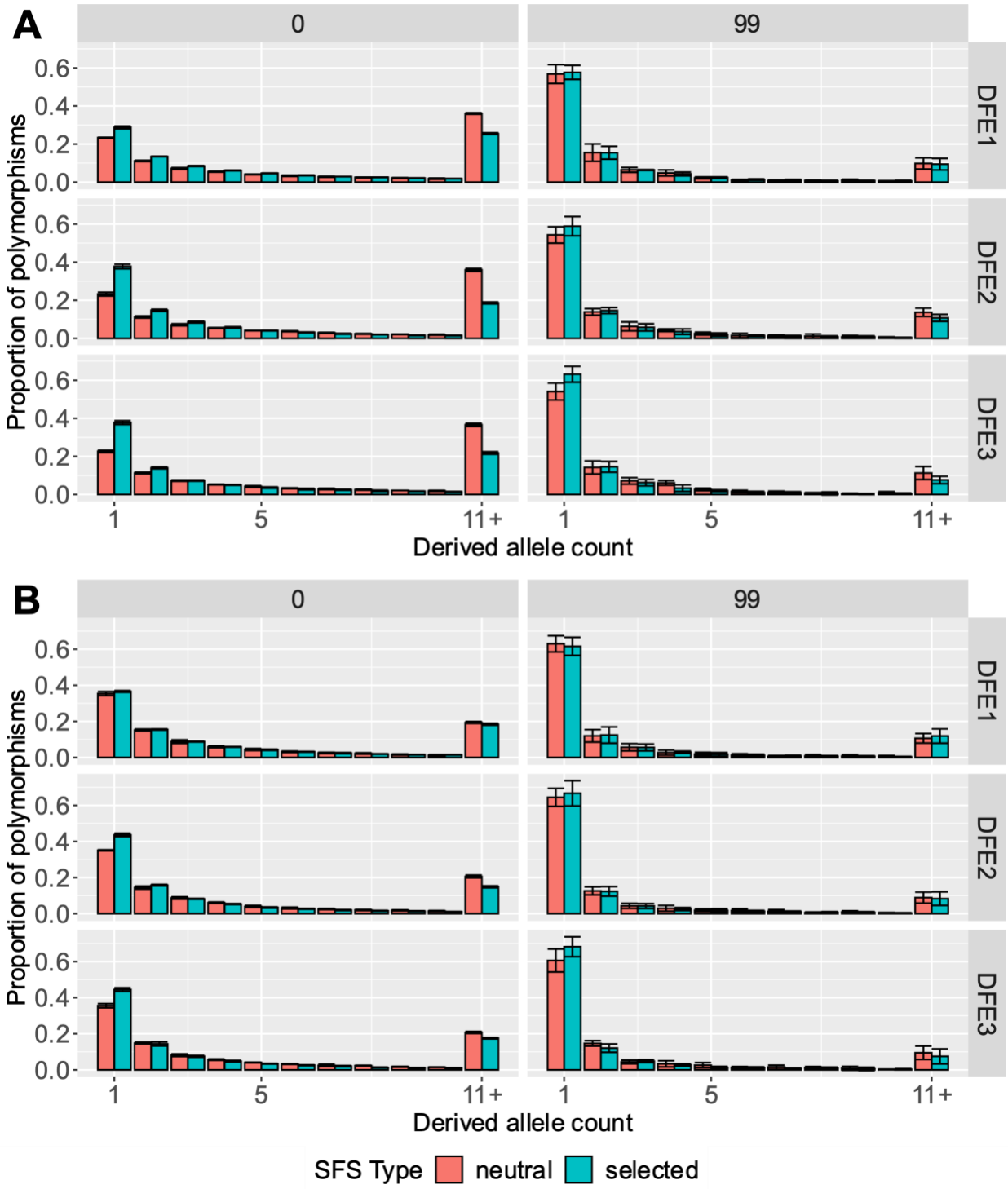

Supplementary Figure 22: Site frequency spectra of neutral vs selected sites when a full DFE was simulated (*i.e.*, both deleterious and beneficial mutations were present). 100 genomes were sampled and the y-axis depicts the proportion of segregating polymorphisms that fall into the given allele-count class. Panel **A** shows simulations where 0.1% of new mutations at selected sites were beneficial and Panel **B** shows simulations where 1% of new mutations at selected sites were beneficial. The error bars denote the standard deviation of proportions estimated from 5 independent replicates.

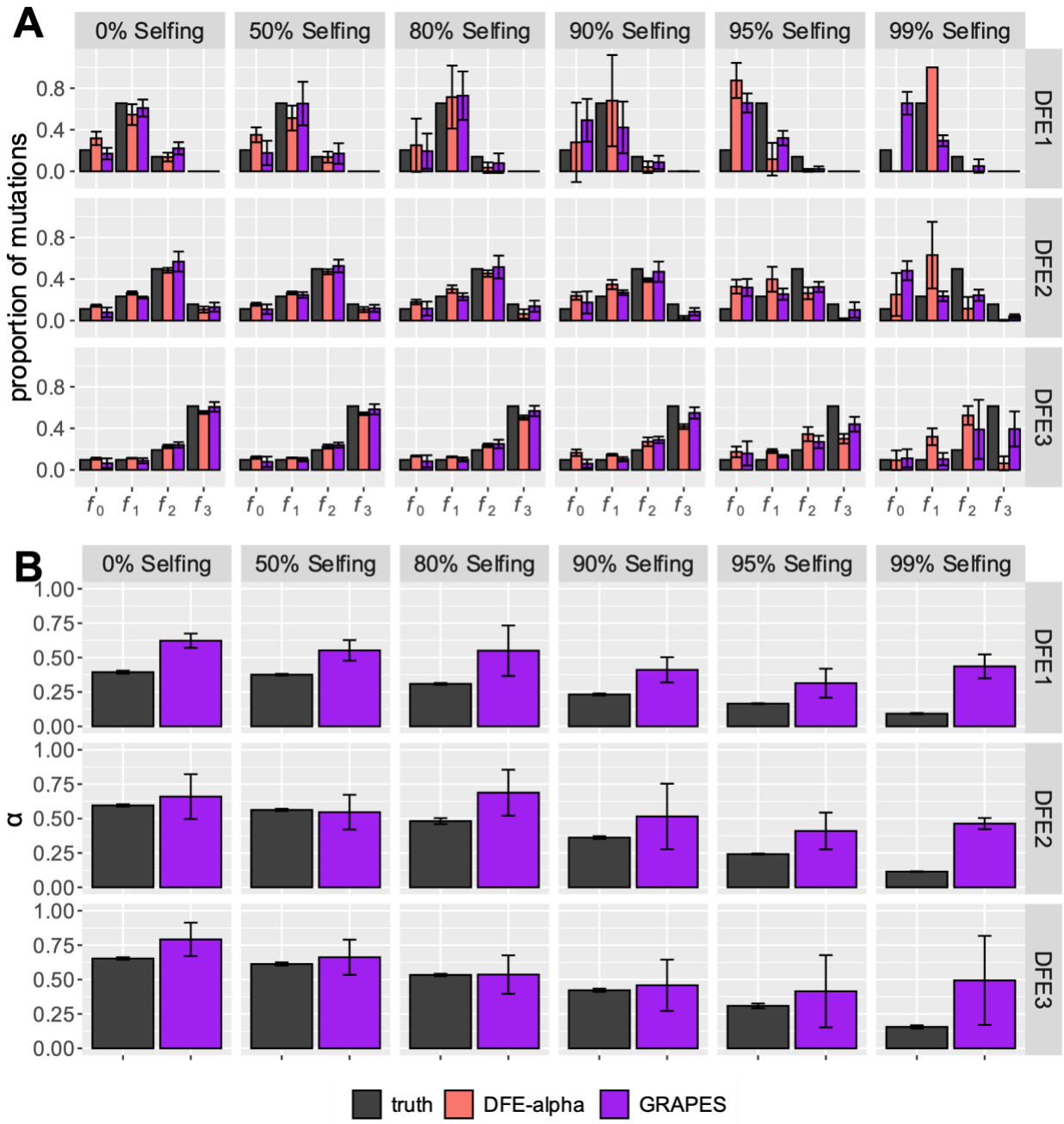

Supplementary Figure 23: Effects of selfing on the inference of (A) the DFE of new deleterious mutations and (B) the proportion of beneficial fixations (α) using DFE-alpha and GRAPES, when beneficial mutations were rare. Results for A are shown in terms of the proportion of mutations in effectively neutral (f_0), weakly deleterious (f_1), moderately deleterious (f_2) and strongly deleterious (f_3) classes. Here, 0.1% of new exonic mutations were beneficial and exponentially distributed with a mean $2Ns_a = 200$. Here, the folded SFS was used for inference. The error bars denote the standard deviation of proportions estimated from 5 independent replicates.

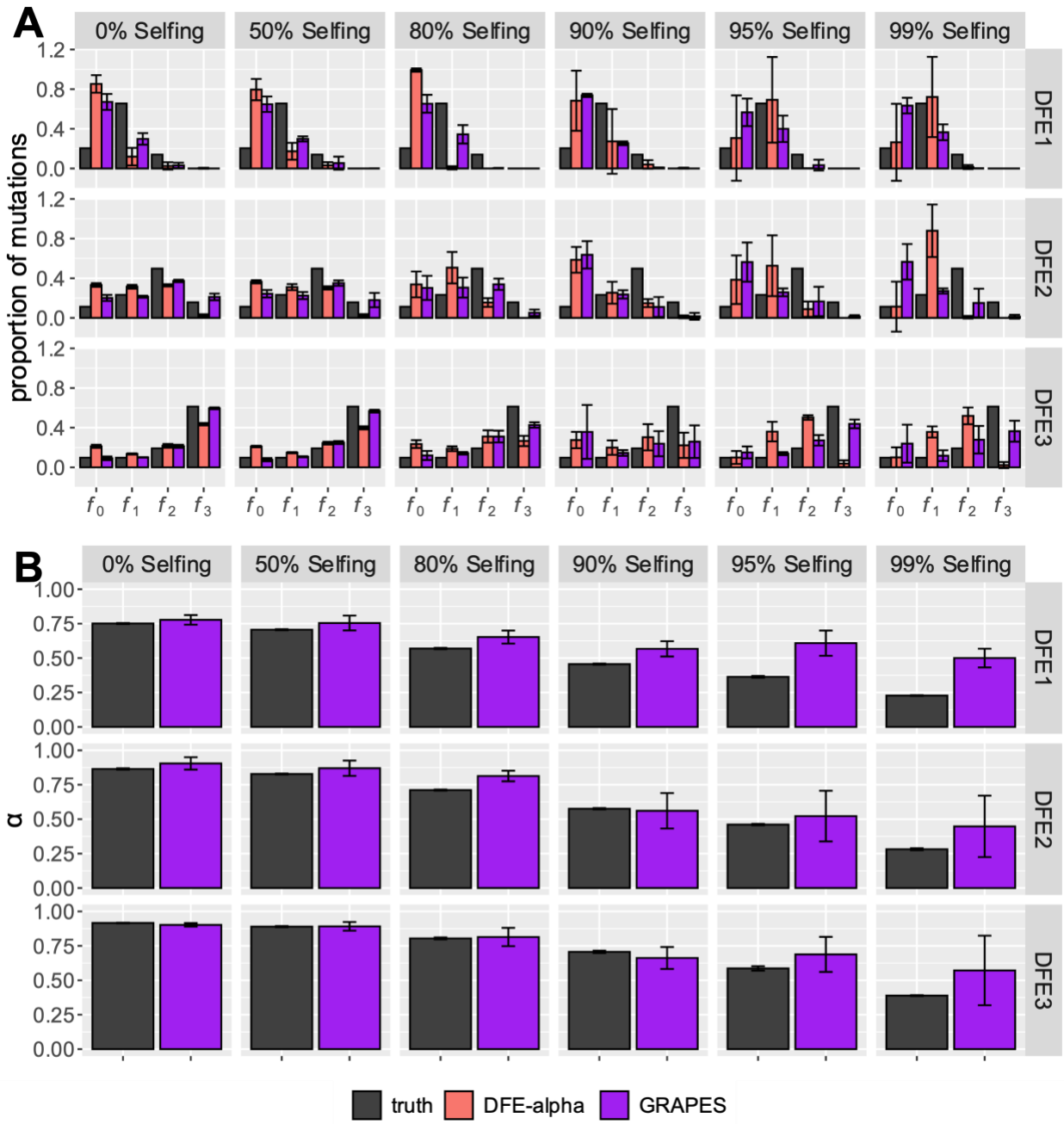

Supplementary Figure 24: Effects of selfing on the inference of (A) the DFE of new deleterious mutations and (B) the proportion of beneficial fixations (α) using DFE-alpha and GRAPES, when beneficial mutations were common. Results for A are shown in terms of the proportion of mutations in effectively neutral (f_0), weakly deleterious (f_1), moderately deleterious (f_2) and strongly deleterious (f_3) classes. Here, 1.0% of new exonic mutations were beneficial and exponentially distributed with a mean $2Ns_a = 200$. Here, the folded SFS was used for inference. The error bars denote the standard deviation of proportions estimated from 5 independent replicates.

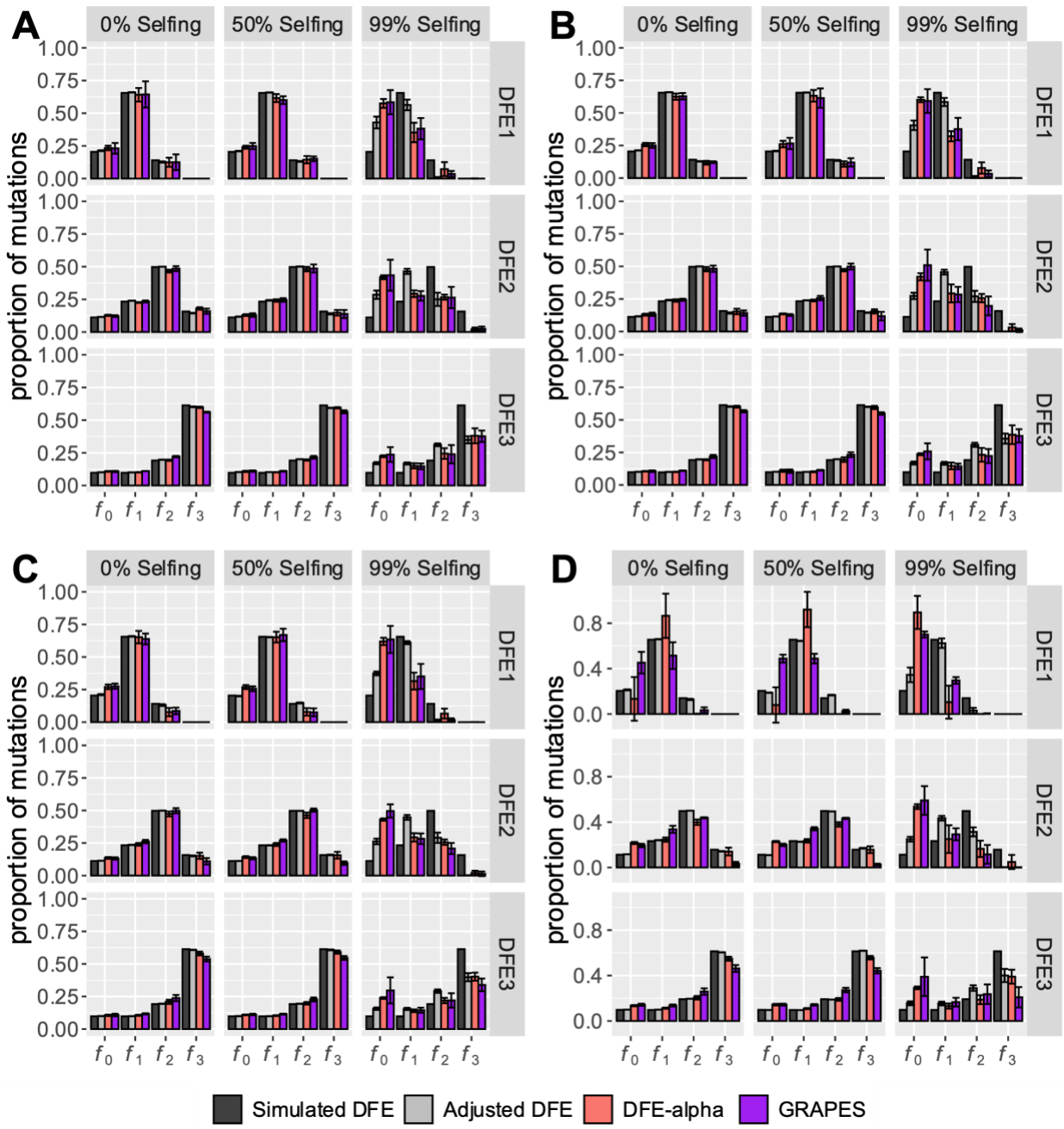

Supplementary Figure 25: Effects of population structure and selfing on the inference of the DFE of new deleterious mutations using DFE-alpha and GRAPES. Populations were simulated under an island model with five demes, and genomes were sampled evenly from each deme. Here the metapopulation effective size was equal to 5000 at 0% selfing (see methods). Results are shown when $N_{deme}m$ was (**A**) 2 (**B**) 1, (**C**) 0.5, and (**D**) 0.1. Results are shown in terms of the proportion of mutations in effectively neutral (f_0), weakly deleterious (f_1), moderately deleterious (f_2) and strongly deleterious (f_3) classes. The nucleotide site diversity with background selection (B) relative to its expectation under strict neutrality is shown in each panel. The adjusted DFE represents the distribution of $2NBs_d$. The error bars denote the standard deviation of proportions estimated from 5 independent replicates.

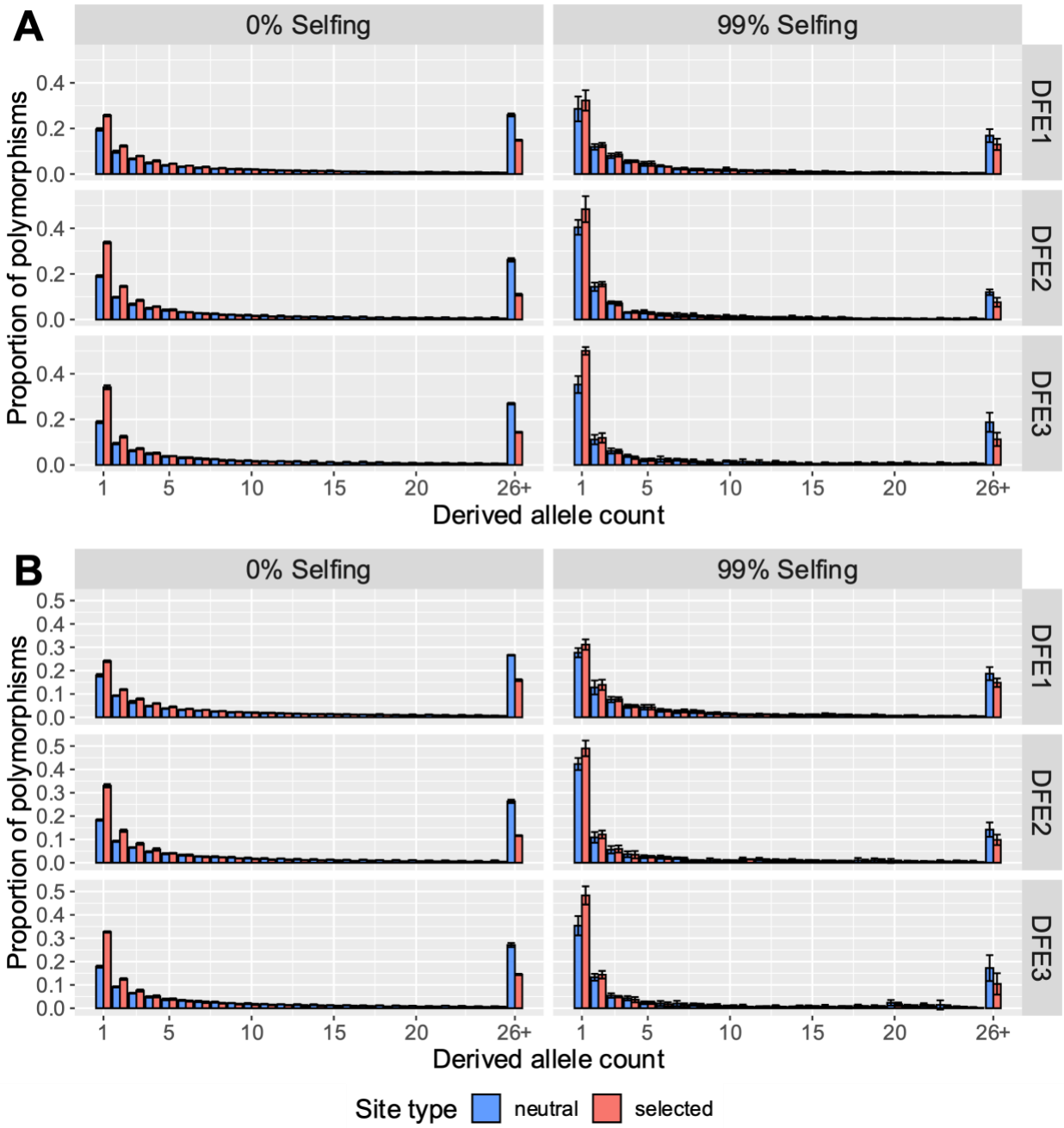

Supplementary Figure 26: Effects of population structure and selfing on the SFS. Populations were simulated under an island model with five demes, and genomes were sampled evenly from each deme. Here the metapopulation effective size was equal to 5000 at 0% selfing (see methods). Results are shown when $N_{deme}m$ was (**A)** 2 **(B)** 1. The error bars denote the standard deviation of proportions estimated from 5 independent replicates. The last class (26+) refers to the derived allele counts 26-100.

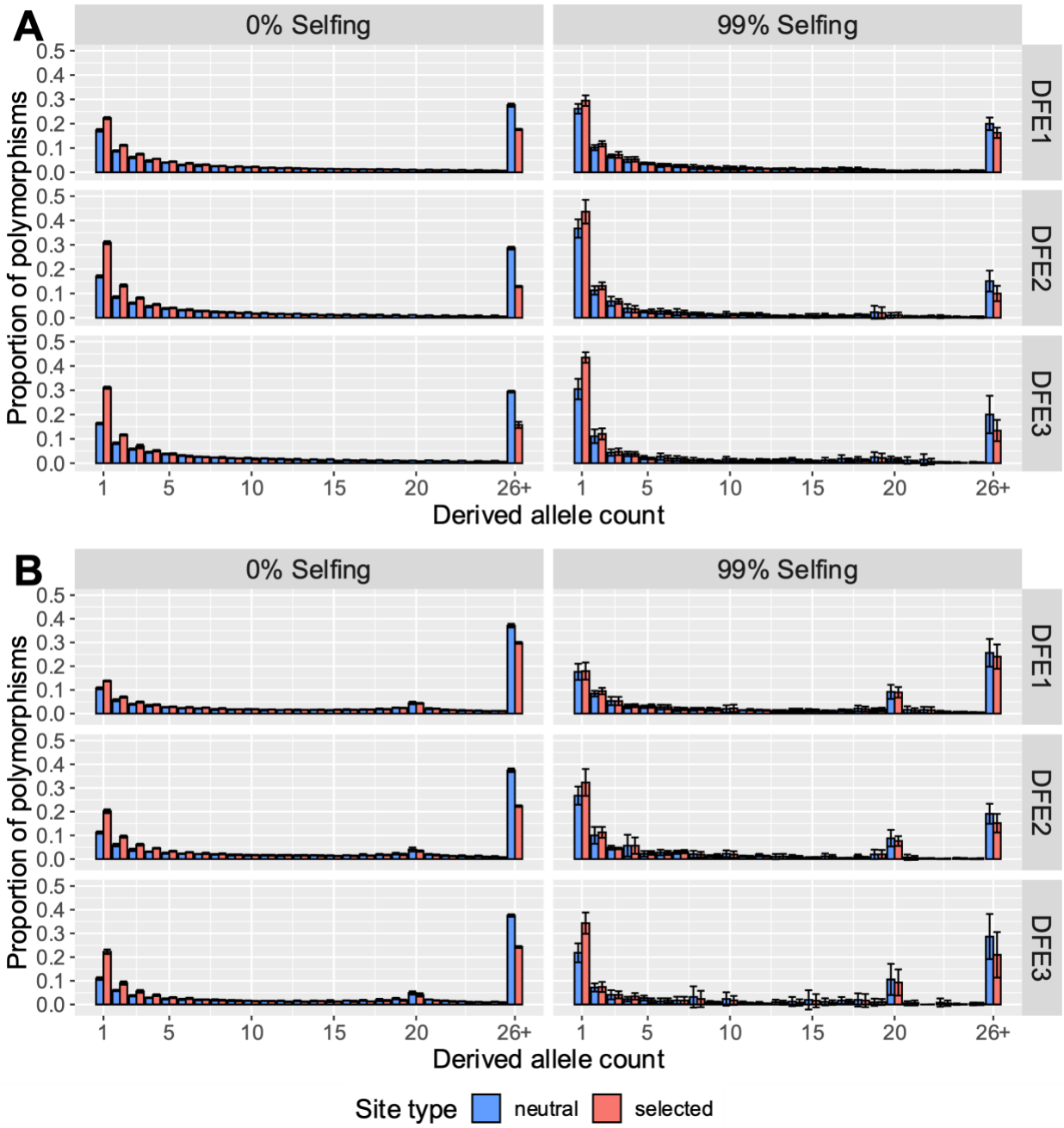

Supplementary Figure 27: Effects of population structure and selfing on the SFS with even sampling. Populations were simulated under an island model with five demes, and genomes were sampled evenly from each deme. Here the metapopulation effective size was equal to 5000 at 0% selfing (see methods). Results are shown when $N_{deme}m$ was (**A**) 0.5 (**B**) 0.1. The error bars denote the standard deviation of proportions estimated from 5 independent replicates. The last class (26+) refers to the derived allele counts 26-100.

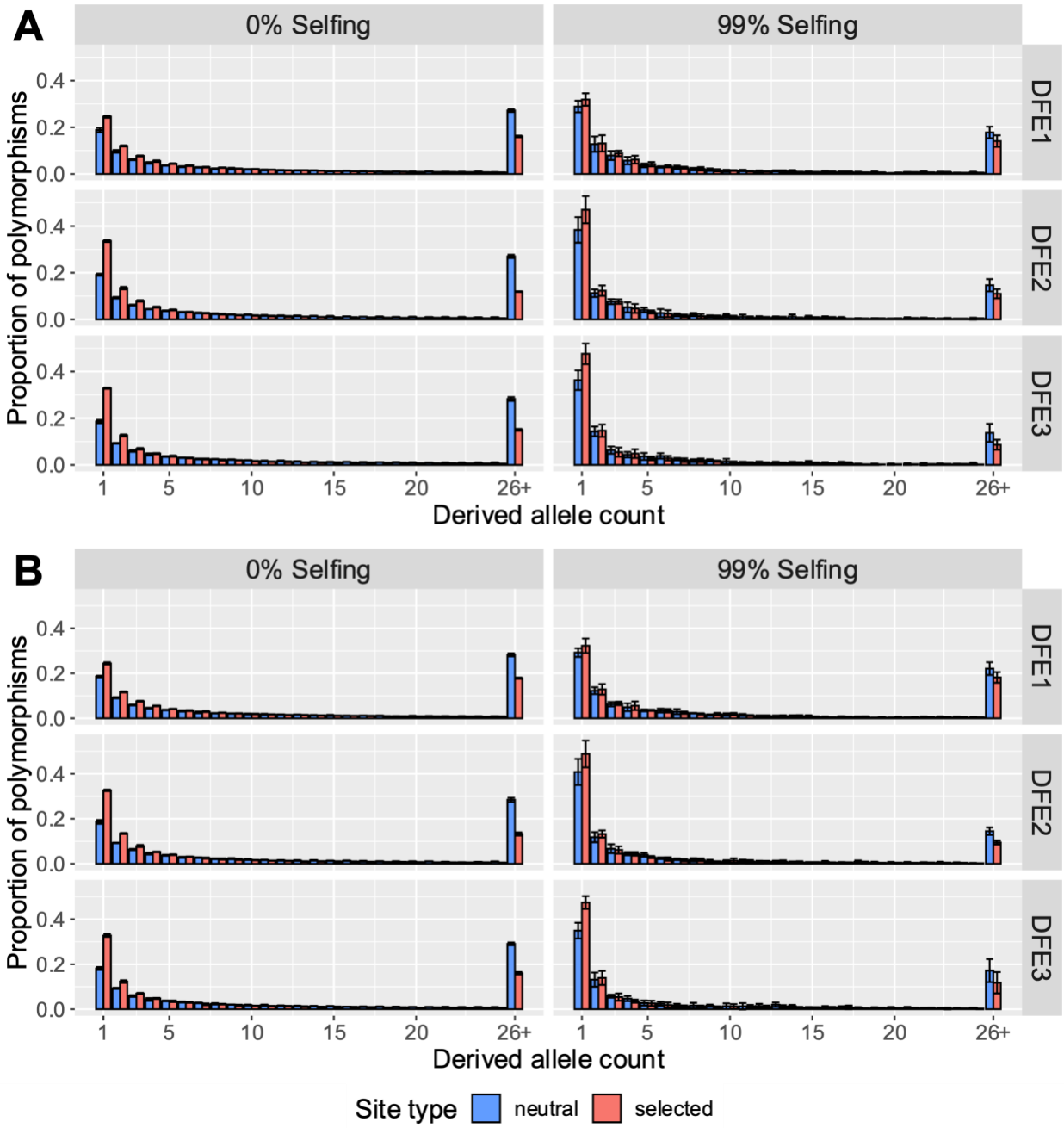

Supplementary Figure 28: Effects of uneven sampling, population structure, and selfing on the SFS at high migration rates. Populations were simulated under an island model with five demes, and genomes were sampled unevenly (60 genomes from one deme, and 10 from the remaining four demes). Here the metapopulation effective size was equal to 5000 at 0% selfing (see methods). Results are shown when $N_{deme}m$ was (**A**) 2 (**B**) 1. The error bars denote the standard deviation of proportions estimated from 5 independent replicates. The last class (26+) refers to the derived allele counts 26-100.

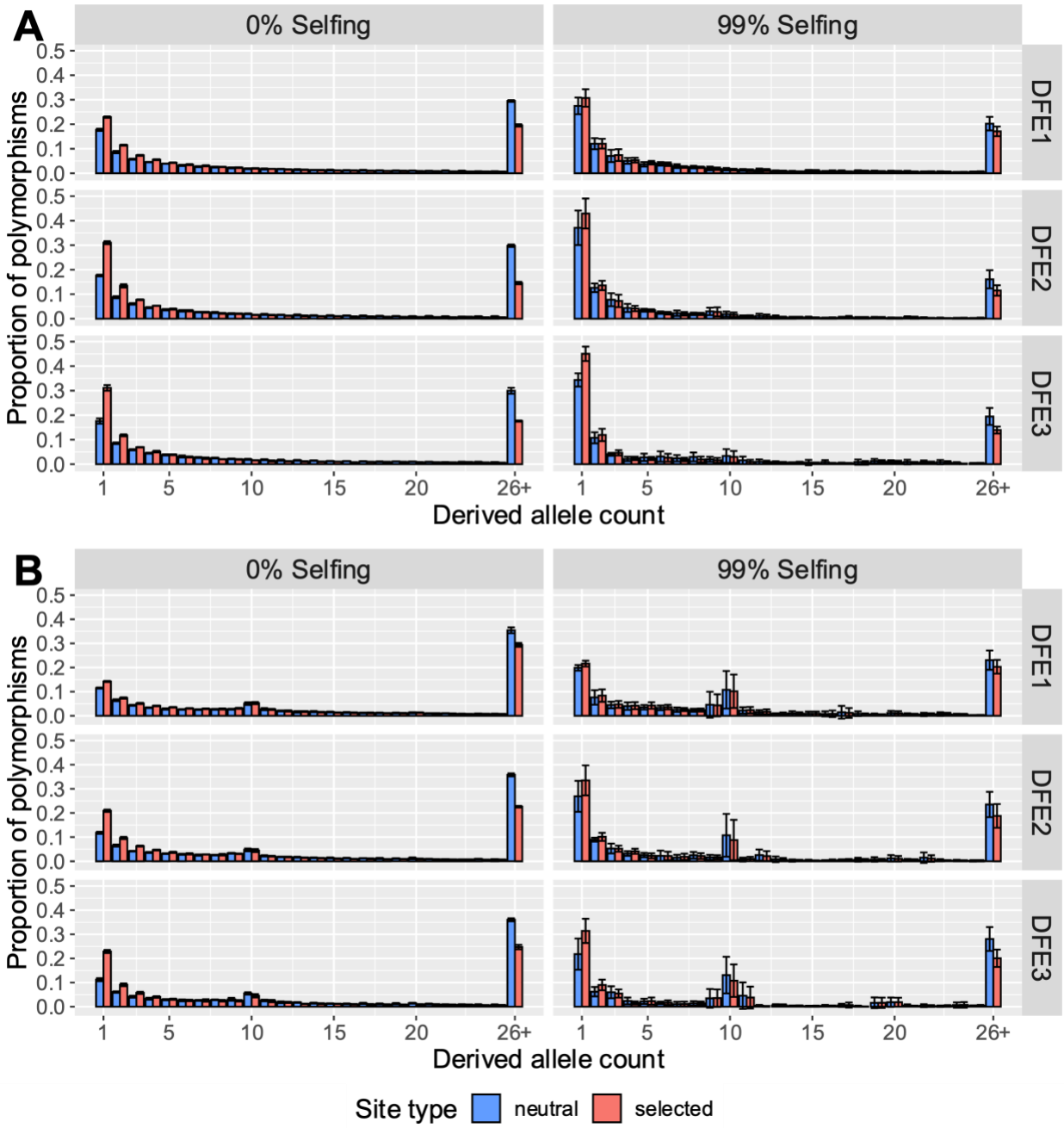

Supplementary Figure 29: Effects of uneven sampling, population structure, and selfing on the SFS at lower migration rates. Populations were simulated under an island model with five demes, and genomes were sampled unevenly (60 genomes from one deme, and 10 from the remaining four demes). Here the metapopulation effective size was equal to 5000 at 0% selfing (see methods). Results are shown when $N_{deme}m$ was (**A**) 0.5 (**B**) 0.1. The error bars denote the standard deviation of proportions estimated from 5 independent replicates. The last class (26+) refers to the derived allele counts 26-100.

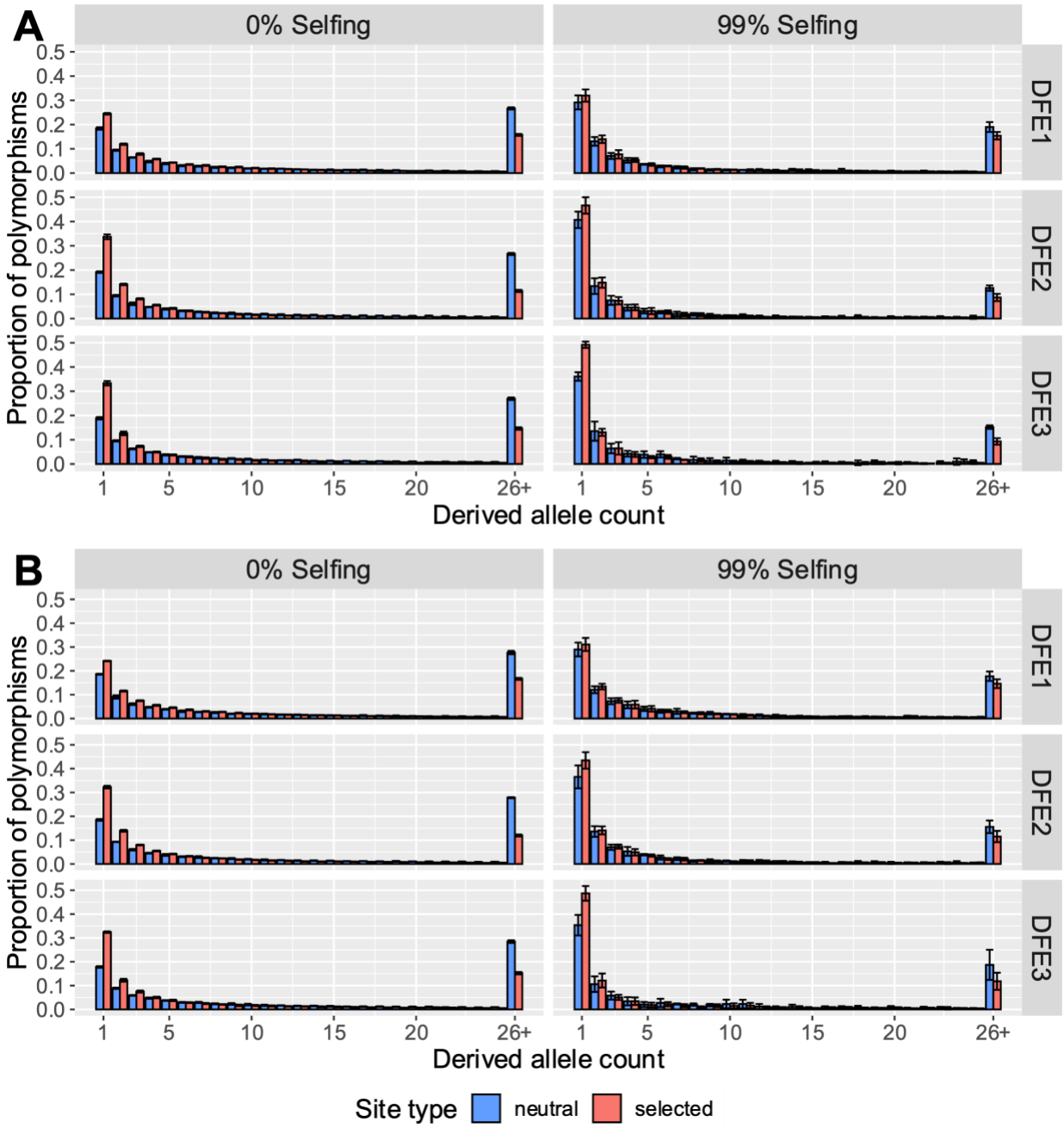

Supplementary Figure 30: Effects of uneven sampling, population structure, and selfing on the SFS at high migration rates. Populations were simulated under an island model with five demes, and genomes were sampled unevenly (35 genomes from two demes, and 10 from the remaining four demes). Here the metapopulation effective size was equal to 5000 at 0% selfing (see methods). Results are shown when $N_{deme}m$ was (**A**) 2 (**B**) 1. The error bars denote the standard deviation of proportions estimated from 5 independent replicates. The last class (26+) refers to the derived allele counts 26-100.

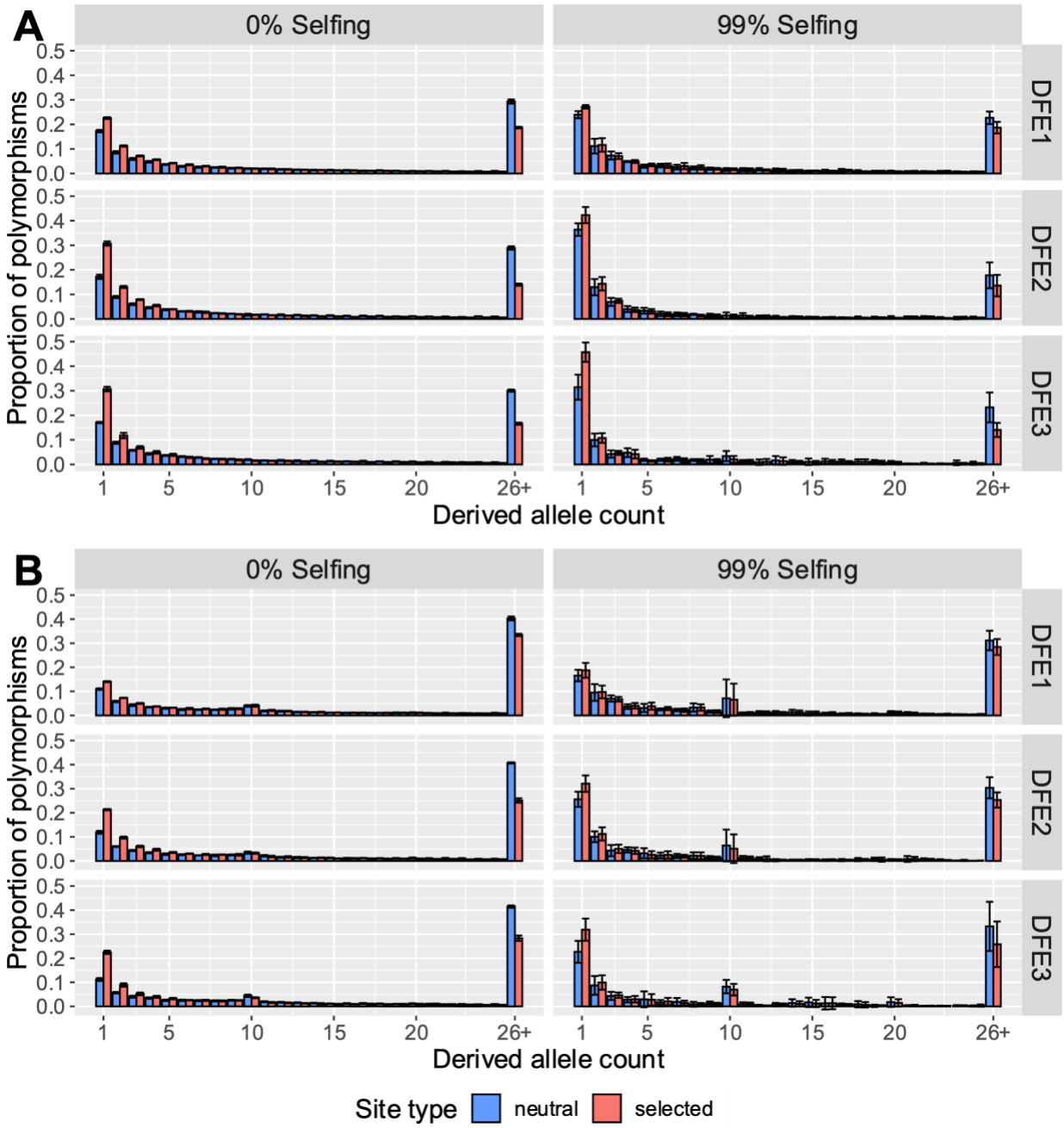

Supplementary Figure 31: Effects of uneven sampling, population structure, and selfing on the SFS when rates of migration are low. Populations were simulated under an island model with five demes, and genomes were sampled unevenly (35 genomes from two demes, and 10 from the remaining four demes). Here the metapopulation effective size was equal to 5000 at 0% selfing (see methods). Results are shown when $N_{deme}m$ was **(A)** 0.5 **(B)** 0.1. The error bars denote the standard deviation of proportions estimated from 5 independent replicates. The last class (26+) refers to the derived allele counts 26-100.

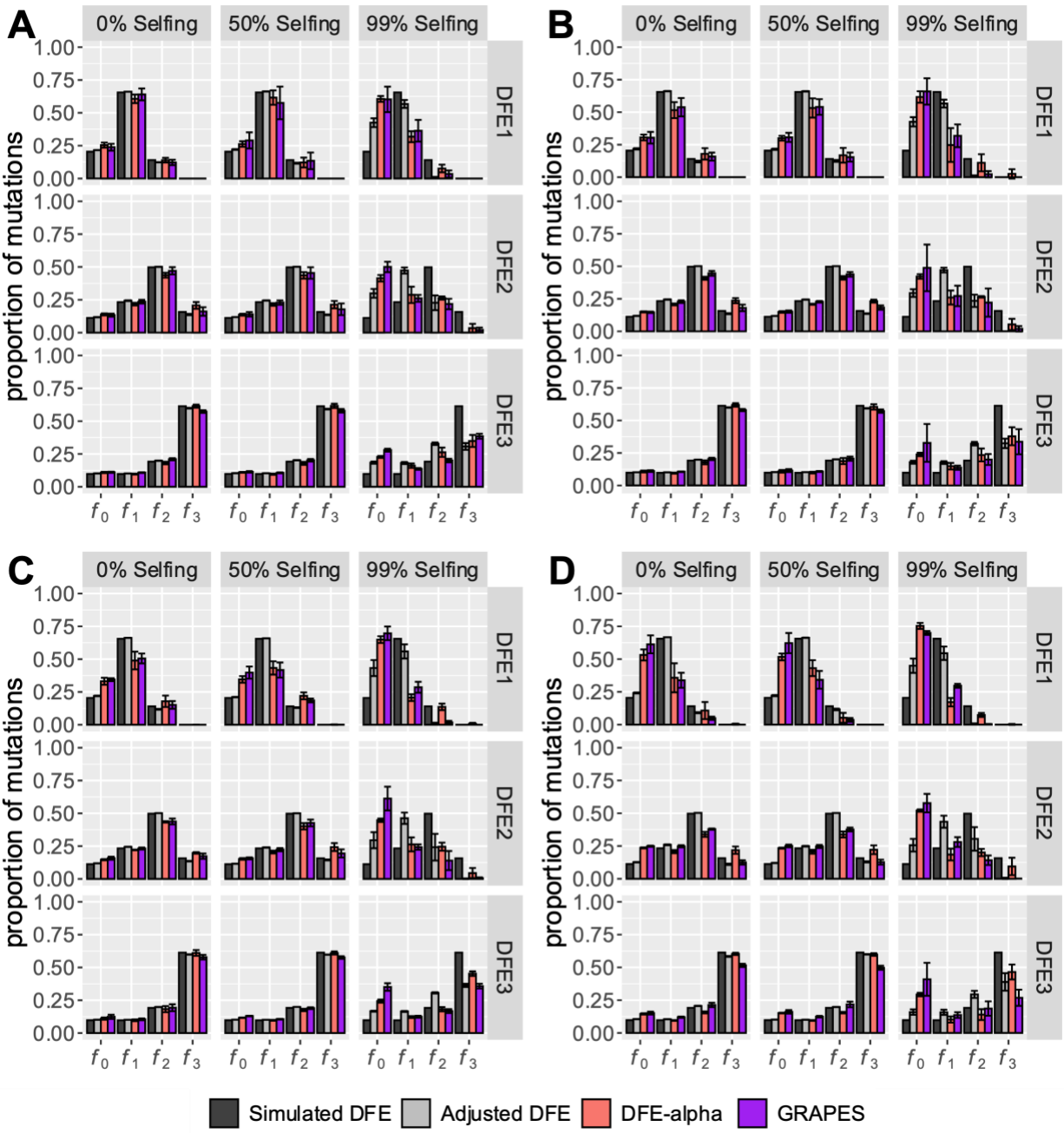

Supplementary Figure 32: Effects of uneven sampling, population structure, and selfing on the inference of the DFE of new deleterious mutations using DFE-alpha and GRAPES. Populations were simulated under an island model with five demes, and genomes were sampled unevenly (60 genomes from one deme, and 10 from the remaining four demes). Here the metapopulation effective size was equal to 5000 at 0% selfing (see methods). Results are shown when $N_{deme}m$ was **(A)** 2 **(B)** 1, **(C)** 0.5, and **(D)** 0.1. Results are shown in terms of the proportion of mutations in effectively neutral (f_0), weakly deleterious (f_1), moderately deleterious (f_2) and strongly deleterious (f_3) classes. The nucleotide site diversity with background selection (B) relative to its expectation under strict neutrality is shown in each panel. The adjusted DFE represents the distribution of $2NBs_d$. The error bars denote the standard deviation of proportions estimated from 5 independent replicates.

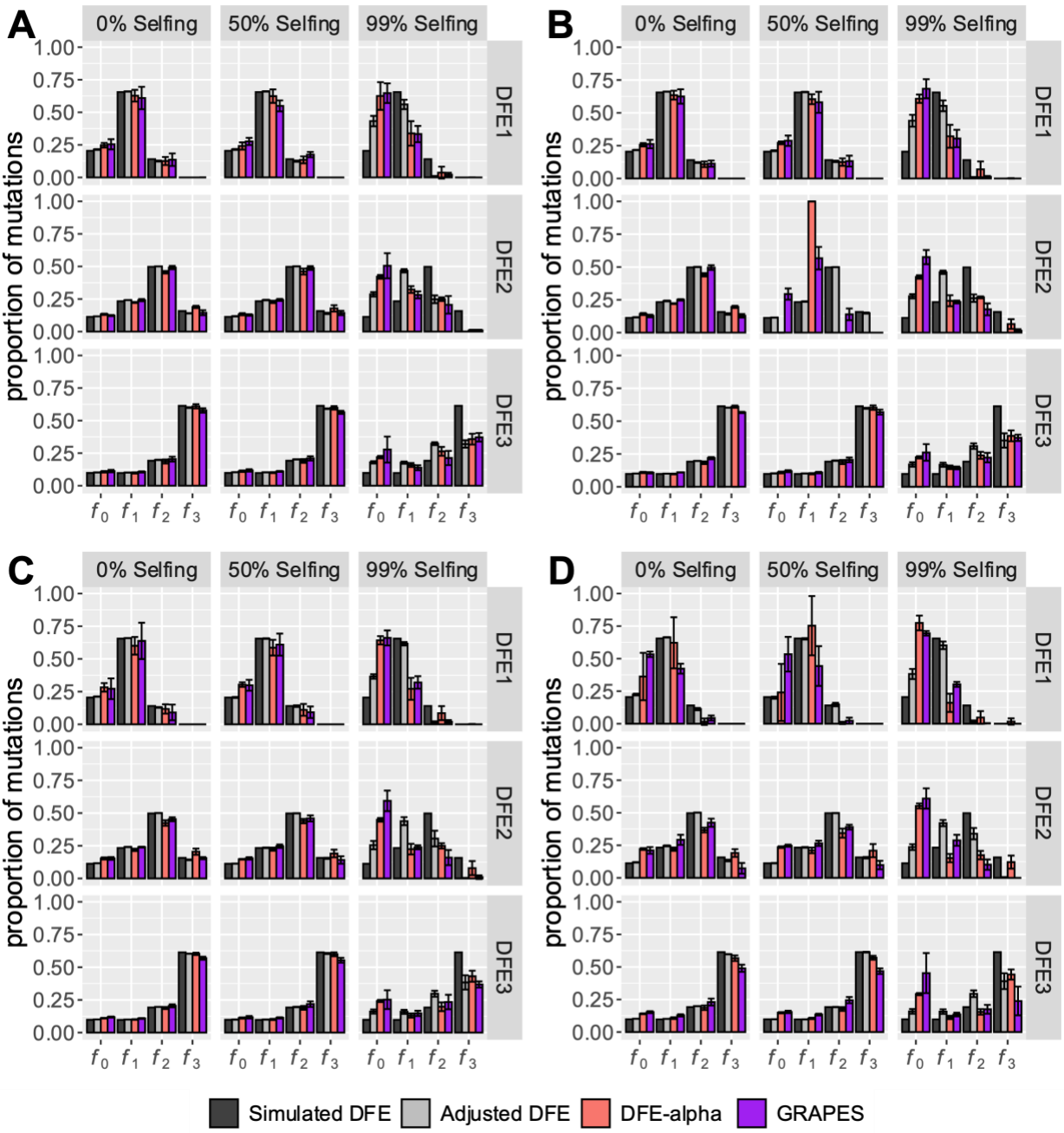

Supplementary Figure 33: Effects of uneven sampling, population structure and selfing on the inference of the DFE of new deleterious mutations using DFE-alpha and GRAPES. Populations were simulated under an island model with five demes, and genomes were sampled unevenly (35 genomes from two demes, and 10 from the remaining three demes). Here the metapopulation effective size was equal to 5000 at 0% selfing (see methods). Results are shown when $N_{deme}m$ was **(A)** 2 **(B)** 1, **(C)** 0.5, and **(D)** 0.1. Results are shown in terms of the proportion of mutations in effectively neutral (f_0), weakly deleterious (f_1), moderately deleterious (f_2) and strongly deleterious (f_3) classes. The nucleotide site diversity with background selection (B) relative to its expectation under strict neutrality is shown in each panel. The adjusted DFE represents the distribution of $2NBs_d$. The error bars denote the standard deviation of proportions estimated from 5 independent replicates.

Supplementary Table 1 Effects of selfing on the mean values of parameters of the DFE of new deleterious mutations, estimated by DFE-alpha. Here $E[s]$ represents the mean efficacy of selection, before being scaled by a 2-epoch model of population size change, where $N1$ represents the ancestral population size, $N2$ represents the relative population size after the first epoch, and $t2$ represents the duration of time after the population size change (in generations).

	Selfing rate	$E[s]$	$N1$	$N2$	$t2$
DFE1	Truth	-0.025	100	NA	NA
	0%	-0.027	100	145	16
	50%	-0.025	100	153	7
	80%	-0.021	100	162	5
	90%	-0.023	100	150	17
	95%	-0.019	100	179	29
	99%	-0.013	100	394	77
DFE2	Truth	-0.25	100	100	NA
	0%	-0.269	100	158	5
	50%	-0.263	100	150	6
	80%	-0.223	100	168	5
	90%	-0.187	100	238	5
	95%	-0.099	100	322	22
	99%	-0.026	100	1000	57
DFE3	Truth	-5	100	100	NA
	0%	-4.712	100	144	5
	50%	-5.465	100	156	5
	80%	-4.62	100	162	5
	90%	-2.665	100	198	11
	95%	-1.722	100	319	17
	99%	-0.687	100	798	59

Supplementary Table 2 Estimated parameter values of the deleterious DFE by GRAPES and DFE-alpha for simulations with only semi-dominant deleterious mutations.

		β				$2N_e s_d$			
		GRAPES		DFE-alpha		GRAPES		DFE-alpha	
	Selfing rate	mean	SD	mean	SD	mean	SD	mean	SD
DFE1	Truth	0.9	0	0.9	0	5	0	5	0
	0%	0.77	0.16	0.74	0.04	5.43	0.58	5.4	0.33
	50%	0.85	0.09	0.82	0.16	4.97	0.15	5.12	0.5
	80%	0.93	0.30	1	0.29	4.5	0.81	4.27	0.59
	90%	0.65	0.11	0.78	0.16	5.25	1.07	4.8	0.92
	95%	0.57	0.15	0.68	0.14	4.42	0.39	4	0.48
	99%	0.34	0.03	0.26	0.03	2.34	0.59	3.2	0.9
DFE2	Truth	0.5	0	0.5	0	50	0	50	0
	0%	0.50	0.01	0.48	0.01	50.6	4.12	54.23	5.35
	50%	0.48	0.04	0.47	0.02	52	6.64	53.12	3.45
	80%	0.49	0.06	0.48	0.03	44.4	7.33	45.14	3.73
	90%	0.45	0.05	0.47	0.03	41.87	10.37	37.87	6.4
	95%	0.39	0.07	0.46	0.07	29.44	9.1	21.12	5.89
	99%	0.33	0.15	0.35	0.04	8.93	1.38	6.39	1.41
DFE3	Truth	0.3	0	0.3	0	1000	0	1000	0
	0%	0.32	0.02	0.3	0.01	627.15	107.89	949.56	138.64
	50%	0.30	0.02	0.29	0.02	730.72	133.39	1102.76	243.83
	80%	0.30	0.05	0.29	0.03	743.11	415.73	933.55	448.17
	90%	0.28	0.04	0.29	0.01	663.41	468.89	546.89	156.22
	95%	0.26	0.04	0.28	0.01	512.23	233.45	363.49	62.58
	99%	0.17	0.06	0.26	0.03	619.02	344.14	171.07	99.41

Supplementary Table 3 The number of segregating sites and reduction in population size due to BGS and selfing for varying selfing rates and DFEs as observed in our simulations. Here N=5000 and $B = \pi_{neu}/(4N_{self}\mu)$, where μ is the mutation rate per site/generation.

	Selfing rate	Number of deleterious segregating sites		π_{neu}	N_{emp}	N_{self}	B
		mean	SD				
DFE1	0%	13564	137	0.00626	4746	5000	0.949
	50%	10077	121	0.00464	3512	3750	0.936
	80%	7950	112	0.00352	2664	3000	0.888
	90%	6997	131	0.00299	2264	2750	0.823
	95%	6260	190	0.00244	1850	2625	0.705
	99%	4281	293	0.0011	835	2525	0.331
DFE2	0%	7930	103	0.00614	4654	5000	0.931
	50%	5837	105	0.00448	3392	3750	0.905
	80%	4463	95	0.00322	2440	3000	0.813
	90%	3559	137	0.00225	1706	2750	0.620
	95%	2656	244	0.00114	865	2625	0.329
	99%	1628	135	0.00028	212	2525	0.084
DFE3	0%	4273	49	0.0059	4470	5000	0.894
	50%	3003	36	0.00406	3078	3750	0.821
	80%	2048	68	0.00257	1946	3000	0.649
	90%	1602	25	0.00165	1254	2750	0.456
	95%	1213	54	0.00097	737	2625	0.281
	99%	818	69	0.00032	241	2525	0.096

Supplementary Table 4 Nucleotide site diversity (π) from single-site simulations of neutral and semidominant deleterious mutations in populations with varying selfing rates.

	Selfing rate	Theoretical π at neutral sites	Simulation π at neutral sites
DFE1	0	0.00660	0.00653
DFE2	0	0.00660	0.00653
DFE3	0	0.00660	0.00653
DFE1	0.50	0.00495	0.00499
DFE2	0.50	0.00495	0.00499
DFE3	0.50	0.00495	0.00499
DFE1	0.99	0.00333	0.00321
DFE2	0.99	0.00333	0.00321
DFE3	0.99	0.00333	0.00321

Supplementary Table 5 Estimates of the parameters of the deleterious DFE (a gamma distribution with mean $\gamma = 2N_e\overline{s_d}$ and shape parameter β) inferred by DFE-alpha and GRAPES. Since DFE-alpha and GRAPES assume semidominance, the mean strength of selection γ was multiplied by 0.5 to be equivalent to $2N_{self}s_dh_{self}$.

DFE	Selfing rate	$2N_{self}s_dh_{self}$ (expected)	DFE-alpha γh	GRAPES γh	β (expected)	DFE-alpha β	GRAPES β	h
DFE1	0	3.75	4.29	4.33	0.9	0.62	0.64	0.75
DFE1	0.50	4.04	3.32	3.49	0.9	0.68	0.66	0.75
DFE1	0.99	4.17	1.40	1.01	0.9	0.42	0.34	0.75
DFE2	0	37.5	41.45	34.99	0.5	0.44	0.48	0.75
DFE2	0.50	40.38	30.68	27.77	0.5	0.46	0.49	0.75
DFE2	0.99	41.67	4.23	4.54	0.5	0.30	0.19	0.75
DFE3	0	750.00	791.63	493.84	0.3	0.29	0.31	0.75
DFE3	0.50	807.69	630.82	429.23	0.3	0.28	0.30	0.75
DFE3	0.99	833.32	50.93	222.49	0.3	0.29	0.18	0.75
DFE1	0	2.50	2.70	2.71	0.9	0.74	0.77	0.50
DFE1	0.50	3.08	2.56	2.48	0.9	0.82	0.85	0.50
DFE1	0.99	3.33	1.60	1.17	0.9	0.26	0.34	0.50
DFE2	0	25.00	27.11	25.30	0.5	0.48	0.49	0.50
DFE2	0.50	30.77	26.56	26.00	0.5	0.47	0.48	0.50
DFE2	0.99	33.33	3.19	4.46	0.5	0.35	0.33	0.50
DFE3	0	500.00	474.78	313.57	0.3	0.30	0.32	0.50
DFE3	0.50	615.38	551.38	365.36	0.3	0.29	0.30	0.50
DFE3	0.99	666.64	85.53	309.51	0.3	0.26	0.17	0.50
DFE1	0	1.25	1.28	1.33	0.9	2.66	2.07	0.25
DFE1	0.50	2.12	1.66	1.74	0.9	1.54	1.49	0.25
DFE1	0.99	2.50	1.56	0.98	0.9	0.32	0.39	0.25
DFE2	0	12.50	10.73	10.62	0.5	0.63	0.64	0.25
DFE2	0.50	21.15	18.06	15.95	0.5	0.51	0.56	0.25
DFE2	0.99	25.00	4.50	4.65	0.5	0.29	0.20	0.25
DFE3	0	250.00	263.78	217.20	0.3	0.31	0.31	0.25
DFE3	0.50	423.08	316.34	253.83	0.3	0.31	0.32	0.25
DFE3	0.99	499.97	54.93	183.24	0.3	0.28	0.25	0.25
DFE1	0	0.50	0.91	0.88	0.9	100	16.45	0.10
DFE1	0.50	1.54	1.24	1.31	0.9	3.44	9.15	0.10
DFE1	0.99	2.00	1.32	0.84	0.9	0.40	0.36	0.10
DFE2	0	5.00	4.54	4.92	0.5	1.05	0.94	0.10
DFE2	0.50	15.38	12.19	12.42	0.5	0.58	0.56	0.10
DFE2	0.99	20.00	5.02	6.41	0.5	0.32	0.22	0.10
DFE3	0	100.00	69.53	63.27	0.3	0.38	0.39	0.10
DFE3	0.50	307.69	192.87	159.62	0.3	0.33	0.33	0.10
DFE3	0.99	399.96	72.07	213.35	0.3	0.26	0.19	0.10

Supplementary Table 6 Effects of selfing on the number of fixations of deleterious and beneficial mutations. Here, deleterious mutations were drawn from the DFEs defined in Table 1, while 0.1% of new exonic mutations were beneficial and exponentially distributed with a mean $2Ns_a = 200$.

Selfing rate	DFE	Deleterious substitutions avg.	Deleterious substitutions SD	Beneficial substitutions avg.	Beneficial substitutions SD	α avg.	α SD
0	DFE1	1438.4	31.48	935.8	32.09	0.39	0.01
50	DFE1	1514.2	56.92	912.2	30.19	0.38	0.01
80	DFE1	1820.8	28.03	813.4	17.9	0.31	0.01
90	DFE1	2253.6	68.2	681.8	14.75	0.23	0.01
95	DFE1	2785	77.11	552.4	19.55	0.17	0
99	DFE1	3363.8	56.91	343.4	15.53	0.09	0
0	DFE2	618.2	7.82	912	40.21	0.6	0.01
50	DFE2	682	28.57	878.2	33.25	0.56	0.01
80	DFE2	810	46.98	753.4	33.07	0.48	0.02
90	DFE2	1087.4	31.5	617.6	20.02	0.36	0.01
95	DFE2	1451.2	28.01	464	5.7	0.24	0
99	DFE2	2133	26.54	276.6	7.83	0.11	0
0	DFE3	460.8	11.76	869.2	24.38	0.65	0.01
50	DFE3	509	16.39	806.6	25.75	0.61	0.01
80	DFE3	543.2	27.22	620.6	18.99	0.53	0.01
90	DFE3	635.6	34.25	464.8	25.96	0.42	0.01
95	DFE3	762.2	24.94	341.4	20.95	0.31	0.02
99	DFE3	1040.8	36.62	191.6	18.77	0.16	0.01

Supplementary Table 7 Parameters used for five-deme island model simulations.

$N_{deme}m$	m	N_{deme}
10	0.0102	984
2	0.00216	926
1	0.00116	862
0.5	0.00066	785
0.1	0.00026	385

Supplementary Table 8 Table showing how theoretical expectations for T_T, T_S, and F_{st} match values estimated from neutral simulations.

$N_{deme}m$	Selfing rate	π_{meta} expected	π_{meta} observed	π_{deme} expected	π_{deme} observed	F_{st} expected	F_{st} observed
0.1	0	0.00660	0.00659	0.00254	0.00259	0.61515	0.60713
0.1	0.50	0.00597	0.00599	0.00191	0.00211	0.68063	0.64825
0.1	0.99	0.00534	0.00567	0.00128	0.00140	0.75991	0.76400
0.5	0	0.00678	0.00661	0.00518	0.00507	0.23595	0.23265
0.5	0.50	0.00549	0.00537	0.00389	0.00375	0.29166	0.30229
0.5	0.99	0.00422	0.00425	0.00262	0.00291	0.37947	0.31402
1.0	0	0.00660	0.00659	0.00569	0.00564	0.13794	0.14426
1.0	0.50	0.00518	0.00519	0.00427	0.00434	0.17584	0.16317
1.0	0.99	0.00378	0.00402	0.00287	0.00305	0.24062	0.24016
2.0	0	0.00660	0.00657	0.00611	0.00611	0.07407	0.06951
2.0	0.50	0.00507	0.00508	0.00458	0.00457	0.09638	0.09950
2.0	0.99	0.00358	0.00345	0.00309	0.00295	0.13674	0.14377

Supplementary Table 9 Estimated levels of background selection (B) in highly selfing species for the range of previously reported selfing rates. All species are diploid except *C. bursa-pastoris*. The number of deleterious mutations per genome per generation (U_d) was estimated by multiplying the number of coding sites by 0.7. The strength of BGS was calculated with $B = \exp\left(-\frac{U_d}{R_{self}}\right)$, where $R_{self} = R \times F$. This supplementary table contains all mutation and recombination rate data used for the calculations in Table 2 of the main text.

(table stored in a separate attachment)